12-2012

Testing a Novel Technique to Improve Aluminum-26 Accelerator Mass Spectrometry Measurements for Earth Science Applications

Meghan Sarah Janzen
mjanzen1@utk.edu

To the Graduate Council:

I am submitting herewith a thesis written by Meghan Sarah Janzen entitled "Testing a Novel Technique to Improve Aluminum-26 Accelerator Mass Spectrometry Measurements for Earth Science Applications." I have examined the final electronic copy of this thesis for form and content and recommend that it be accepted in partial fulfillment of the requirements for the degree of Master of Science, with a major in Geology.

Alfredo Galindo-Uribarri, Major Professor

We have read this thesis and recommend its acceptance:

Edmund Perfect, Yingkui Li

Accepted for the Council:
Carolyn R. Hodges

Vice Provost and Dean of the Graduate School

(Original signatures are on file with official student records.)

Testing a Novel Technique to Improve Aluminum-26 Accelerator Mass Spectrometry Measurements for Earth Science Applications

A Thesis Presented for
The Master of Science
Degree
The University of Tennessee, Knoxville

Meghan Sarah Janzen
December 2012

DEDICATION

To my mother
Heather Ann Janzen

and my father
Victor Paul Janzen

ACKNOWLEDGMENTS

I wish to express my deep gratitude to my advisor Dr. Alfredo Galindo-Uribarri at Oak Ridge National Laboratories (ORNL) for providing me with the opportunity to pursue a higher education at ORNL and for opening up doors to many other opportunities and collaborations during my tenure in graduate school. Thanks also to the rest of my thesis committee Prof. Ed. Perfect and Prof. Yingkui Li for their continuous support and guidance. I would also like to thank the entire team at the Holifield Radioactive Ion Beam Facility for their assistance in my research; especially Dr. Yuan Liu for her help operating the test stand and Gerald Mills for his help operating the stable ion beam injector negative ion source. I would also like to thank the employees at the PRIME Lab at Purdue University; in particular Greg Chmiel and Tom Clifton for the use of their labs and for their help in the quartz sample preparations. Special thanks also to my father Dr. Victor Janzen for inspiring me to pursue higher education. I also wish to thank Michael Lawson as well as Bill Deane, Arya Udry, Avril Meza, Latisha Brengman and Rachel Storniolo for their encouragement and friendship throughout my studies.

I would like to express my appreciation to the U.S. Department of Energy for providing funding for my work and to HRIBF for providing the equipment and materials used in this project. I would also like to thank Prof. Yingkui Li for providing me with the purified quartz samples for the preparation of my AMS targets.

ABSTRACT

The measurement of cosmogenic ^{26}Al [aluminum-26] in geological samples by accelerator mass spectrometry (AMS) is typically conducted on Al_2O_3 [aluminum oxide] targets. However, Al_2O_3 is not an ideal source material because it does not form a prolific beam of Al^- [negative atomic aluminum ions] required for measuring low-levels of ^{26}Al. This thesis presents the performance of AlN [aluminum nitride], AlF_3 [aluminum fluoride] and mixed AlN + Al_2O_3 as novel alternative source materials for the analysis of ^{26}Al. A negative ion cesium sputtering source at the Holifield Radioactive Ion Facility was used to measure the currents of stable atomic $^{27}Al^-$ ions as well as molecular AlX^- ions of commercially prepared target samples. Here it is shown that an AlN target produces an Al^- current seven times greater than that of an Al_2O_3 target and a molecular AlN^- current that is four times greater. The performance of AlN in producing negative ion beams is shown to be dependent on the length of exposure to moist air, which is known to cause AlN to hydrolyze to $Al(OH)_3$. A peak in performance is observed after one hour of exposure. This suggests that the formation of an intermediary product of hydrolysis, such as AlOOH, may increase the ionization efficiency of the AlN material. The AlF_3 and mixed AlN + Al_2O_3 targets did not yield prolific ion beams of Al species and therefore were not promising source materials. The applicability of using AlN as a source material for geological samples was explored by preparing quartz samples as Al_2O_3 and converting them to AlN using a carbothermal reduction technique, which involves reducing the Al_2O_3 with graphite powder at 1600°C within a nitrogen atmosphere. The material was successfully converted to AlN and yielded an atomic Al^- current higher than

the Al_2O_3 sample. However, a large excess of carbon bonded with the aluminum in the sample forming AlC_2 [aluminum carbide] and inhibited the production of AlN. While AlN represents a promising source material for the analysis of ^{26}Al, further work is needed to optimize the conversion process for geological samples.

TABLE OF CONTENTS

LIST OF TABLES

LIST OF FIGURES

1. INTRODUCTION

1.1 Origin and Production of Cosmogenic Nuclides

Primary cosmic rays are high-energy, charged particles, originating from outer space and impinge on the Earth from all directions. As seen in Figure 1, at the top of Earth's atmosphere the majority (~90%) of these high-energy particles are hydrogen atomic nuclei (protons) with a smaller component comprising of α particles (~10%) as well as electrons, positrons, heavier nuclei and other subatomic particles (~1%) (Dunai, 2010). The large range of particle energies of cosmic rays reflects the wide variety of outer space sources. Most cosmic rays are galactic cosmic rays derived from supernova explosions and have energies in the range of 100 MeV to 10 GeV (Dunai, 2010). A smaller fraction of cosmic rays are derived from solar winds that transport protons and ionized atoms to Earth. However, solar cosmic rays have a much lower energy of about 1 to 100 MeV and do not contribute significantly to nuclide production at Earth's surface (Dunai, 2010).

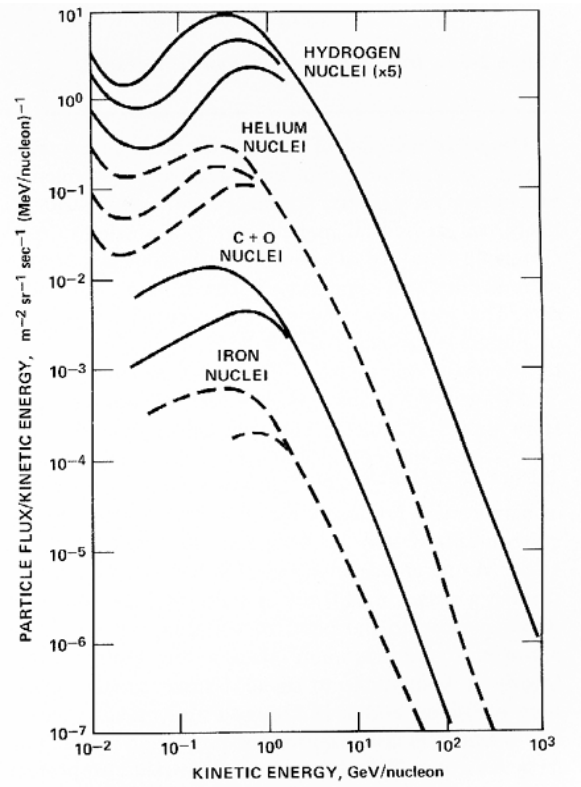

Figure 1: At the top of Earth's atmosphere the composition of primary cosmic ray flux is dominated by protons (H^+) and alpha-particles ($^4He^{2+}$). Carbon ($^{12}C^{6+}$) and oxygen ($^{16}O^{8+}$) nuclei represent the next most significant particle contributions, but total less than 1% of the proton flux. Nuclei heavier than oxygen, such as iron ($^{56}Fe^{26+}$), are less common and as such contribute even less to the total cosmic ray flux (NASA, 2010). This figure is taken from Dunai (2010).

As cosmic rays travel through Earth's atmosphere, they lose energy through the interaction with surrounding particles and therefore display an increased attenuation with greater atmospheric depth. The energy of primary cosmic rays is well in excess of the binding energy for atomic nuclei, which ranges from 7-9 MeV. Most primary cosmic rays will cause a spallation reaction (Dunai, 2010). In spallation reactions the high-energy particles strike target nuclei in the atmosphere or at the Earth's surface and sputter off protons, neutrons and even other nucleons, leaving behind lighter nuclides. In the upper atmosphere the most common target molecules are N_2 and O_2. Upon entering Earth's atmosphere primary cosmic rays collide with surrounding atoms and produce nuclear spallation reactions, which cause cascades of secondary particles such as neutrons,

protons and mesons. These secondary, lower energy cosmic ray particles can subsequently cause additional nuclear reactions as they travel through Earth's atmosphere and reach the Earth's surface.

Since neutrons do not lose energy to ionization in the same way protons do the cosmic ray flux shifts towards neutron-dominated during a nuclear cascade. The energy of the secondary neutrons is much less than the primary neutrons and at sea level the neutron energy spectrum peaks around 100 MeV (high energy neutrons), 1-10 MeV (fast neutrons) and <1 eV (thermal neutrons) (Dunai, 2010) as depicted in Figure 2. Even though the abundance of secondary neutrons decreases exponentially with increasing atmospheric depth, they are responsible for most of the reactions at Earth's surface (Dunai, 2010). Overall, secondary cosmic ray particles represent 98% of all cosmic ray associated reactions.

Most of the mesons sputtered away are pions, which decay within a couple meters to form muons (Dunai, 2010). Muons are an unstable subatomic particle of the same class as an electron (lepton) but are about 200 times heavier. They are typically produced high in the atmosphere and lose about 2 GeV to ionization leaving them with a mean energy of ~4 GeV at sea level (Dunai, 2010). Because muons react relatively weakly with matter they do not attenuate as quickly as neutrons and are the most abundant cosmic ray particle at sea level.

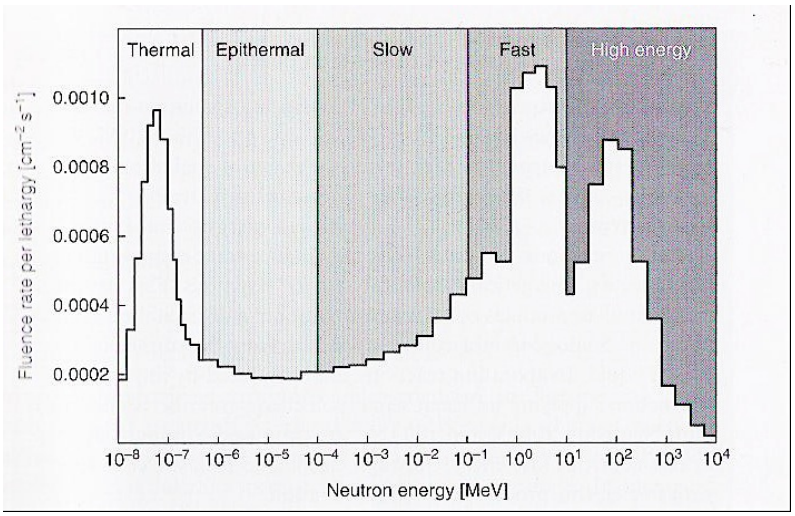

Figure 2: Neutron energy spectrum at sea level, which has peaks at 100 MeV, 1-10 MeV and <1 eV. The units of lethargy are the natural logarithm of energy. This figure is taken from Dunai (2010).

The nucleonic component dominates cosmogenic nuclide production at Earth's surface. This nucleonic component is primarily composed of secondary neutrons given that the large majority of protons are consumed in nuclear reactions during transport through the atmosphere (Lal, 1988). Much like the attenuation seen in the atmosphere, cosmic ray particles also attenuate within the solid material at Earth's surface, the main difference being that material is much denser. The fast and high-energy neutron fluxes decrease exponentially with increasing depth below the surface (Dunai, 2010). The attenuation path length, which is the distance over which the cosmic-ray flux decreases by a factor of 1/e where e is the natural log, decreases for increasing rock density. In common rock types with a density of about 2.65 g/cm^3 the attenuation path length is about 50 - 60 cm (Nishiizumi *et al.*, 1993). Once a depth of five attenuation path lengths is reached (2.5 - 3 m of rock), less than 1% of the high-energy neutron flux remains (Dunai, 2010), as depicted in Figure 3. In contrast to high-energy neutrons, muons have the ability to penetrate deeper into materials and as such the cosmogenic nuclide production at depth is dominated by muons.

Cosmogenic radionuclides are the products of interactions with primary and secondary cosmic ray particles. While most of these nuclear reactions occur in the atmosphere, a fraction of the secondary cosmic ray particles reach the Earth's surface where they are involved in nuclear reactions with exposed material. Such nuclear reactions within the Earth's crust and the crust of other planetary bodies are of particular interest to geologists because of the potential to form rare long-lived radionuclides within surface materials. Any exposed material at Earth's surface with the appropriate target elements has the potential to accumulate cosmogenic nuclides. The target nucleus and the resulting cosmogenic nuclide are usually only a few atomic mass units in difference (see Table 1).

Table 1. Cosmogenic radionuclides commonly used for dating terrestrial surface samples.

Nuclide	Half-life (years)	Target Elements	Primary Target Minerals
^{3}He	Stable	Spallation of all major elements and Li	Olivine, Pyroxene and other He-retentive minerals
^{10}Be	1.36×10^{6}	Spallation on O, Si, (Fe and Mg)	Quartz (rarely Pyroxene and Olivine)
^{14}C	5730	Spallation on Si and O	Quartz
^{21}Ne, ^{22}Ne	Stable	Spallation on Mg, Al, Si	Quartz, Pyroxene, Olivine
^{26}Al	7.05×10^{5}	Spallation on Si	Quartz
^{36}Cl	3.01×10^{5}	Spallation of K, Ca, Cl, (Fe and Ti)	Carbonates, Feldspars, Whole Rock
^{36}Ar, ^{38}Ar	Stable	Spallation of K, Ca	Feldspar, Amphibole, Pyroxene
^{41}Ca	1.04×10^{5}	Fe, Ti, (Ca)	Fe-Ti Oxides
^{53}Mn	3.7×10^{6}	Fe, Mn	Fe-bearing minerals

Source: Revised from T. Dunai "Cosmogenic Nuclides: Principles, Concepts and Applications in Earth Surface Sciences" Cambridge University Press (2010)

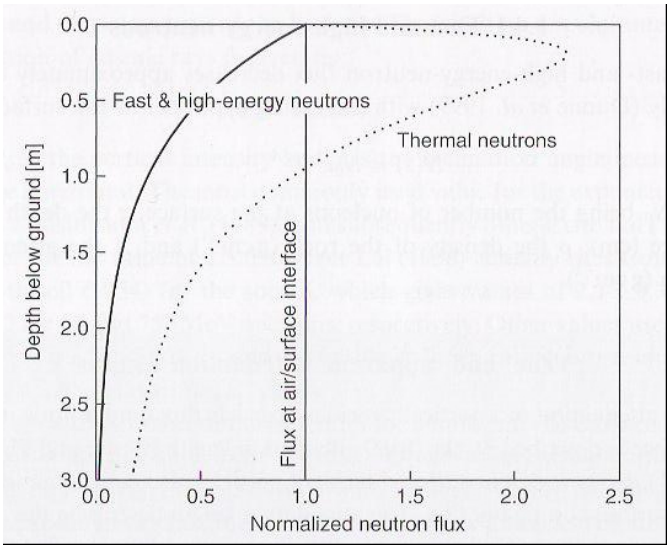

Figure 3: Neutron flux below Earth's surface. The fast and high-energy neutron flux decreases exponentially with depth beneath Earth's surface. The thermal neutrons that are created near the surface can leak back into the atmosphere, hence the humped profile. This figure is taken from Dunai (2010).

1.2 Applications of ^{26}Al and ^{10}Be in Earth Sciences

Following production, cosmogenic radionuclides begin to decay. After an exposure time equivalent to 2-3 times the radionuclide's half-life the rate of radioactive decay and the rate of cosmogenic production become similar and the concentration approaches equilibrium, as shown in Figure 4 (Dunai, 2010). The ideal environment for measuring the exposure age of a geological feature would be within a fully exposed non-eroding surface. For a non-eroding surface the cosmic ray accumulation increases with exposure time until equilibrium is reached. The total cosmogenic radionuclide concentration, C_{total}, at a subsurface depth, z, is described by Equation 1.

$$C_{total}(t,z) = C_{inh}(z)e^{-t\lambda} + \sum_i \frac{P_i(z)}{\lambda}(1 - e^{-t\lambda}) \qquad (1)$$

Where C_{inh} is the inherent nuclide present before exposure, subscript *i* denotes the different reaction pathways, λ denotes the decay constant and t is time. For cases where C_{inh} and the production rate (P) is known, the cosmogenic nuclide concentration can be used to determine the exposure age (T_{exp}) for surface samples using Equation 2.

$$T_{exp} = -\frac{1}{\lambda}\ln\left(1 - \frac{C_{inh}\lambda}{\sum_i P_i(z) * e^{-\rho z/\Lambda_i}}\right) \qquad (2)$$

Where ρ is the density of the sample's overburden and Λ is the attenuation factor. With a half-life of 0.7 million years (Gosse, 2007), ^{26}Al is used for dating exposures with absolute ages between 10^3 and 10^6 years old (Schaefer and Lifton, 2007). Once a system reaches equilibrium only a minimum exposure age can be given. For surfaces that have experienced erosion Equations 1 and 2 become more complicated. The production rate (P_i) by reaction pathway *i*, is generally dominated by neutron-induced spallation and neutron capture reactions within the top meter of exposed material. As previously discussed, at depth the production rate is mainly a function of muon-induced reactions. As seen in Figure 3 the spallation-induced reactions resulting from interactions with fast and high-energy neutrons decreases exponentially with depth. Therefore, the production rate can be modeled using a simple exponential law as shown in Equation 3.

$$P = P_0 e^{-\rho z/\Lambda_i} \qquad (3)$$

The applications of cosmogenic nuclides span across numerous fields of science. The field of cosmogenic nuclides is relatively young, approximately 25 years old, and the study of cosmogenic nuclides within Earth Sciences is less mature still. As analytical methods for their measurements are improving new applications for the use of cosmogenic nuclides are being identified. For a cosmogenic nuclide to be useful for Earth

Sciences it has to meet the following necessary criteria. First, the nuclide must be naturally rare in geological material, making it easier to resolve the relatively few atoms produced from the natural background concentration. In addition, it is important that naturally occurring interferences can be resolved analytically. Secondly, the nuclide must be either stable or a long-lived radioactive nuclide with a half-life that is the same order as or greater than the timescale of the geological process. Thirdly, there must be a reasonable understanding of the mechanisms required for the production of the nuclide, including knowledge of the different target elements and nuclide production contributions from spallation, thermal neutron and muon reactions. Finally, the nuclide of interest must be produced and retained within reasonably common minerals and, perhaps most importantly, the analytical effort involved in preparing and measuring the nuclide must be feasible.

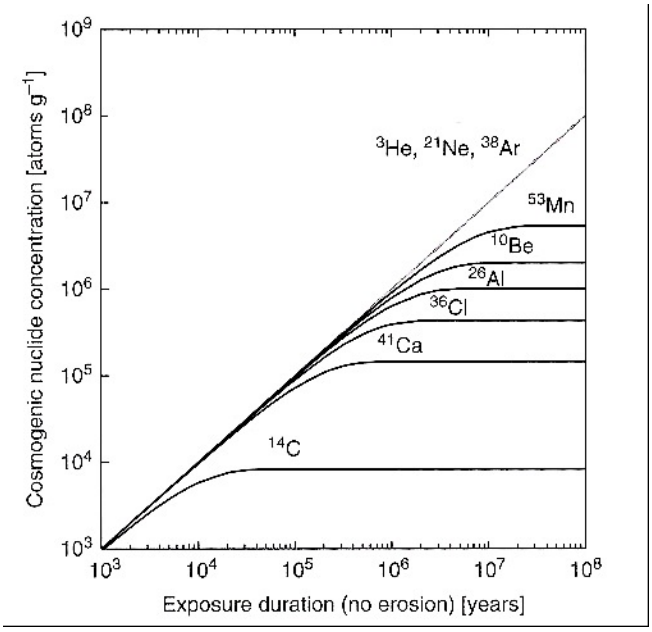

Figure 4: Accumulation of cosmogenic nuclides in a non-eroding surface. Once sufficient time is reached the production rate and decay rate of the radionuclide reache equilibrium. This figure is taken from Dunai (2010).

Cosmogenic radionuclides are commonly used as a tool to provide erosion rates. As previously mentioned the production rates for cosmogenic radionuclides decrease exponentially beneath Earth's surface (Faure & Mensing, 2005). The loss of radionuclides at Earth's surface due to erosion gives the impression that the radionuclides are decaying faster than expected. The concept of using cosmogenic nuclides to give an erosion rate is based on the fact that mineral grains in transit from their shielded subsurface position will accumulate cosmogenic nuclides at a rate that is proportional to the transit time to the surface. For surfaces that erode sufficiently slowly so that the radionuclides produced at greater depths by negative muon reactions have decayed before they reach the surface (<10 Ma^{-1} for ^{10}Be), the erosion rate (ε) can be calculated using Equation 4 (Dunai, 2010).

$$\varepsilon = \left(\frac{P(0)}{C(0)} - \lambda\right)\frac{\Lambda}{\rho} \qquad (4)$$

Here, if the concentration C(0) of a spallogenic cosmogenic nuclide with decay constant λ at the surface can be measured, and the production rate at the surface P(0), the density of the eroding material ρ, and the attenuation coefficient Λ for the nucleonic component of the cosmogenic radiation is known, the steady-state erosion rate ε can be determined.

The use of a single nuclide such as ^{26}Al or ^{10}Be individually is not in itself such a useful tool because it could only be applied to geological issues in which there is only one unknown variable. For example, a single nuclide would prove to be useful in a situation where the erosion of the surface is negligible, or the surface erosion or exposure time is known through another mechanism or there is evidence that the site has reached

an erosional equilibrium (Li & Harbor, 2009). However, in many cases there are at least two unknowns, such as erosion rate and exposure age. By analyzing two nuclides within the same sample more complicated scenarios involving two unknowns can be solved and fewer assumptions regarding a sampling site need to be made.

Within Earth sciences the $^{26}Al/^{10}Be$ ratio is the most commonly used pairing of isotopes for several reasons. First of all, both nuclides are produced through similar nuclear reactions. Both Al and Be are deposited by meteoric precipitation and dry fallout from the atmosphere as well as being produced *in situ* within exposed quartz. Both ^{26}Al and ^{10}Be have longer half-lives compared to other cosmogenic nuclides, 0.705×10^6 years and 1.5×10^6 years respectively, and so will take longer to reach a state of equilibrium within exposed material (Faure & Mensing, 2005). In addition, the ions of both elements are strongly sorbed to the charged sites on the surface of solid materials and remain in suspension in seawater so their production and accumulation within material is proportional to one another other. These properties, alongside the similar behavior and occurrences of cosmogenic ^{10}Be and ^{26}Al in various reservoirs, has supported the following common lines of research within the earth sciences; geochronology of deep sea sediments and continental ice sheets, cosmic ray exposure dating as well as burial ages of rock surfaces, measurements of surface erosion rates and the measurement of terrestrial ages and break off ages for stony meteorites.

In 1984, shortly after the discovery of ^{26}Al within natural samples (Nishiizumi *et al.*, 1986), the prime motivation for developing a technique capable of measuring ^{26}Al at naturally occurring levels was so a $^{26}Al/^{10}Be$ chronology technique could be established. The idea behind the $^{26}Al/^{10}Be$ chronology is that once a material becomes exposed to the

atmosphere it begins to accumulate cosmogenic nuclides. By measuring the amount of accumulated cosmogenic nuclide within geological material it is possible to date any fresh surface that is stable and continuously exposed to cosmic rays. These exposed surfaces can be geological deposits such as moraines, fluvial deposits, gravity and lava flows, or erosional features carved by glaciers, fluvial deposits, meteoritic impacts, gravity and eolian forces or features created by endogenic forces, such as fault scarps (Dunai, 2010).

The most common use of the $^{26}Al/^{10}Be$ pair together is to evaluate exposure and burial ages, as well as the histories and erosion styles from a plot of the nuclide ratio. For this, the ratio of $^{26}Al/^{10}Be$ is plotted against the log of ^{10}Be and the differences in half-lives of these nuclides creates an upper curve, which represents the expected values for the accumulation of the nuclides under zero erosion, as shown in Figure 5. Samples that experience erosion will plot and form a curve beneath the zero erosion curve and their deviation from the curve can be used to give an erosion rate. In contrast, samples that become buried will cease to accumulate ^{10}Be and will plot beneath the zero erosion curve, which can therefore be used to give an age of burial. This is also shown for samples 1 and 2 in Figure 5.

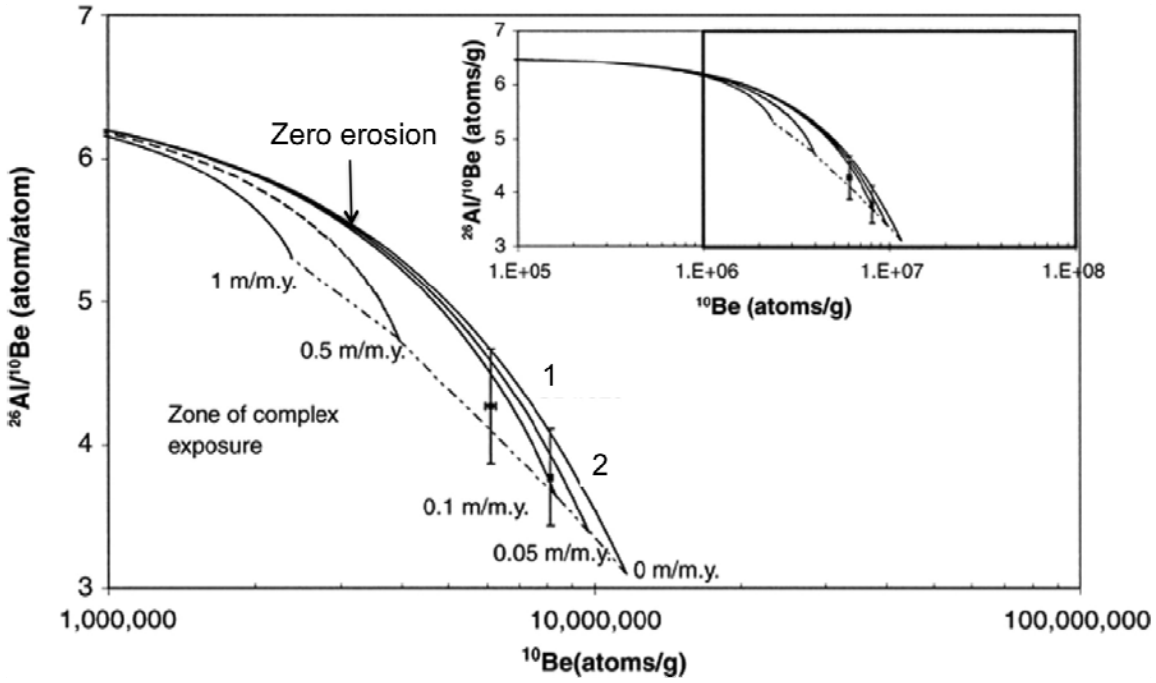

Figure 5: The $^{26}Al/^{10}Be$ ratio plotted against the log of ^{10}Be concentration. This figure has been revised from Fogwill *et al.* (2004).

While numerous studies have utilized the $^{26}Al/^{10}Be$ technique for providing exposure ages of geologic samples, there are several assumptions that limit the accuracy of exposure ages derived from ^{10}Be or ^{26}Al. First of all it is assumed that during exposure the rate of *in situ* production is constant, the sample has been continuously irradiated without interruptions and the rate of deposition of the nuclide from all sources has remained constant. This is likely an over simplification in natural systems where the accumulation of a nuclide may be interrupted by intervals of non-deposition or erosion caused by physical processes such as bioturbation, turbidity currents, landslides or the movement of glaciers (Balco *et al.*, 2008). Secondly, it is assumed that the material was not temporarily shielded from cosmic rays, and hence the production of cosmogenic nuclides, during the history of the site. A correction to the cosmogenic signature should be applied if shielding of the sample site is apparent during sample collection (e.g. when

samples are collected on the side of a slope or when physical objects block the exposure to the atmosphere). Thirdly, it is assumed that all initial ^{10}Be and ^{26}Al present in the sample before the period of interest has decayed away and that the activity of the radionuclides changed following this period only as a result of decay. Finally, it is assumed that the activities of ^{10}Be and ^{26}Al in the atmosphere are in steady-state equilibrium maintained by production rate and removal from the atmosphere.

Another common use of ^{26}Al/^{10}Be chronology is the dating of the advancement and retreat of large ice masses, which provides dates for short-lived periods of glaciation as well as ice ages. Once ice begins to accumulate the underlying rock surfaces become shielded and any new cosmogenic radionuclide production is on the surface of newly formed ice. The material that is no longer exposed to the atmosphere will therefore no longer accumulate cosmogenic radionuclides.

1.3 Cosmogenic Production of *In Situ* ^{26}Al in Quartz

In situ nuclear spallation reactions in rocks with incoming neutrons and muons produce cosmogenic radionuclides, with some of the more common ones being beryllium (^{10}Be), carbon (^{14}C), aluminum (^{26}Al), chlorine (^{36}Cl) and argon (^{39}Ar). While each of these cosmogenic isotopes have a range of practical applications, this thesis will primarily focus on the production and accumulation of cosmogenic aluminum (^{26}Al) in geological materials. Cosmogenic beryllium will provide a secondary focus given that both ^{10}Be and ^{26}Al are commonly associated with the key target mineral investigated in this thesis i.e. quartz.

The production and yield of cosmogenic nuclides within an exposed surface depends on the chemical composition of the target rocks. The target elements from which ^{10}Be and ^{26}Al are produced are primary rock forming elements such as O, Mg, Al, Si and Fe. Cosmogenic Al is most commonly produced through spallation reactions involving ^{27}Al and Si, although an additional contribution may derive from protons from cosmic ray cascades interacting with ^{26}Mg (Faure and Mensing, 2005). In non-silicate minerals the production of ^{26}Al from P, S, Cl, K and Ca can become important and measurements can become complicated when there are numerous mineral sources of a cosmogenic nuclide. However, many of the variables associated with alternative sources of aluminum can be avoided by using quartz as a target mineral.

Quartz is an attractive target mineral for the measurement of ^{26}Al/^{10}Be ratios for several reasons. Quartz is a very common mineral within silicate rocks and as such is relatively abundant in most exposed rock surfaces. In addition, quartz has been shown to be a resistant mineral to chemical and mechanical weathering, allowing for the accumulation of cosmogenic nuclides within the exposed surface. Given these properties, one of the unique applications of ^{26}Al analysis in quartz is as a proxy for tracing erosion and cosmogenic nuclide production rates. Another beneficial property of quartz is that the mineral formula SiO_2 contains two of the most important target minerals, O and Si, for the production of cosmogenic beryllium and aluminum but effectively excludes all other elements. The majority of ^{10}Be is produced through the spallation of ^{16}O and ^{28}Si, while ^{26}Al is primarily produced through the spallation of ^{28}Si. Therefore, both nuclides can be extracted from the same sample and so it can be assumed that production rates will be proportional to one another. Lastly, quartz is relatively easy to process in the laboratory

and can be concentrated by conventional mineral separation techniques to produce high-purity samples. This preparation process allows for Al and Be to be extracted congruently.

Aluminum is a major element present in many minerals and high levels of native ^{27}Al will make the $^{26}Al/^{27}Al$ ratio increasingly low and difficult to measure. A useful property of using *in situ* quartz as a target mineral is that the native stable nuclides, ^{9}Be and ^{27}Al, are present in negligible amounts within most quartz samples. Also worth noting is that *in situ* samples can have a small contribution from meteoric ^{26}Al produced through the spallation of ^{40}Ar and transported to Earth's surface through dry fallout and precipitation. However, typically contributions of meteoric ^{26}Al are considered to be negligible as there are not many appropriate target elements for ^{26}Al within the atmosphere. Furthermore, the rigorous cleaning procedure required for ^{10}Be during sample preparation should remove any meteoric ^{26}Al that may be present. Currently, only low-aluminum quartz is being used for *in situ* applications of ^{26}Al.

Within exposed quartz only particles with sufficient kinetic energy, such as secondary neutrons and to a lesser extent negative muons, can drive the *in situ* nuclear reactions that form ^{26}Al and ^{10}Be (Hunt, 2008). Secondary neutrons have the appropriate kinetic energy to cause spallation reactions, and negative muons have the appropriate kinetic energy to cause negative muon capture reactions with the silicon and oxygen atoms of the quartz lattice. However, the cross-section for reactions involving neutrons is much larger than that for negative muon capture reactions. Therefore, spallation reactions involving high-energy neutrons are the primary source for cosmogenic nuclide production (Nishiizumi *et al.*, 1993). Almost all of the spallation reactions by secondary

neutrons (see Table 2) occur within the top 2 m of exposed material. The predominant reaction pathways that proceed through spallation reactions with secondary neutrons and the reaction pathways that proceed through negative muon capture with negative muons are given in Table 2 for ^{10}Be and ^{26}Al (Dunai, 2010). Negative muon capture reactions account for only 2.0% and 2.1% of the ^{10}Be and ^{26}Al respectively produced at sea level (Dunai, 2010). However, because secondary neutrons interact with surrounding atoms to a larger degree at greater depths below the surface, the secondary neutron flux attenuates and muon reactions become more important. In total, muon reactions account for 4.5% of all ^{26}Al production in quartz and this value increases with increasing depth (Heisinger *et al.*, 2002). On average, at sea level, the total production rate of cosmogenic ^{26}Al in quartz is about 30 atoms/g/a (Balco *et al.*, 2008).

Table 2: The reaction pathways that process through both spallation reactions and negative muon capture for the target elements in quartz (O and Si) for both ^{10}Be and ^{26}Al.

Radionuclide	**Target Element**	**Spallation Reactions**	**Negative Muon Capture Reactions**
^{10}Be	^{16}O	^{16}O(n, ^{3}Heα)^{10}Be or ^{16}O(n,4p3n)^{10}Be	^{16}O(μ^-,αpn)^{10}Be
^{10}Be	^{28}Si	^{28}Si(n,6p3n)2^{10}Be	^{28}Si(μ^-,x)^{10}Be
^{26}Al	^{28}Si	^{28}Si(n,2np)^{26}Al	^{28}Si(μ^-,2n)^{26}Al

1.4 Synergy With Other Fields

Some of the earliest applications of ^{26}Al arose within the fields of biology and pharmacy. After Accelerator Mass Spectrometry (AMS) techniques were developed for ^{26}Al in the early 1990's the use of ^{26}Al as a tracer arose within the biomedical field. It

was determined that ^{26}Al could be used as a tracer for the following pathogeneses; Alzheimer's disease, renal failures, anemia, metabolism studies and dialysis encephalopathy (Day *et al.*, 1991 and Barker & Day, 1990). In the late 1980's it became recognized that aluminum was a generally toxic element and the accumulation within the body was implicated as the cause to well-recognized serious medical conditions, such as Alzheimer's and renal disease (Day, 1991). The use of ^{26}Al as an isotopic tracer coupled with AMS measurements quickly became appealing because of the isotope's negligible natural abundance and the low radiological hazard resulting from the low detection limit. To date new applications continue to open up for ^{26}Al as an isotopic tracer for aluminum incorporation and uptake into biological tissues, in particular the brain (Ajormand, 2010).

In addition to the fields of geology and medicine, ^{26}Al has many astrophysical applications some of which are currently being explored at the Holifield Radioactive Ion Beam Facility (HRIBF) at Oak Ridge National Laboratory (ORNL). The system used for AMS at HRIBF allows for the tandem accelerator to provide acceleration for radioactive ion beams (RIBs) produced from the RIB injector. One line of interdisciplinary research involving the production of ^{26}Al radioactive ion beams is aimed at helping to understand and calibrate observational data from NASA's Compton Gamma-Ray Observatory. NASA has identified centers of intense ^{26}Al radiation within the galaxy. Proposed research at HRIBF is focused on constraining the rates of the astrophysical ^{25,26} Al(p,γ)^{26,27} Si reactions, which can be made by scattering a low-energy ^{26}Al ion beam on protons and observing the resonances in ^{27}Si (Beene, 2011). These constraints directly affect the predictions made for ^{26}Al nucleosynthesis in astrophysical events and could lead to an increased destruction of ^{26}Al than is currently predicted.

1.5 Accelerator Mass Spectrometry (AMS)

The field of Accelerator Mass Spectrometry can be traced back to 1939 when Luis Alvarez and Robert Cornog at the University of California, Berkeley first used a cyclotron, which is a type of accelerator, as a mass spectrometer to demonstrate that ^{3}He was stable (Alvarez and Cornog, 1939). Meanwhile, in the late 1940's it was discovered that radiocarbon was produced through interactions with cosmic rays and henceforth it was developed into a widely used tool for the dating of organic matter (Arnold & Libby, 1949). Advantage was taken of the relatively short half-life of ^{14}C (5730 years) and initially decay counting techniques were used (Faure & Mensing, 2005). It wasn't until 1977 when Richard Muller, a student of Luis Alvarez, recognized that modern accelerators could accelerate radioactive particles to an energy high enough such that the background interferences could be separated out and low-level isotopes could be detected using particle identification techniques (Tuniz *et al.*, 1998). Richard Muller then went on to demonstrate how accelerators, could be used for detection of isotopes such as; radiocarbon (^{14}C), tritium (H^{3}) and beryllium (^{10}Be). Richard Muller was also responsible for accomplishing the first successful radioisotope date experimentally obtained using tritium (^{3}H) (Tuniz *et al.*, 1998). It wasn't long afterwards that the successful detection of ^{10}Be, an isotope now widely used in geology, was made. From these discoveries emerged the field of AMS as used to measure cosmogenic isotopes within natural samples. Simultaneously, work done with electrostatic tandem accelerators by two groups at Rochester and McMaster led to the modern era of AMS (Nelson *et al.*, 1977 and Bennett

et al., 1977). Nowadays the vast majority of the AMS machines are electrostatic accelerators.

AMS is an ultrasensitive tool that takes conventional mass spectrometry techniques and pairs them with a particle accelerator. The high acceleration voltages permit an excellent discrimination against isobaric, isotopic and molecular interferences (Hellborg & Skog, 2008). Isotopic ratios as low as 10^{-16} are achievable and ratios of 10^{-15} are commonly measured (Kutschera, 2005). In addition, with AMS the sample size is reduced from tens of grams to milligrams because of the higher efficiency of direct atom counting. The AMS techniques superseded the older decay counting techniques and have opened up the field of cosmogenic isotopes within the geological community as it allows for measurements of nuclide concentrations that were otherwise impossible to detect.

The earliest adoption of cosmogenic tools arose within extraterrestrial material due to the higher production rates, which were orders of magnitude higher than at the Earth's surface. The meteoritic, lunar, atmospheric and oceanic scientific communities have widely used cosmogenic nuclides since the 1960's (Weiler, 2002 and Lal, 1998). As depicted in Figure 6 the concentrations of cosmogenic radionuclides at the Earth's surface are relatively low and this has delayed their use for geochronology because the sensitivity of low-level radiation detectors was limited (Faure & Mensing, 2005). In the mid 1980's ^{36}Cl became the first *in situ*-produced nuclide to be detected in rocks and its discovery coincided with the development of the methodological principles for exposure dating (Davis & Schaeffer, 1955). The discovery of other *in situ* cosmogenic nuclides were discovered in late 1986 with reports of ^{3}He, ^{21}Ne, ^{22}Ne, ^{10}Be, ^{26}Al and ^{36}Cl

emerging as high profile papers in rapid succession (Craig & Poreda, 1986, Kurz, 1986, Nishiizumi *et al.*, 1986, Phillips *et al.*, 1986 and Lal *et al.*, 1987).

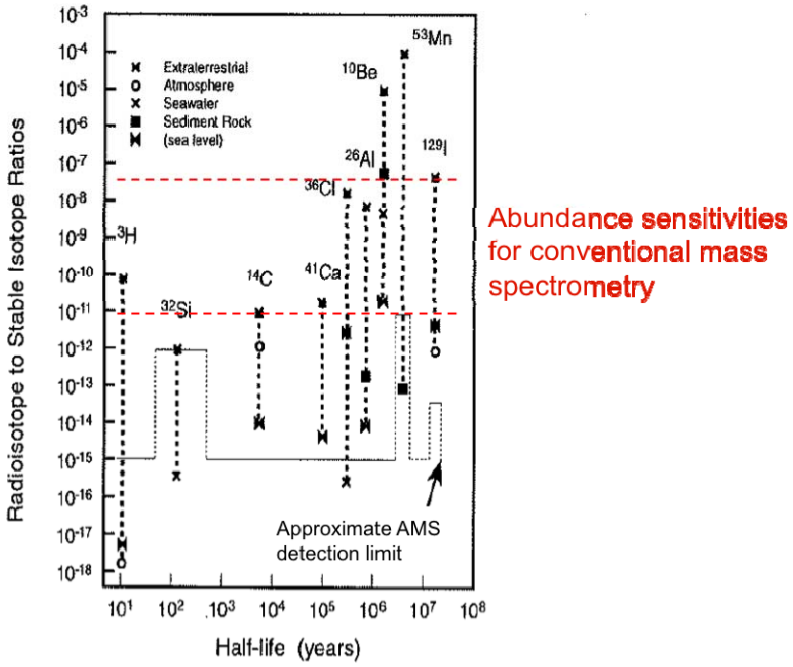

Figure 6: This graph shows the range of cosmogenic isotopic ratios within natural samples along with the AMS detection limits as compared to the abundance sensitivities for conventional mass spectrometry. The ranges for ratios of radioisotope to stable isotope for natural samples are shown by the vertical thick black dashed line for each cosmogenic nuclide. The detection limits for the AMS measurements for each of the cosmogenic nuclides are shown by the thin black dashed lines. The abundance sensitivities for conventional mass spectrometry are approximated by the dashed horizontal red lines. This figure is revised from G. Aardsma (1984).

The main advantages of AMS over conventional mass spectrometers allow for the elimination of molecular interference, determination of the total ion energy E, by ionization methods and the determination of the atomic number Z of an ion through differential energy loss in the final detector (Hellborg & Skog, 2008). The use of a tandem accelerator can have even greater advantages because of the use of negative ions as opposed to positive ions used in conventional mass spectrometry. For cosmogenic radionuclide studies some of the more important inferring isobars do not form negative

ions (i.e. ^{14}N in the case of ^{14}C and ^{26}Mg in the case of ^{26}Al) (Middleton, 1990). As well, doubly negative ions are not observed experimentally so any ambiguities in M/Q (mass/charge) and E/Q (energy/charge) that could arise from having a charge greater than one do not exist (Middleton, 1990). All of these advantages combine together to give mass abundance sensitivities, which is the ratio of the peak at mass "M" to the "M±1" peak intensity, at least five orders of magnitude better than a conventional mass spectrometer (Tuniz, 1998). As shown in Figure 6 the sensitivities for conventional mass spectrometry do not encompass a large range of the natural abundances for many of the cosmogenic nuclides. The key differences between a conventional mass spectrometry system and an accelerator mass spectrometry system can be viewed in Figure 7.

The AMS measurement technique for ^{26}Al within geological samples involves mixing a small amount (few mg) of prepared material with a metal matrix powder. The mixture is then pressed into a small (typically copper or stainless steel) metal target holder called a cathode (see Figure 8). The sample is then loaded into the negative ion cesium-sputtering source where a beam of negative ions is formed from the sample material. The beam is then accelerated from ground potential, focused and passed through a magnetic mass analyzer. The selected ions are then injected into a particle accelerator where they accelerate towards a high positive voltage. At the acceleration terminal electrons are stripped from the ions as they pass through a foil or gas stripper. Whereas negative ions can only be singularly charged, multiple electrons can be removed from the ions, which imparts a multiple positive charge on the ions and has the effect of dissociating any molecular ions. The now positive ions are repelled from the accelerator terminal at a much higher velocity. Now at high voltage the ion beam passes through a

second magnetic mass analyzer and then an electrostatic mass analyzer. The ions are then individually counted using particle detectors, which are based on measuring the residual energy after identification as having the correct atomic number and mass.

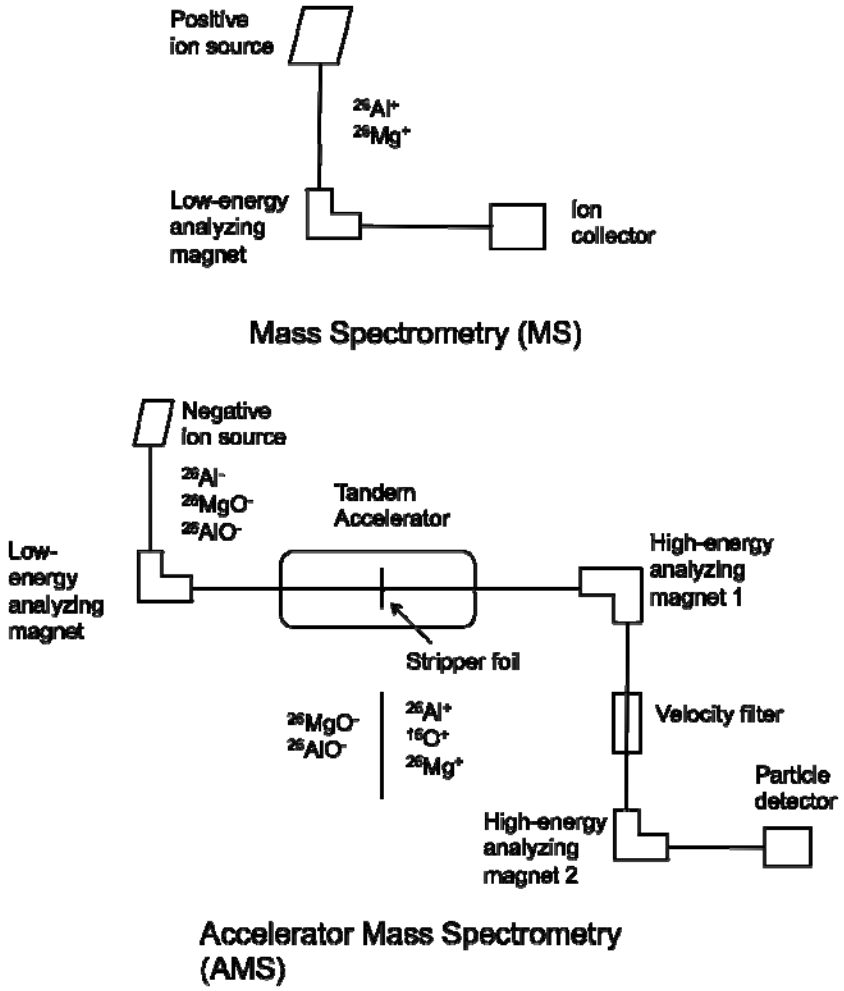

Figure 7: Simplified schematic of an Accelerator Mass Spectrometry system versus a conventional Mass Spectrometry system. This figure has been revised from Hellborg and Skog (2008).

Figure 8: Photo of a copper cathode used for the stable injector. Cathode is packed with an Al_2O_3 and Ag mixture so that the powder is flush with the surface.

Even though the arrival of the AMS systems allowed for the counting of single ions, a huge advantage to ^{26}Al measurements, the technique is not without limitations. The need for a particle accelerator greatly increases the cost of acquiring an AMS machine as well as the increased electrical costs of running the machine. Generally these instruments are expensive to construct and maintain and until more recently were limited to all but the highest funded research facilities. The current trend in AMS systems is moving towards smaller machines, such as the tabletop 0.25MV AMS system at Eidgenössische Technische Hochschule (ETH) in Zurich (Jull & Burr, 2006). However, presently these smaller systems are limited mostly to ^{14}C measurements, which are much more straightforward and do not require the high voltages needed for ^{26}Al analysis.

1.6 AMS Measurements of ^{26}Al

The implications associated with the discovery of ^{26}Al in natural samples were slightly delayed due to the extremely low decay rates of ^{26}Al. However, soon afterwards

in the 1980's the obstacles associated with ^{26}Al measurements were overcome by the use of electrostatic accelerators to count individual ions with unparalleled sensitivity (Raisbeck *et al.*, 1979). A traditional analysis of ^{26}Al using β-decay counting techniques used to require ~1x10^{6} kg of sample (Hunt, 2008). Compare that to an AMS analysis of the same sample material, which requires only ~30 g of sample prior to sample preparation (Chmiel, 2012).

The AMS measurement techniques for ^{26}Al have improved since the discovery of the nuclide, however, they are still much more difficult than those of ^{10}Be. A couple reasons behind the difficulty of the ^{26}Al measurement are simply due to the natural abundances of aluminum in the environment. The lower production rate of ^{26}Al in the atmosphere due to fewer target elements compared to ^{10}Be (argon~0.93% compared to nitrogen~78% and oxygen ~21%) account for a lower meteoric accumulation within materials at the Earth's surface (Aardsma, 1984). As well there is a larger natural abundance of stable aluminum (81.3x10^{3} ppm) compared to stable Be (6 ppm) in the Earth's crust. The ^{26}Al can be diluted by the stable ^{27}Al in geological samples (Aardsma, 1984). In addition, the natural abundances of ^{26}Al are so low (modern ocean sediment ^{26}Al/^{27}Al ~ 10^{-14}) that AMS is the only technique that allows routine measurements within natural samples (Aardsma, 1984).

Experimentally ^{26}Al is more difficult to measure than ^{10}Be because of its chemical properties. In fact, when using a conventional mass spectrometer the ^{26}Al signal is completely overwhelmed by ^{26}Mg and other elements with atomic mass unit (amu) 26. Magnesium is a fairly common element within geological samples and so the ^{26}Mg isobar poses a large threat to ^{26}Al measurements. Additionally ^{26}Al decays by beta-plus or

electron capture resulting in the stable daughter nuclide of ^{26}Mg. When using AMS techniques and transmitting a beam of negative atomic aluminum the isobar ^{26}Mg is removed as magnesium does not form negative ions. Magnesium does, however, form molecular negative ions and so, typically, even if a molecular species of Al forms a more prolific beam, measurements, for most systems, must be made using atomic Al. The conundrum lies in the fact that geological samples must be prepared as an aluminum oxide, which is impractical to measure due to the prevalence of magnesium oxide impurities, a molecular isobar. So even though the atomic ion is formed in relatively low yields it is Al^- that must be extracted from the ion source, mass separated and injected into the accelerator so that there are no large isobaric interferences from ^{26}Mg. Using this method of creating an Al_2O_3 cathode AMS ion beam currents are typically around a few μA (Flarend, 2004). A few μA of beam current for AMS measurements is relatively low and insufficient and therefore continues to be a problem when attempting to measure ^{26}Al within samples. To date the utility of cosmogenic ^{26}Al has remained limited within the cosmogenic isotope community.

1.7 Negative Ion Beam Production

The yield of negative sputtered ions greatly depends on a number of factors inherent to the source material used. One of the factors affecting the yield of negative ions from a source material is the electron affinity of the element of interest. Higher yields of negative ions are observed for elements with a higher electron affinity and lower yields are observed for elements with a low electron affinity. If an atomic ion yield is low for an element of interest then the selection of one of the possible negative molecular ions

(i.e. oxides, hydrides, nitrides, carbides etc.) may be preferred. Another factor that can affect the negative ion yield is the physical conditions affecting the surface atoms of the sample. Physical conditions such as the presence of a thin Cs layer and a secondary electron cloud at the surface of the sample will enhance the probability that the collision by Cs^+ ions will sputter off negative ions. As well, the nature of the bonding of the sample material can affect how easily the material is sputtered away. Lastly, because the sputtering process, which is caused by the collision of Cs^+ ions with the sample atoms, is a kinematic mechanism, heavier elements will have a harder time being sputtered away. Lighter elements will have a higher yield of sputtered ions.

Due to its versatility the cesium sputter ion source is currently the source of choice for most AMS experiments (Pegg, 2004). It is especially suited to produce beams of materials that are resistant to negative ion formation. Nowadays most commercial cesium sputter ion sources are based on the designs created by Middleton (Middleton, 1990). This type of source has been used to generate a wide variety of atomic, molecular and clustered negative ions (Pegg, 2004). Negative ions are formed in exoergic attachment processes in which an electron attaches itself to a neutral atom or molecule. If the incident electron has kinetic energy, E, prior to the collision and the electron affinity of the atom is E_a then an amount of energy $E + E_a$ is released upon capture and is dissipated in some manner (Pegg, 2004).

The process of forming a negative ion beam is often referred to as "ion sourcery" as there are many factors involved and the mechanisms involved are complicated and very sensitive to changing parameters. For example, the negative ion currents and ionization efficiencies are very dependent upon the creation of a deep sputter crater and

the formation of an intense plasma ball (Middleton, 1990). Ion source operations can also vary substantially and the source must be tuned to maximize the negative ion production by changing parameters such as cesium oven temperature, sputtering voltage, beam focus on the cathode material, aperture diameter, etc.

The production of negative ion beams is a complex process and there is an entire field dedicated to examining the production and behavior of negative ions, however, a more in depth discussion is outside the scope of this thesis. Papers by Belchenko (1993), Yu (1978) and Middleton (1977 and 1990) can provide a more detailed description on the production of negative ions within cesium sputtering sources.

1.8 AMS at Holifield Radioactive Ion Beam Facility (HRIBF)

Nowadays many of the AMS systems used to make routine measurements are smaller machines including tandem accelerators with terminal voltages are less than 3MV (Galindo-Uribarri *et al.*, 2007). Some of the larger tandem accelerators that are being used for AMS research include HVEC's (High Voltage Engineering Corporation) FN (10-MV) and MP (13-MV) and NEC's (National Electrostatic Corporation) 15-MV unit (Galindo-Uribarri *et al.*, 2007). The tandem accelerator at HRIBF is unique for AMS in the sense that it is 25 MV machine and capable at operating at the highest terminal potential in the world, which makes it an excellent system to explore the potential for AMS measurements of cosmogenic nuclides. The tandem accelerator is a model 25 URC accelerator built to ORNL specifications by NEC. The high-voltage generator is located inside a 100-ft high, 33-ft diameter pressure vessel which has a built in folded geometry configuration (Beene, 2011). The folded geometry of the accelerator allows for both low-

energy and a high-energy acceleration tubes to be contained within the same column structure with a 180-degree mass-analyzing magnet at the terminal of the column. The mass-analyzing magnet at the high-voltage terminal provides the reversal of ion direction from the low-energy and high-energy acceleration tubes (see Figure 9).

The beam is accelerated through the system by a series of attractions and repulsions. A charged repeller plate attracts anions and repels cations, accelerating them towards other electrodes. As the beam of negative ions travels through the system it experiences a combination of electric and magnetic fields that act as charge and mass separators to reject unwanted ions and purify the beam. The first mass separation occurs as the beam leaves the injection beamline and the ions are separated out using a mass-analyzing magnet. As the ions travel through the magnetic field the magnetic force serves to move the particles in a circular path. The radius (r) of the circular path is proportional to the velocity of the particle (see Equation 5).

$$r = mV/qB \qquad (5)$$

The charge of the particle (q) is always -1, the velocity (V) of the particle is known and so by changing the magnetic field the trajectory can be changed for the mass of interest (m) allowing it to pass through slits in the electrodes. The lighter ions are deflected more than heavier ones and so the machine can be tuned to preferentially allow ions of a known mass to pass through the electrode slits and continue through the system.

The aluminum isotope separation techniques are applied at both low energy (prior to acceleration) and at high energy (post acceleration). A huge advantage of the set up at the HRIBF is the extremely high operating voltages. Because of the dependence on energy the differences between the radii of curvature for ions of varying masses will be

much greater, allowing for a more effective ion separation. As well the 180° magnet at the terminal allows for excellent mass separation as the ions are deflected twice as much as a 90° magnet.

As the beam of negative ions is accelerated it interacts with a 2-3μg/cm^2 carbon stripper foil at the terminal (see Figure 9). Stripping removes a number of the electrons from the ions, which results in the destruction of molecules due to Coulomb forces between the nuclei of constituent atoms. At charge state >2+ molecular ions are essentially absent (Masarik & Beer, 1999). As aluminum ions interact with the foil stripper a variable number of electrons are removed giving rise to a charge-state distribution. Aluminum will exhibit a different charge state distribution for different energy levels. This charge-state distribution for aluminum is well documented and is taken into consideration when counting ions post-acceleration. Although charge-state distributions for molecular ion species is not as well known.

A beam of individual, positive, multiply-charged ions is formed ahead of the 180° magnet at the terminal of the accelerator. The location of the stripper foil offers excellent charge-state separation as the ions pass through the magnetic field. The newly created positive ions are now repelled by the positive terminal and are accelerated to a much larger degree back down the accelerator. The extent to which the ions are accelerated down is dependent on the charge of the ions and those with higher positive charges will be accelerated to a larger degree. The energy at which the anions enter the tandem accelerator is given in Equation 6 and the energy at which the ions leave the accelerator is given in Equation 7.

$$E_i = V_i e \quad (6)$$

$$E = E_i + (q+1)eV_t \quad (7)$$

Where V_i and V_t are injection and terminal voltages respectively, q is the ion charge and e is the elementary charge (Argento, 2010). The higher terminal voltage allows for higher charge-states and therefore energy has a greater than linear dependence on the terminal voltage.

Once the beam exits the accelerator it passes through a second carbon stripper foil, this time at extremely high voltages (see Figure 9). At high enough energies it is possible to strip all the electrons off a portion of the aluminum ions, creating Al^{+13} ions. At HRIBF it is possible to fully strip ions up to mass 55 (manganese) (Galindo-Uribarri, 2012). Fully stripping the ions effectively creates a charge difference between ^{26}Al (+13) and its isobar ^{26}Mg (+12) and once the beam enters a magnetic field the ^{26}Mg isobars can be removed due to the difference in charge state. This technique is somewhat unique to the machine at the HRIBF due to the extremely high terminal voltages needed to fully strip ions.

Stable aluminum isotope detection and counting is done at both low energy and high energy using a Faraday Cup. The beam of stable chlorine ions strikes the cup and is neutralized while giving the metal cup a slight charge. As shown in Equation 8 the observed current (I) can then be converted using the elementary charge (e) to the number of ions (N) observed over time (t in seconds) (Heisinger, 2002).

$$N/t = I/e \quad (8)$$

Where N is number of ions observed in time t (sec), I is the measured current (amperes) and e is the elementary charge (1.6×10^{-19} C). The electrical current produced in

the conductive metal is proportional to the number of charges being carried by the ions in the vacuum part of the circuit. The stable ^{27}Al isotopes are measured using Faraday Cups located at low energy (FC 13-1) and high energy (FC 17-1) typically for a 30 second counting period (see Figure 9). The Faraday Cup must then be removed and ^{26}Al measurements take place for 10 minutes afterwards using a Bragg detector located at the end of the beam line after FC 17-1 (Galindo-Uribarri, 2012). The Bragg curve detector is filled with CF_4 gas at a pressure of 220 Torr (Galindo-Uribarri, 2007). The gas sealed within the detector is ionized by the collision of the high-energy Al ions as well as other isobars that are not removed during beam travel. The ions are swept towards an electrode and it is possible to analyze the target ions by collecting and quantifying the electrical charges released. Each ion that interacts with the detector will emit a different energy loss trend and so discrimination of individual ions is done through multiple measurements of energy loss. The mass spectrum is represented as a vertical bar graph for each desired element with ions of a given mass to charge ratio located along the x-axis the number of ions present along the y-axis. So identification of an isotope requires determination of its nuclear mass and charge. Because there is little discrimination between ions of similar mass and charge most unwanted particles must be removed before the ion beam strikes the detector.

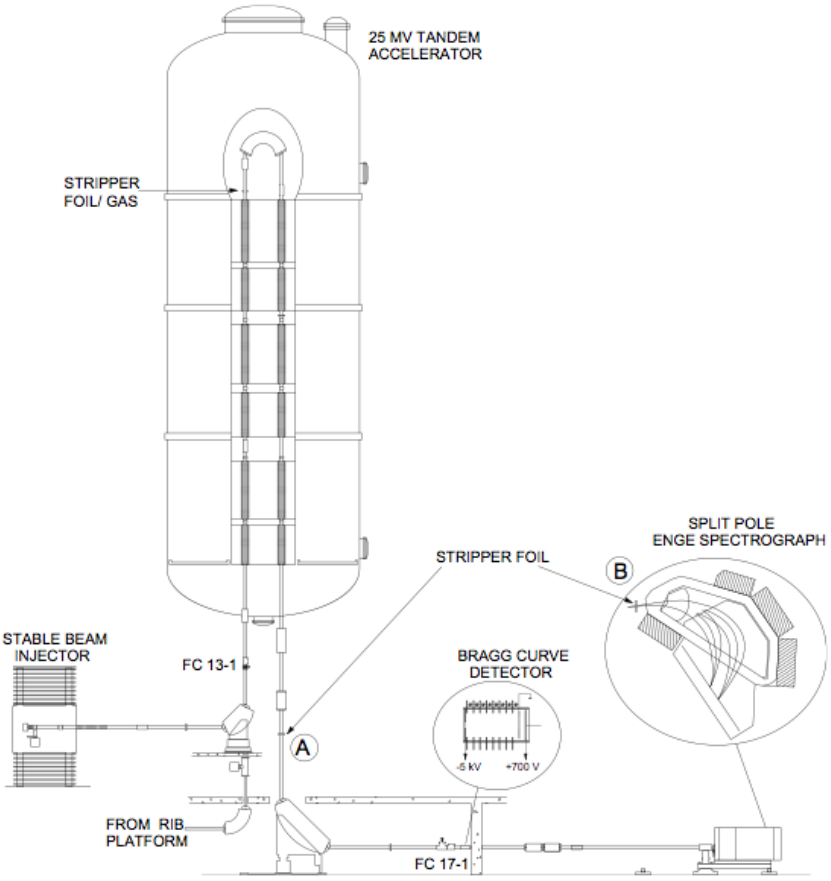

Figure 9: Schematics of the experimental set-up used for AMS measurements at HRIBF. This figure has been taken from Galindo-Uribarri (2007).

1.9 Goals and Objectives

The goal of this study is to develop a new and improved technique for the ultrasensitive AMS measurements of ^{26}Al. To date, quartz is the only target mineral used for the measurement of cosmogenic Al and few studies within Earth sciences have ever used individual ^{26}Al measurements. Because of the poor accuracy and reproducibility of ^{26}Al AMS measurements they are always made in conjunction with ^{10}Be and often ^{26}Al measurements cannot be used because they prove to be unreliable.

In 1990 Middleton demonstrated that a target made of solid aluminum metal yields a much higher negative ion beam than Al_2O_3. However, the practicality for using an aluminum metal as an ion source target for geological purposes just isn't there. As mentioned before, Al_2O_3, which is currently used for geological samples, is easy to synthesize and stable within the ion source, yet it is not an optimal material. The goal of this thesis is to develop a new technique that allows ^{26}Al to be measured more effectively while still remaining applicable to geological samples. This thesis aims to demonstrate the possibility of (aluminum nitride) AlN as novel ion source material, which could improve the AMS measurement of ^{26}Al.

The overall objective behind this thesis is to compare the negative ion source performance for different source materials, in particular aluminum oxide (Al_2O_3) and AlN, and demonstrate a more effective way for measuring ^{26}Al using AMS techniques. Increasing the beam of negative ions of aluminum emitted from the source also increases the counting rate at the detection level, thus increasing the sensitivity and accuracy of the measurement. Optimizing the overall currents produced by the ion source as well as those for both atomic and molecular aluminum ion species will transmit more aluminum ions through the system and allow for a more efficient measurement. ^{27}Al and ^{26}Al are isotopes of one another a while their relative masses are different they have the same number of electrons and so chemically they will behave the same way. Because the stable isotope of aluminum (^{27}Al), with a natural abundance of about 99.9%, is much more abundant than ^{26}Al, and will be detectable using the low-energy Faraday Cup, the system was tuned to examine mass 27 not mass 26 (Faure & Mensing, 2005). ^{26}Al cannot be

detected without the use of the tandem accelerator. However, inferences can be made for the production of ^{26}Al ions as it will behave in an identical fashion as the stable isotope.

The first objective was to demonstrate that AlN as a source material did indeed outperform Al_2O_3. These first exploratory runs were done using the test stand at HRIBF, which is essentially a conventional mass spectrometer and has no high voltage or accelerator capabilities. Different source parameters were examined so that the effect on the production of negative aluminum ions could be observed and the output optimized.

Once it was demonstrated that AlN could outperform Al_2O_3 in the production of negative aluminum ions the objective grew to demonstrating the potential of using AlN as a source material for AMS measurements. So next the samples were run using the stable injector, which includes the low-energy side of the AMS setup at HRIBF. The stable injector gives a realistic estimate as to the source output and the AMS measurement capabilities for measuring ^{26}Al at HRIBF. The samples were run without using the high-energy side of the AMS setup and currents as measured on Faraday Cup 13 (FC-13) before injection into the tandem accelerator were compared. Transmission through the tandem accelerator and high-energy side of the system for aluminum is known and therefore, currents measured by FC-13 can infer what the overall ^{26}Al ion detection will be.

Up to this point all samples run were commercially prepared AlN, AlF_3, Al_2O_3 and mixed AlN/ Al_2O_3 samples. The next objective was to prepare geological samples, convert them to AlN and then run them using the stable injector. Thus demonstrating that not only is AlN a promising source material but the sample preparation for geological samples is applicable to Earth Sciences.

2. INVESTIGATION INTO DIFFERENT SOURCE MATERIALS FOR ACCELERATOR MASS SPECTROMETRY (AMS) MEASUREMENTS OF COSMOGENIC ^{26}AL NUCLIDES

2.1 Production of Negative Ions at Holifield Radioactive Ion Beam Facility (HRIBF)

At HRIBF, ion beams can be injected from either the Radioactive Ion Beam (RIB) injector, which is primarily used for short-lived isotopes, or the Stable Ion Beam (SIB) injector, which is primarily used for long-lived isotopes. Like other cosmogenic isotopes ^{26}Al is a long-lived isotope and therefore a beam of ^{26}Al is injected from the negative ion source that is mounted in the SIB injector platform. At HRIBF the source of negative ions is a single cathode sputtering negative ion cesium sources (SNICS) from National Electrostatics Corporation (NEC). Because it is a single cathode source each sample must be loaded and removed one at a time using a removable rod (see Figure 10 and 11). Most AMS facilities that routinely measure geological samples employ a multi-cathode wheel so that operators can switch between samples, references and blanks with ease. Located underneath the source is a heated cesium (Cs) reservoir where a jet of Cs vapor is created and sprayed into the cavity in front of the cathode containing the spherical ionizer. Some of the cesium accumulates on the surface of the sample while the rest undergoes thermal ionization at the metal surface of the ionizer producing Cs^+ ions (see Figure 12). A potential is applied between the ionizer and the cathode surface and this potential accelerates and focuses the Cs^+ ions at an angle of 45° to a small spot on the center of the sample. The sample is then physically sputtered away as it is continuously bombarded with Cs^+ ions. The accumulated layer of neutral cesium at the surface of the sample reduces the work function and enhances the probability of negative ion production. As material is sputtered off the sample it interacts with the layer of Cs to form negative ions (Tuniz, 1998). The ionizer electrode, having a positive voltage, serves as an extractor for

the negative ions and the newly created negative ions are accelerated towards it. As the negative ions pass through a hole in the electrode they become focused and form a beam upon entering the injection beamline (see Figure 11 and 12).

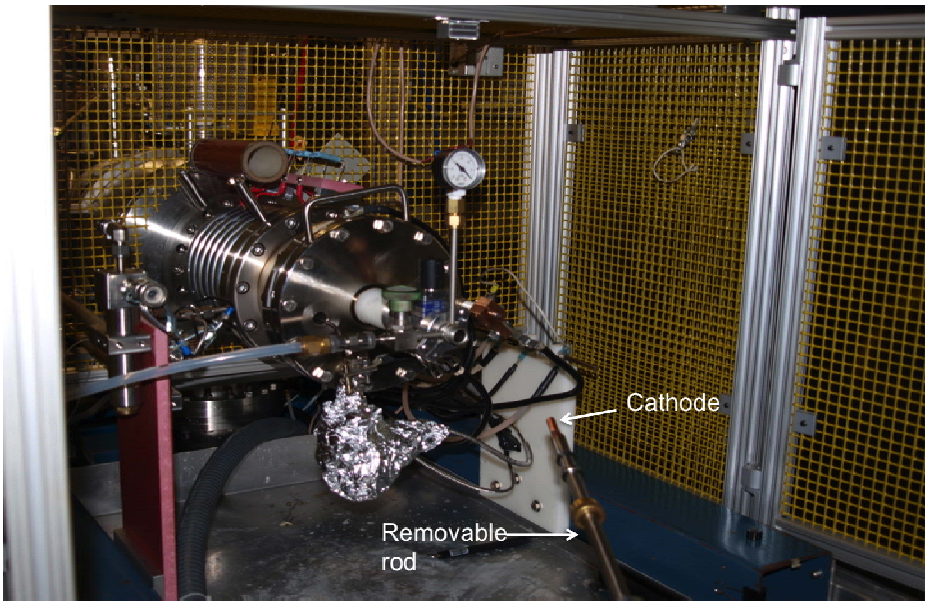

Figure 10: A single cathode SNICS with the cathode containing the sample material being screwed onto the end of a removable rod and inserted into the focal point of the SNICS through a vacuum lock.

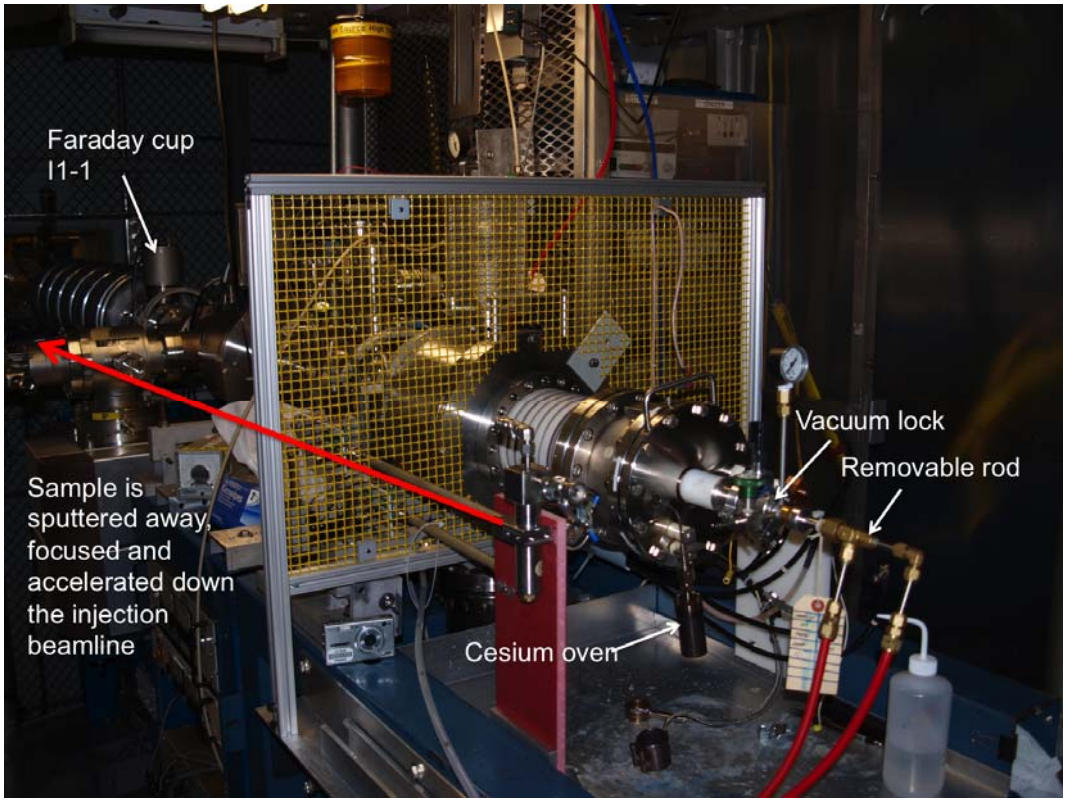

Figure 11: Side view of the single cathode SNICS and injection beamline with the sample rod inserted.

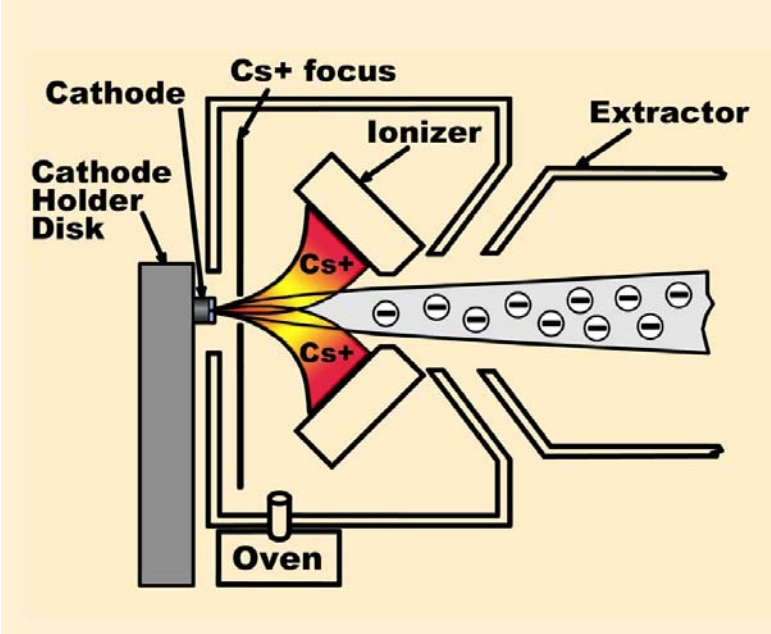

Figure 12: Simplified image of the SNICS operations. The cesium oven supplies heated cesium, which is then thermally ionized by the ionizer and aimed at the center of the sample located in the cathode holder disk. The negative ions that are sputtered away are then accelerated and focused by the extractor. This figure has been taken from the National Electrostatics Corporation website (2007).

2.2 The Production of Al^- Ion Beams

It is notably more difficult to perform AMS measurements for ^{26}Al than for ^{10}Be. One study by Kilius *et al.* (1979) recognized the cesium sputter ion source as the problem (Kilius *et al.*, 1979). Kilius observed that the output current of negative aluminum ions from the source was low due to a low efficiency for producing negative aluminum ions from the sample ions. As previously mentioned the ratio of $^{26}Al/^{27}Al$ within natural samples is on the order of 10^{-14} and AMS is the only technique that allows the routine measurements of ^{26}Al in natural samples. ^{27}Al and ^{26}Al are isotopes of aluminum and so they have equal numbers of electrons and protons but different numbers of neutrons in their nuclei and hence they differ in relative atomic mass but not in chemical properties. ^{26}Al is simply the radioactive form of the elements Al. Chemically and physically ^{27}Al and ^{26}Al will react the same way within the source, however, ^{27}Al is 14 orders of magnitude more abundant. Therefore, when using the low-energy side of the AMS system without the use of the tandem accelerator ^{26}Al is essentially undetectable. Studies involving the investigation into the production of negative aluminum ion beams from a cesium sputtering source have focused on the performance for $^{27}Al^-$ ions as the currents are much stronger and can be detected using a Faraday Cup without the use of the tandem accelerator.

In 1989 Roy Middleton performed one of the earliest investigations into the production of negative ion beams from different source materials. Middleton's goal was to provide a means of producing negative ion beams with particular emphasis on their suitability for injection into a tandem accelerator. Middleton reported that aluminum oxide cathodes, which were not mixed with silver powder, usually provided a steady

beam of about 0.5μA of $^{27}Al^-$ after 10 minutes of running. Over the period of 30 to 40 minutes the current would rise to between 1 and 2 μA of $^{27}Al^-$. Middleton also noted that the yield of molecular aluminum ions was much larger than the atomic aluminum ions. He reported currents as high as 20 to 40 μA for AlO^- and currents up to 4 to 6 μA of AlO^{2-} (Middleton, 1990).

Middleton reported the ionization efficiency for producing $^{27}Al^-$ ions from aluminum oxide to be 0.2% (Middleton, 1990). For aluminum samples the counting rates for negative aluminum ions is so low that ~99.8% of the sample does not become ionized and therefore is wasted (Aardsma, 1984). This implies that a typical cathode containing about 6 mg of aluminum oxide will produce about $2.5x10^4$ μC of $^{27}Al^-$ ions, which indicates an average current of about 2 μA for a little over 3 hours (Middleton, 1990). Middleton also examined the performance of a pure metal aluminum sample noting a higher Al^- beam current of 6 to 8 μA over the cathodes lifetime of 3 or 4 hours (Middleton, 1990).

Since the work done by Middleton, there have been other attempts to use a pure aluminum metal as an ion source material (Flarend *et al.*, 2004, Granger, 2012 and Hunt, 2007). The results have been contradictory for a pure aluminum powder and additionally the applications of using an aluminum powder for geological samples have yet to be demonstrated. Other source materials that have been investigated include aluminum carbide (Al_4C_3) as well as aluminum boride (AlB_2) (Flarend *et al.*, 2004). The aluminum boride produced a large negative ion beam, however, the majority of the mass 26 amu beam was attributed to BO^- not Al^- and so would interfere with ^{26}Al measurements. The

aluminum carbide did not perform as well as the aluminum oxide and so is not a practical source material for ^{26}Al measurements (Flarend *et al.*, 2004).

A recent study by R. Flarend *et al*. (2004) examined the negative ion source outputs for different aluminum compounds and in particular aluminum nitride (AlN). In his search for an optimal source material for Al^- ion beam production Flarend (2004) reported $^{27}Al^-$ ion beam current of 150 nA for an aluminum oxide sample, 74 nA for a pure aluminum powder and 100-600 nA for an aluminum nitride sample (Flarend *et al.*, 2004). Flarend found that the performance of AlN in producing negative ions of Al^- depended on the length of exposure of the sample to an air atmosphere (Flarend *et al.*, 2004). They noted that an exposure of one hour yielded the highest beam currents, more so than a longer exposure or no exposure at all.

Flarend's observations regarding the different exposure times were a result of the fact that AlN decomposes to form aluminum hydroxide ($Al(OH)_3$) and ammonia (NH_3) in moist air (see Reaction 4). Kameshima *et al*. found, by using X-ray photoelectron spectrometry (XPS), that the surface of AlN powders reacted slowly with atmospheric moisture during several years of storage in a capped container (Kameshima, 1998). It is possible that the formation of a thin layer of $Al(OH)_3$ around the grains of AlN encourages the formation of negative ions. However, once exposed for longer periods of time, more AlN decomposes and the negative ion formation is hindered.

$$AlN(s) + 3H_2O(g) \rightarrow Al(OH)_3 + NH_3 \qquad (4)$$

2.3 Source Materials of Interest

In an attempt to find a more effective source material for AMS measurements of ^{26}Al several different compounds were tested. The only conditions a potential source material must meet is that it is stable within the source at high temperatures under vacuum. An AlN source material is expected to perform better than an Al_2O_3 based on the observation that nitrogen does not form negative ions and therefore will not interfere with the production of Al^- (Middleton, 1990). The previous finding by Flarend *et al*. (2004) demonstrates AlN to be a promising source material for the measurement of ^{26}Al and that the effectiveness of AlN in producing a negative ion beam depends on the length of exposure to air (Flarend *et al.*, 2004).

The length of exposure of AlN to air determines the extent to which the sample hydrolyzes to form $Al(OH)_3$. By investigating samples of AlN with different lengths of exposure to air the effects of decomposition can be observed. Primarily AlN samples with no exposure ("no exposure" AlN), a short exposure to air ("one-hour" AlN) and those with a long exposure to air ("2 day" and "14 day" AlN) were examined.

An AlN sample that is hydrolyzed by moist air is chemically different than an Al_2O_3 sample that has been converted to AlN. The amount of oxygen and degree of hydrolysis within an AlN sample may affect the performance of the source material. The primary interest behind the mixed AlN + Al_2O_3 sample was to investigate a sample that better represents that of a geological sample that has been prepared as an Al_2O_3 and then converted to AlN for AMS measurements.

In addition to AlN, aluminum fluoride (AlF_3) is another source material of interest. While the usefulness of preparing an aluminum sample as an aluminum fluoride

has yet to be examined fluorine has proven to be a useful carrier for other elements such as Be, Ca, Pb, Sm, Nd and Pu (Zhao *et al.*, 2004 and Kieser *et al.*, 2012). Fluorine is the most electronegative of the reactive elements and studies have shown that embedding an element of interest in a fluoride matrix can facilitate the production of fluoride molecular anions (Kieser *et al.*, 2012).

2.4 Sample Preparation

The investigated samples included commercially produced aluminum oxide (Al_2O_3, Fischer A-540), aluminum nitride (AlN, Sigma-Aldrich 241903) and aluminum fluoride (AlF_3, Sigma-Aldrich 449628) as well as a mixed sample of AlN and Al_2O_3 (50:50 volume %). Each material was mixed with a fine silver (Ag) powder to form a 3:1 wt % sample to silver ratio. The silver powder is added to help increase the conductivity of the sample and encourage the production of negative ions as well as facilitate the handling of low volume samples that might otherwise prematurely expire (Hunt, 2007). In addition the silver powder creates a more malleable sample, allowing it to be more easily packed into a cathode.

In each case, excluding the AlN samples that were exposed for days, the samples were weighed out, mixed with Ag powder and packed into copper cathodes immediately prior to loading them into the source. Initially the short exposure to air for AlN samples was investigated out of convenience, as it is difficult to contain the entire sample preparation procedure within an argon atmosphere. The “one-hour” AlN samples were measured out in an argon atmosphere chamber and then mixed with Ag powder and left in an air atmosphere for an hour prior to packing into a cathode. In the case where AlN

was exposed for several days the remaining "one-hour" AlN + Ag material was left stored in an air atmosphere, and then packed into a cathode immediately prior to placing in the source. In the case of the "no exposure" AlN the sample was measured out, mixed with Ag and packed into a cathode all within an argon glovebox. The mixed AlN + Al_2O_3 sample was prepared so that it was 50% Al_2O_3 and 50% AlN by volume and the sample was exposed to an air atmosphere for one hour to try and yield the best results for AlN. The technique of mixing the samples ahead of time and packing them into a cathode immediately prior to loading into the source ensures that the entire sample is exposed to air, not simply the surface of the sample.

2.5 Source Operations

The initial investigation involved comparing three different compounds (AlN, Al2O3 and a mixed AlN + Al_2O_3) using the low-energy test stand. The test stand operates as a conventional mass spectrometer and is an ideal system for testing numerous samples as well as taking multiple mass scans and examining the effects of varying source system parameters. Parameters such as the cesium oven temperature, sputter voltage, and focusing lenses were adjusted so that each sample yielded the optimum atomic or molecular aluminum negative ion beam current. Figure 13 shows a schematic of the negative ion source that is associated with the test stand.

After loading the sample and pumping down the vacuum to 10^{-6} torr the ionizer current is slowly increased at a rate of ~2 Amps every 10 minutes. The current must be slowly increased to avoid burning out the ionizer. Increasing the ionizer current has the effect of increasing the sputtering rate and ultimately the overall beam current. It was

observed that the ideal ionizer current for the test stand is 22 Amps, any higher and there exists the danger of burning out the ionizer. Once the ionizer reaches a current of about 16 Amps the cesium oven was turned on to 100°C. Turning on the cesium oven while the ionizer is still cool will result in a build up of cesium within the system. Once the ionizer is increased to 22 Amps the cesium oven is raised to 160°C and then slowly increased to 200°C. The ideal cesium oven temperature is approximately 200°C. If the cesium oven temperature is too low then the sample will not form a prolific beam current and if cesium oven is too high then too much cesium is released and it will accumulate on surfaces within the source, including the sample (see Figure 14). If the cesium builds up too much it will coat everything and overwhelm the system prohibiting negative ion beam production. Once too much cesium is released it can take a couple hours to sputter away the excess.

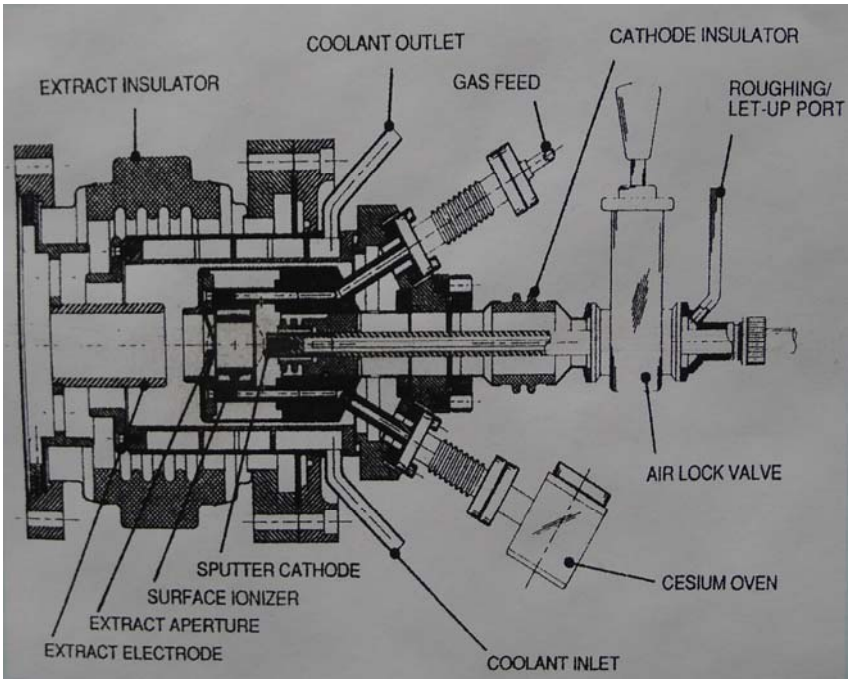

Figure 13: Schematic of the negative ion source associated with the test stand. This figure has been taken from a poster presented by Liu (2011).

Figure 14: Cathode containing Al_2O_3 with a layer of cesium (black) coating the sample surface. This was the first sample that was run on the test stand and the effect of varying source conditions were being examined. The cesium oven was turned up to 210°C, which clogged the system and coated the sample in cesium.

In an attempt to further quantify whether or not AlN is a source material that outperforms Al_2O_3 for AMS measurements the samples runs were repeated using the low-energy Stable Ion Beam (SIB) injector platform, which forms the low-energy side of the AMS system at HRIBF. The schematics of the negative ion source on the stable injector are very similar to that of the test stand. The source was run so that the cathode voltage was 3 kV, the source voltage was 20 kV with an acceleration voltage of 180 kV, giving a total of 200 kV. The cesium oven was heated to 200°C, the ionizer current was set to 27 Amps and the aperture was set to 4mm. Increasing the aperture slit allows for a greater portion of the ion beam to pass through, however measurements become less accurate as a larger percentage of unwanted ions are allowed to pass through the system (Mills, 2012).

In addition to the previously run AlN, Al_2O_3 and mixed sample materials, a new sample of AlF_3 was introduced. Once placed in the source each sample was run 8 hours a day and in some cases they were run for multiple days in a row. The total current output

from the source was recorded using Faraday Cup FC I1-1 to ensure consistent source behavior. As well the mass analyzed currents of atomic $^{27}Al^-$ and molecular species of $^{27}Al^-$ were monitored and recorded using mass scans from mass 0 to mass 140 amu every couple of hours. Mass scans also allowed for the relative peak intensities to be examined between the numerous aluminum species. The isotope ^{27}Al is much more abundant than ^{26}Al, however, both isotopes will have identical source behaviors. Therefore, inferences can be made about the AMS measurements of ^{26}Al by examining the behavior of $^{27}Al^-$ beam production for different source materials using the stable injector platform.

2.6 Experimental Results and Discussion

Often the source parameters for the test stand were altered during a run, and on many occasions the negative ion production was too low or the beam current wasn't stable enough to get a proper measurement. As a result measurements from the test stand are difficult to compare and quantitative conclusions are difficult to state. Primarily the observations from the test stand were used as an investigation into the potential of AlN as a source material and to optimize the source performance for the stable ion beam (SIB) injector. The same trends that were seen on the test stand were observed using the SIB injector platform (se Figure 15). The overall magnitudes of the observed negative ion currents were much greater using the SIB injector compared to the test stand, however, the relative beam intensities between the two systems remain very similar. The results from the SIB injector yielded reasonably stable beam currents.

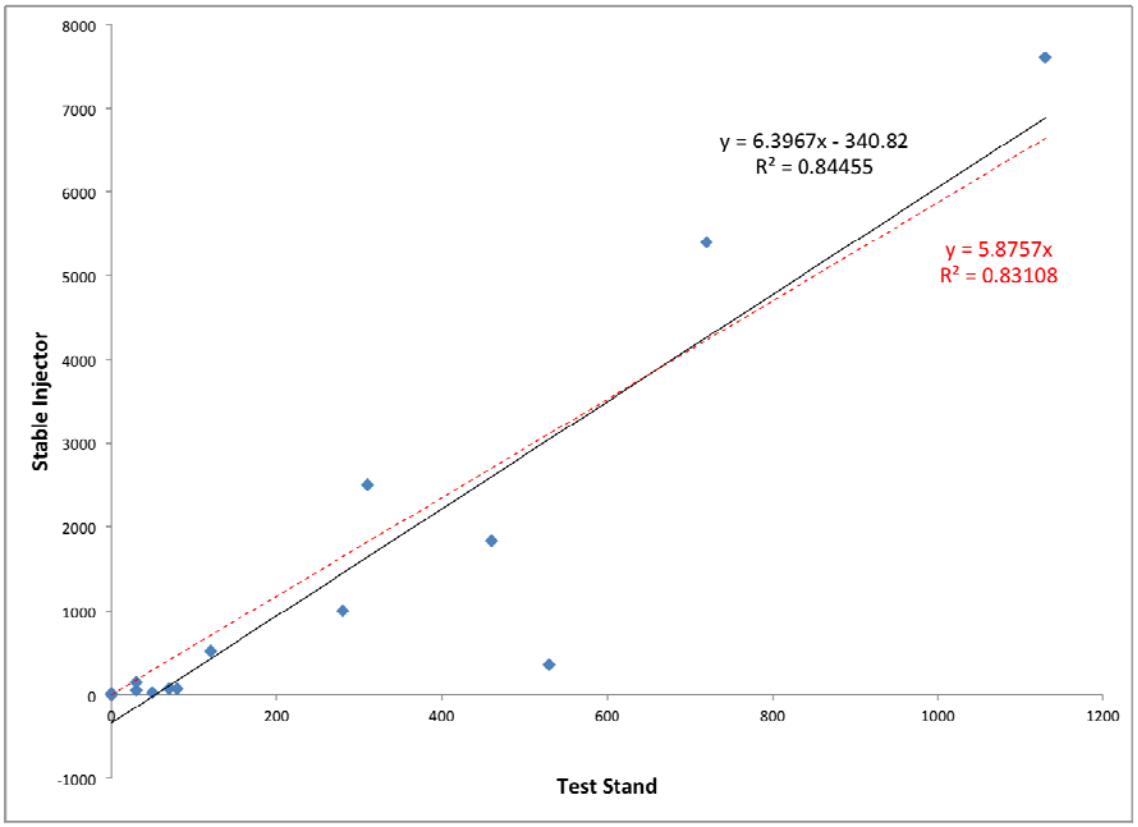

Figure 15: The correspondence between the stable injector and test stand data for AlN (1hr) samples. While the stable injector yields overall higher beam currents the trends seen for both the stable injector and the test stand are similar.

For the AlN samples the total beam current increases quickly at the start of a run and approaches its maximum current within 1.5 hours of operation under ideal source conditions. A common trend amongst all of the AlN samples is that the molecular aluminum negative ion beams AlN^- and Al_2N^-, with masses 41 and 68 amu respectively, yielded higher currents than the atomic or diatomic species of aluminum. However, in each case the diatomic negative ion of aluminum, Al_2^- at mass 54 amu, also yielded a higher beam current than the atomic species (see Table 2). In fact, for each of the AlN samples, the beam of atomic aluminum ions Al^- yielded the lowest currents of any of the aluminum species. As shown in Appendix 6, the data collected from the test stand shows the beam of AlN^- the Al^- current continuing to increase over the course of an 8-hour run.

The highest observed currents for any of the AlN samples were for the AlN^- negative ion beam (mass 41 amu), which continues to increase over the course of a run (see Appendix 6). In each AlN sample the order of the most prolific beam to the least prolific beam of negative ions for the aluminum species is as follows; $AlN^- > Al_2N^- > Al_2^- > Al^-$ (see Table 2*).* The relative peak intensities between the various aluminum species remain fairly constant between each of the AlN sample.

When comparing the AlN samples with various exposure times it was observed that the AlN sample with a shorter exposure to air (1 hour) performed much better than material that had been exposed for a couple days (2 days) or weeks (14 days). However, even for longer exposure times, the AlN samples with some exposure to air, yielded better results than no exposure at all (see Figures 16, 17 and 18). The highest observed currents for any aluminum species were for the "one-hour" AlN sample with a maximum AlN^- current of 1130 nA and 7600 nA on the test stand and SIB injector respectively. The maximum AlN^- currents for the longer exposed AlN samples were 590 nA and 2050 nA for the test stand and SIB injector respectively and a maximum current of 1260 nA for the "no exposure" AlN sample using the SIB injector (see Table 2).

Similar trends were seen for the negative ions beams of atomic aluminum. The "one-hour" AlN sample yielded the highest Al^- currents with maximums of 280 ηA and 1000 nA for the test stand and SIB injector respectively. The longer exposed AlN samples displayed lower Al^- currents with maximums of 150 nA and 290 nA for the test stand and SIB injector. As well, the lowest atomic aluminum current was seen in the "no exposure" AlN sample with a maximum Al^- current of 230 nA using the SIB injector (see Table 2).

Regardless of the length of exposure to air, the AlN samples always yielded a more prolific beam of atomic and molecular aluminum than the Al_2O_3 samples. For samples of Al_2O_3 the most prolific negative ion beam was always $^{16}O^-$, which comprised approximately 12% of the total beam (see Appendix 1). The most prolific negative ion beams of aluminum species for the Al_2O_3 samples were AlO^-, AlO_2^- and Al^- with maximum currents of 460, 120 and 30 nA for the test stand and 1830, 520 and 150 nA for the stable injector respectively (see Figure 19). When comparing similar runs for the stable injector for samples of AlN and Al_2O_3 the Al^- current is approximately 7 times higher in the "one-hour" AlN sample than the Al_2O_3 sample and the AlN^- current is approximately 4 times higher than the AlO^- current. For the "one-hour" AlN sample the AlN^- current comprised as much as ~33% of the total beam. Compare this to an Al_2O_3 sample where the AlO^- beam comprised only ~2% of the total beam. As shown in Figure 16 the AlO^- negative ion current was actually higher within the "one-hour" AlN sample than the Al_2O_3 sample, which had a maximum current of 3100 nA and comprised 13% of the total beam compared to 1830 nA and 1.7% of the total beam (see Appendix 1).

However, for AlN to outperform Al_2O_3 there needs to be some decomposition of the AlN in moist air. As shown in Figures 16-18 the "one-hour" AlN sample, which performed the most prolific beams, also had the highest peak of oxygen of any of the AlN samples. The increased oxygen content that is introduced through the decomposition of AlN coincides with the maximum peaks observed for aluminum species. The "no exposure" AlN sample yielded an Al^- beam current that was less than Al_2O_3. The mixed AlN + Al_2O_3 sample showed some promise on the test stand with higher Al^- currents than the Al_2O_3 sample, 50 nA compared to 30 nA. However, as seen in Table 2 the results

from the stable injector indicated that the mixed sample did not perform very well and yielded the lowest currents of all the samples (see Figure 20).

Table 2: Maximum currents for molecular and atomic aluminum negative ion species for AlN (with different exposure times), Al_2O_3 and mixed AlN + Al_2O_3 samples. Results are for both the test stand and stable injector platform. The given values for the currents have been rounded to the nearest ten nA.

System	Sample	Negative Ion	Maximum Current Observed (nA)
Test Stand	"one-hour" AlN	Al^-	280
		AlN^-	1130
		Al_2^-	310
		Al_2N^-	720
Test Stand	"14 day" AlN	Al^-	150
		AlN^-	590
		Al_2^-	170
		Al_2N^-	360
Test Stand	AlN + Al_2O_3	Al^-	50
		AlN^-	70
		AlO^-	530
		Al_2^-	0
		AlO_2^-	80
		Al_2N^-	30
Test Stand	Al_2O_3	Al^-	30
		AlO^-	460
		Al_2^-	0
		AlO_2^-	120
Stable Injector	"one-hour" AlN	Al^-	1000
		AlN^-	7600
		Al_2^-	2500
		Al_2N^-	5400
Stable Injector	"2 day" AlN	Al^-	290
		AlN^-	2050
		Al_2^-	620
		Al_2N^-	1800
Stable Injector	"no exposure" AlN	Al^-	230
		AlN^-	1260
		Al_2N^-	1050
Stable Injector	AlN + Al_2O_3	Al^-	30

System	Sample	Negative Ion	Maximum Current Observed (nA)
		AlN^-	70
		AlO^-	360
		Al_2^-	20
		AlO_2^-	70
		Al_2N^-	50
Stable Injector	Al_2O_3	Al^-	150
		AlO^-	1830
		Al_2^-	0
		AlO_2^-	520

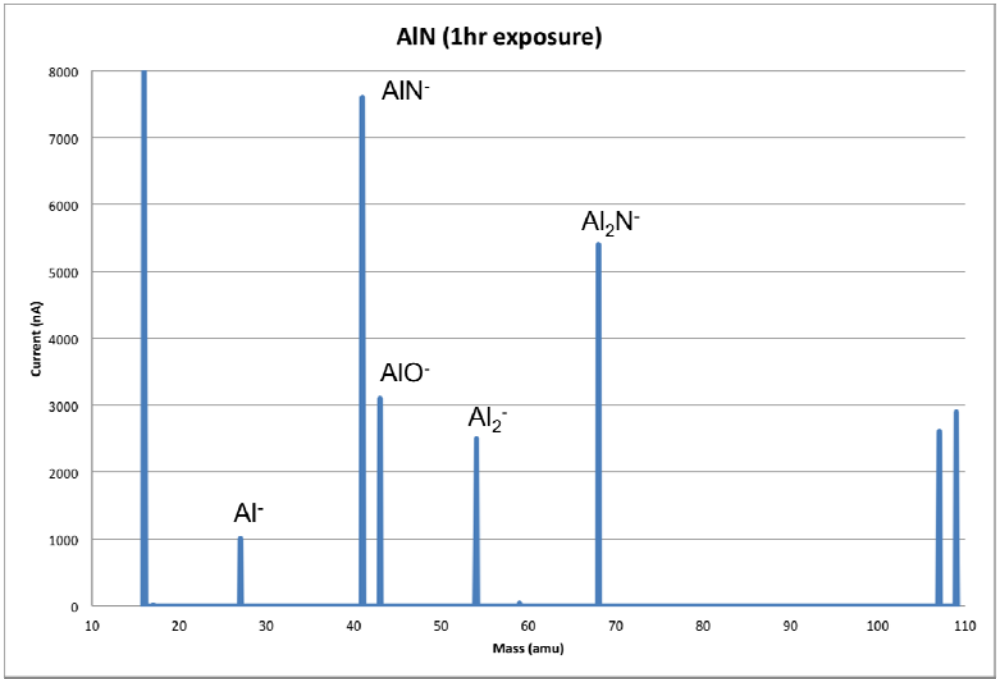

Figure 16: Mass scan for a "one-hour" AlN sample depicting the highest currents achieved for AlN^- and Al^- ion beams (mass 41 and 27 amu) using the stable injector platform. Note the large $^{16}O^-$ beam at mass 16 amu.

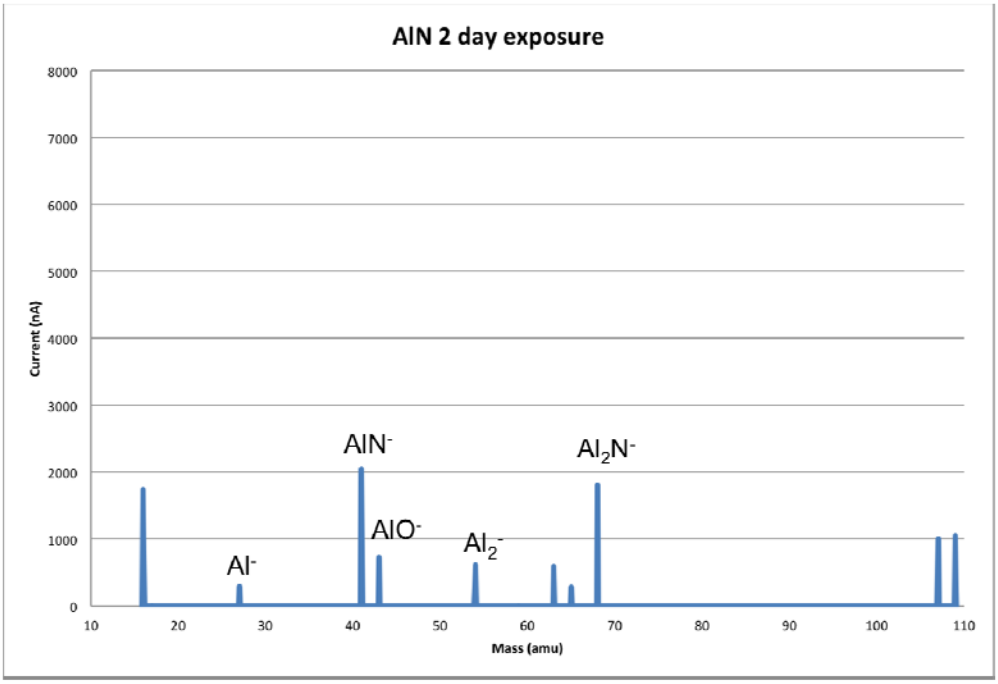

Figure 17: Mass scan for a "2 day" AlN sample depicting the highest currents achieved for AlN^- and Al^- ion beams (mass 41 and 27 amu) using the stable injector platform.

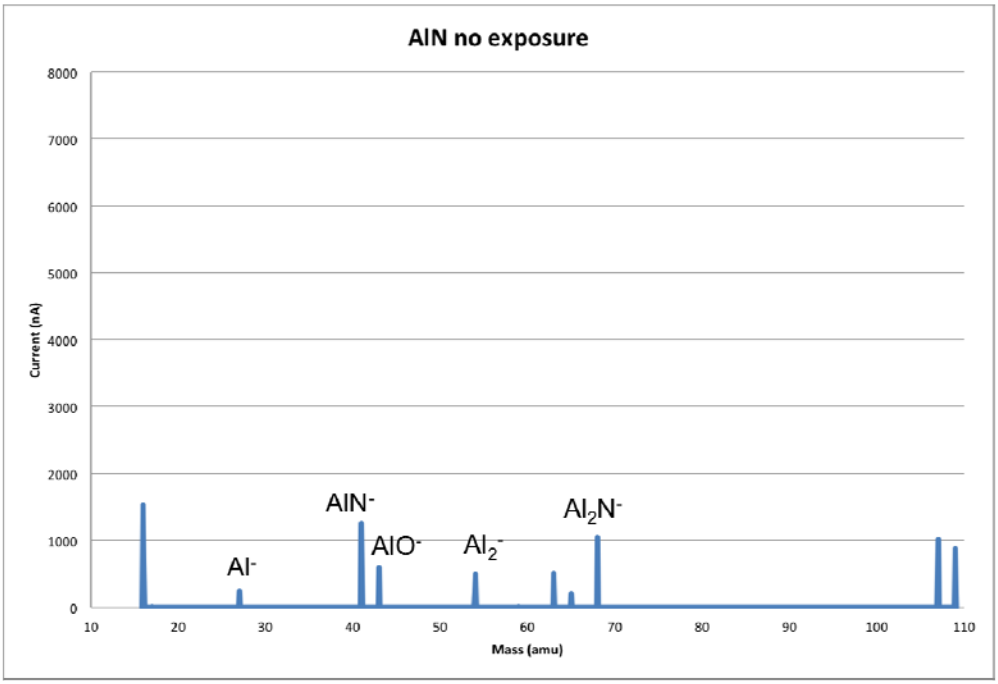

Figure 18: Mass scan for a "no exposure" AlN sample depicting the highest currents achieved for AlN^- and Al^- ion beams (mass 41 and 27 amu) using the stable injector platform.

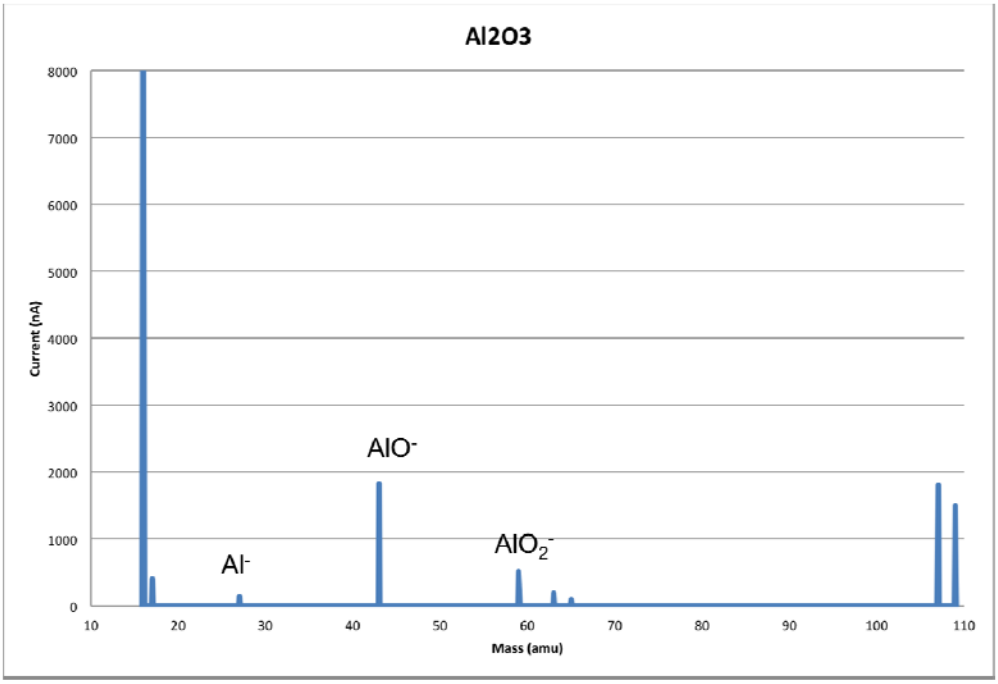

Figure 19: Mass scan for an Al_2O_3 sample depicting the highest currents achieved for AlO^- and Al^- ion beams (mass 43 and 27 amu) using the stable injector platform.

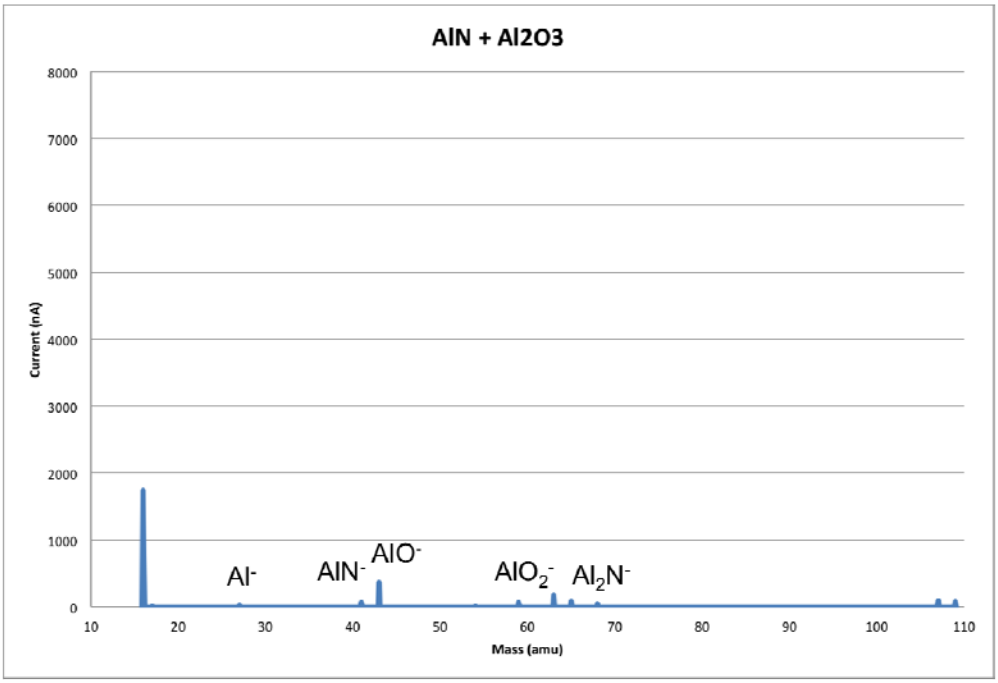

Figure 20: Mass scan for a mixed $AlN+Al_2O_3$ sample, where the AlN has been exposed for 1 hour, depicting the highest currents achieved for AlN^- and Al^- ion beams using the stable injector platform.

To better examine the variability between the different source materials the Al^- currents measurements for the "one-hour" AlN, Al_2O_3 and the mixed $AlN+Al_2O_3$ samples were examined using an ANOVA (ANalysis Of VAriance between groups) test using the SAS (Statistical Analysis System) software. The "2 day" AlN and the "no exposure" AlN samples had too few data points to run a statistical analysis and so they were omitted from the ANOVA test. The results from the ANOVA test showed that the variance in the Al^- currents between runs due to both the sample material and the source operations are significant (see Appendix 2). In addition, the mean Al^- current for the "one-hour" AlN sample is statistically different from the Al_2O_3 sample and the mixed sample (see Appendix 2).

Statistically the atomic Al^- currents for the "one-hour" AlN and Al_2O_3 samples are different, with "one-hour" AlN samples having higher Al^- currents (see Figure 21). As well there is a statistical difference between the "one-hour" AlN sample and the mixed $AlN + Al_2O_3$ but there is no statistical difference between the Al_2O_3 sample and the mixed $AlN + Al_2O_3$ sample. However, the mixed sample has fewer runs to compare. As seen from Figure 21 there is a large range in currents for the "one-hour" AlN samples. This large range demonstrates the need to optimize the source operations for the AlN source material. The maximum currents for the AlN source material demonstrate what is achievable, however in order to repeatedly measure such currents the numerous parameters involved in the source operation and production of negative ions from the AlN material need to be examined and optimized. One must exercise caution when doing a statistical analysis on the results from these types of negative ion beam experiments, as

fluctuations in the currents observed are very common in the exploratory stage. Often it can take years to optimize a system to measure a particular nuclide of interest.

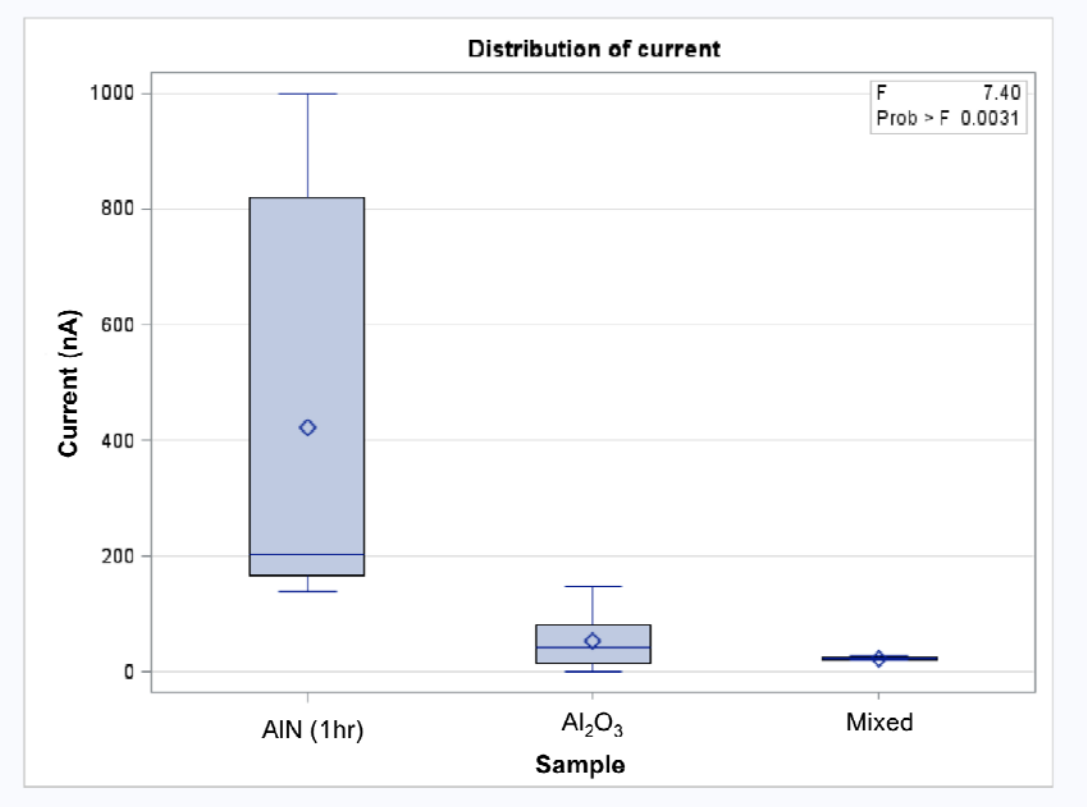

Figure 21: The distribution of Al^- currents for the "one-hour" AlN, Al_2O_3 and mixed AlN+Al_2O_3 samples. As depicted there is a statistical difference in Al^- currents between the "one-hour" AlN and Al_2O_3 samples as well as the "one-hour" AlN and mixed samples. However, the mixed sample is not statistically different from the Al_2O_3 sample.

The AlF_3 sample performed poorly and the total beam of negative ions was dominated by the formation of F^- (mass 19 amu) negative ions and the sample yielded no notable currents of Al^-. As shown in Figure 22 there was a substantial current peak at mass 103 amu, which is most likely the molecule AlF_4^-. In all of the AlF_3 samples the highest negative ion current observed for AlF_4^- is about 500 nA (see Appendix 1). However, the maximum currents for AlF_4^- are still much lower than the observed currents for aluminum nitride and aluminum oxides samples.

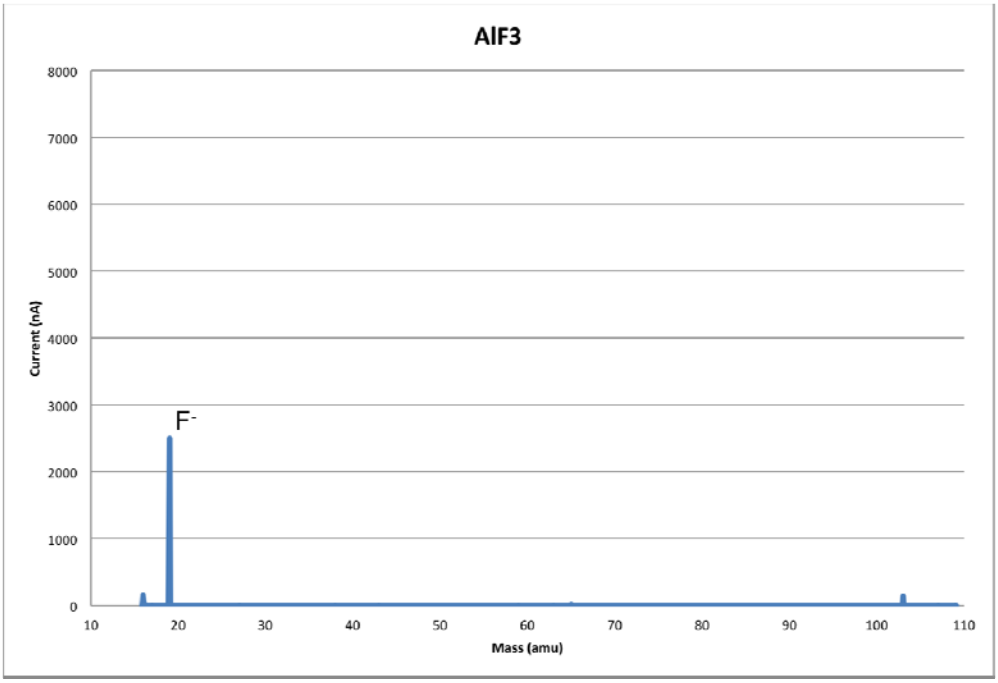

Figure 22: Mass scan for an AlF_3 sample depicting the highest currents achieved for F^- and Al^- ion beams using the stable injector platform.

There are many variables that can affect source operations such as; how long the source was shut down prior to running, or how many days in a row the source has been running, or what samples have been run previously and how clean the ionizer and other surfaces within the source are. For example, the source was disassembled and cleaned over 08/30/2012 to 09/05/2012 and the source performance from before and after it was cleaned changed rather drastically. After cleaning there was a decrease in overall beam production for atomic and molecular aluminum negative ion species for all samples (see Appendix 1). One possibility is that the cleaning of the ionizer removed any residual material that may have facilitated in the production of negative ions. Another possibility is that when reassembling the source some of the components were aligned slightly differently, changing the beam focus. It is difficult to say with any certainty what the causes may be as there are many unknowns surrounding the production of negative ions. Any adjustments made to the source that affect operations are taken into consideration.

Typically if any changes to source operations have been made and there is the suspicion that source performance has been affected then an Al_2O_3 sample, whose negative ion beam production is relatively well known, is run until the source operations appear to be consistent between runs.

Due to the varying nature of the negative ion source it is sometimes difficult to compare samples from one run to the next. One method for ensuring consistent and reliable results regarding the performance of source material is to observe the ratios between negative ion peaks. For example, the ratio of AlN^-/AlO^- and AlN^-/Al^- within a sample of AlN remains relatively constant regardless of the overall output of the source. So even if the overall negative ion production is depressed the ratios of AlN^-/AlO^- and AlN^-/Al^- within a sample can determine whether or not the results are reliable. In addition, by comparing the ratios of AlN^-/AlO^- and Al^-/Al^- between samples run under similar source conditions it can be determined if the results are comparable and consistent even though the overall source output varies.

Each of the AlN samples, regardless of exposure time, displayed the same trend and showed an increase in the AlN^-/AlO^- ratio over the course of an 8-hour run. It is difficult to graph the change in AlN^- current over time using the SIB injector as it takes approximately 1.5 hours to perform a mass scan and collect data, and so typically only 2 or 3 mass scans are done over the course of an 8-hour period. However, some trends can further be examined using data from the test stand data. At the beginning of a run the AlN^- current is almost negligible, it then ramps up quickly within the first hour of running. Only the test stand yielded enough data points to graphically represent the change in AlN^- current over the course of a few hours. The results from the test stand are

depicted in Figure 23 and 24, which shows the ratio of AlN^-/AlO^- increasing fairly quickly in the beginning of a run for "one-hour" and "14 day" AlN samples. The largest increase in AlN^- and Al^- ion beam currents over time was seen for the "one-hour" AlN sample (see Appendix 1). Observations from both the test stand and SIB injector show that over the course of a run the AlN^-/AlO^- ratio continuously increases for the "one-hour" AlN sample (see Figure 23). However, for the longer exposed AlN sample the ratio of AlN^-/AlO^- begins to plateau around mid-day as the rate of increase for the AlN^- current slows down (see Figure 24). For the second half of the run both the AlO^- current and AlN^- current increase more proportionately to each other and the overall beam current.

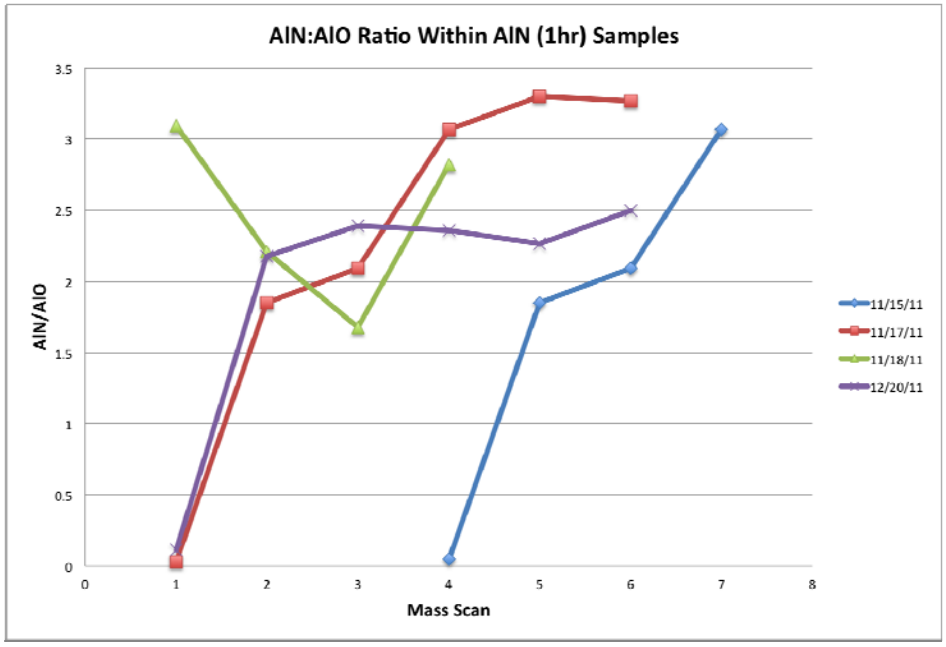

Figure 23: Results from the test stand depicting the ratio of AlN^-/AlO^- within "one-hour" AlN samples. The ratios were calculated from currents of AlN^- (mass 41) and AlO^- (mass 43) recorded using mass scans throughout the course of a run. The mass scans increase in number with increase in running time and the samples are labeled with the date they were run. The results for 11/18/11 vary from the other runs due to the fact that mass scans were acquired after maximum currents were already reached.

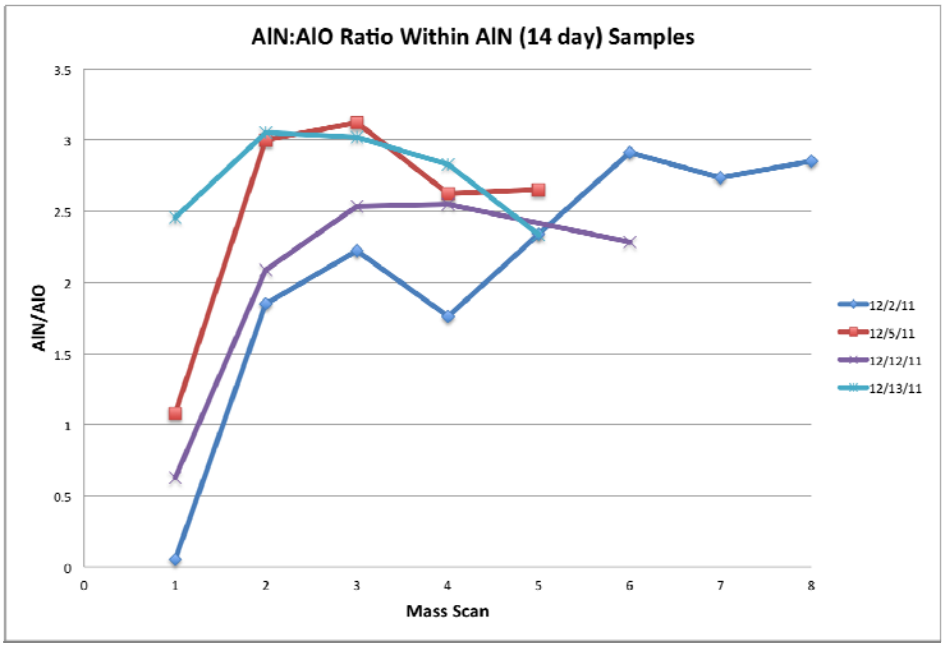

Figure 24: Results from the test stand depicting the ratio of AlN^-/AlO^- within "14 day" AlN samples. The ratios were calculated from currents of AlN^- (mass 41) and AlO^- (mass 43) recorded by multiple mass scans throughout the day using the test stand. The mass scans increase in number with increase in running time.

The trend of an increasing AlN^-/AlO^- ratio is not observed in the mixed AlN + Al_2O_3 sample. The mixed AlN + Al_2O_3 sample did not see such as great a change in the AlN^-/AlO^- ratio within a sample and the rate of change for the AlN^- current wasn't as great in the beginning of the run. Results from the SIB injector showed that the AlN^-/AlO^- ratio actually decreased over the 8 hours of running (see Appendix 3).

Within a sample, the ratio of AlN^-/Al^- for the negative ion currents exhibited the same behavior as the ratio of AlN^-/AlO^-. At the beginning of a run the AlN^-/Al^- ratios increases and then seems to approach a plateau towards the end of an 8-hour run. This indicates that the AlN^- current is growing relative the Al^- current at the beginning of the run. As the AlN^- current ceases to increase at such a rapid rate the AlN^-/Al^- ratio levels off (see Appendix 3). For a "one-hour" AlN sample the yield of AlN^- was almost 8 times

higher than the yield of Al^-. Even for the "2 day" and "no exposure" AlN samples the yield of AlN^- was 7 and 6 times the yield of Al^-.

Perhaps more difficult to compare is the AlN^-/AlO^- ratio between AlN and Al_2O_3 samples of similar runs. It should be noted that only samples run during similar source conditions can be compared. The runs before and after the cleaning of the ion source yielded very different results. After the ion source was cleaned a large portion of the total output from the source is unaccounted for after going through mass analysis (see Appendix 1). This may be due to a change in the alignment of the system after it was reassembled. If the beam isn't properly focused and centered within the system than some of the mass analyzed material may not make it through the gap in the electrodes. Samples that have been run before and after source cleaning or during a period of unusual source behavior were not compared. In addition, due to the increase of beam intensity over the course of a run, measurements taken from mass scans 1.5 hours into a run were not compared with those taken 6.5 hours into a run. For each sample the first mass scan and recorded measurements were taken 1.5 hours after the sample was loaded. Each sample had at least a second mass scan taken 6.5 hours after the sample was loaded towards the end of the run to observe any change in beam intensity over the course of a run.

When comparing samples of AlN to samples of Al_2O_3 the most prolific molecular aluminum currents were compared as well as the atomic aluminum currents. On average the "one-hour" AlN samples yielded a molecular negative ion beam of aluminum as AlN^- that is over 4 times greater than the molecular negative ion beam of aluminum as AlO^- at 1.5 hours and almost 3 times greater at 6.5 hours (see Appendix 7). As mentioned before, the AlN^- current increases much more quickly at the start of a run and so may explain

why the “one-hour” AlN samples yield a higher molecular aluminum current at 1.5 hours. In addition, the atomic aluminum current was almost 12 times greater in the “one-hour” AlN samples than the Al_2O_3 samples at 1.5 hours and about 6 times greater at 6.5 hours. The “one-hour” AlN samples yielded the best results but even the longer exposed “2 day” AlN had an AlN^- current that was about 2 times greater than the AlO^- current in the Al_2O_3 sample at 1.5 hours and slightly better at 6.5. When comparing atomic aluminum currents between samples of “one-hour” AlN and Al_2O_3 the Al^- currents were found to be over 4 times as high at 1.5 hours and over twice as high at 6.5 hours. Comparatively the “no exposure” AlN sample performed the worst and yielded AlN^- currents that were on par with the AlO^- current for Al_2O_3 samples. The Al^- current performed slightly better and was almost 3 times higher in the “no exposure” AlN after 1.5 hours of running and almost twice as high at 6.5 hours (see Appendix 7).

2.7 Conclusions

The formation of negative ions is a very complicated process and there still exists many unanswered questions as to why some atoms or molecules become ionized and other don’t. For example, within a sample of AlN the peaks of Al^-, Al_2N^-, AlN^- and Al_2^- can be observed, this would suggest that the AlN molecule is to some degree dissociating during the sputtering process and forming new molecules, or remaining as individual atoms and becoming ionized. The fact that AlN^- exists as a prolific beam of negative ions could indicate that the entire molecule of AlN^- is being ionized without dissociating or that it is dissociating during sputtering and then reforming as AlN^-. For a sample of Al_2O_3 there does not exist a negative ion beam of $Al_2O_3^-$ and therefore the entire

molecule must be dissociating during the sputtering process. As well, the AlF_3 samples must have been dissociating and since the fluorine atoms can be readily ionized there is a very pronounced beam of F^-. Additionally, the AlF_3 molecules may either be remaining as a whole and picking up an extra F^- to form AlF_4^- or the molecule could be dissociating and reforming.

Observations from the SIB injector show that AlF_3 did not yield any notable currents of atomic aluminum. The AlF_3 produced a somewhat substantial current for the aluminum species AlF_4^-; however the current was still much lower than that for AlN^- or AlO^-. The beam was dominated by the production of F^- ions. It would appear the molecule is dissociating during the sputtering process and fluorine is competing with aluminum for the electrons. In addition, fluorine is a very reactive species and will readily attach itself to materials within the AMS system contaminating the following runs (Mills, 2012). Whereas previous studies have found fluorine compounds to facilitate the production of fluorine molecular anions for aluminum measurements there is no improvement in using AlF_3 as a source material over the now existing Al_2O_3. Therefore, it is highly unlikely AlF_3 would be used as a source material for the AMS measurements of ^{26}Al.

In each comparable case pure AlN, regardless of the exposure time, outperformed pure Al_2O_3 on both the test stand and the SIB injector. Based on the overall source performance the magnitude of the individual peaks may change from sample to sample. However, the relative peak intensities of AlN^-/AlO^- and Al^-/Al^- between samples of AlN and Al_2O_3, which were run under similar source conditions, remained fairly constant. Most of the total beam for an Al_2O_3 sample is attributed to a current of $^{16}O^-$ and in fact

the molecular aluminum negative ion beam (AlO^-) current is even higher in an AlN sample. To achieve the best results for an AlN material it should be prepared and exposed to air for approximately 1 hour. Even if a one-hour exposure is not achievable then a longer exposure to air will still yield reasonable results.

Amongst the exposed samples, the longer the AlN sample was exposed to air the worse it performed in the production of negative ions. Therefore, the slight decomposition of AlN in moist air to form $Al(OH)_3$ and NH_3 somehow facilitates the production of negative ions for aluminum species. However, it is well know within the ceramics industry that oxygen greatly reduces the thermal conductivity of AlN (Li *et al.*, 2005). It would appear that there is an optimal level of oxidization for the AlN compound and if that level is surpassed the compound's performance in the production of negative ions will decrease. This indicates that the optimal source material is in fact not a pure AlN sample but a metastable compound that occurs as AlN hydrolyzes to $Al(OH)_3$ in the presence of moisture. A study by J. Li *et al*. (2005) demonstrated that initially the hydrolysis reaction produces amorphous AlOOH as an intermediate product and then it is further hydrolyzed to polymorphs of $Al(OH)_3$ including mixtures of bayerite, nordstrandite and gibbsite, which form agglomerates around the unreacted AlN (Li *et al.*, 2005). The surfaces of the AlN powders are hydrolyzed first having particles of AlOOH and subsequently $Al(OH)_3$ nucleating and growing around the parent AlN particles. With the proceeding hydrolysis of the AlN the resulting agglomerates become larger and larger and envelope the unreacted AlN inside. Reaction 5 describes the intermediate step to form amorphous AlOOH and Reaction 6 describes further hydrolysis to form $Al(OH)_3$.

$$AlN + 2H_2O \rightarrow AlOOH_{amorph} + NH_3 \quad (5)$$

$$AlOOH_{amorph} + H_2O \rightarrow Al(OH)_3 \quad (6)$$

Based on observations it would be more beneficial to transmit a beam of AlN^- for ^{26}Al measurements rather than Al^-. All of the AlN samples yielded AlN^- currents that were at least 6 times the yield of the Al^- currents. Traditionally when performing ^{26}Al AMS measurements for geological samples the system is tuned to transmit a beam of $^{26}Al^-$ to eliminate the largest isobar, ^{26}Mg. Magnesium atoms do not form negative ions and so by using a beam of atomic aluminum any ^{26}Mg that may be in the sample will not be ionized and cannot be accelerated through the system. However, magnesium can bind with other elements in the sample and become ionized as a molecule. The formation of either magnesium nitride (MgN^-) or magnesium oxide (MgO^-), which will also have mass 41 and 43 amu respectively, would introduce a large isobaric interference for aluminum molecular species. Once the beam of ions reaches the stripper foil at the terminal of the accelerator they are stripped of their electrons and the molecules become dissociated. Since magnesium does form positive ions it can be carried through the system as $^{26}Mg^+$ from this point onward. However, at HRIBF because of the high voltages used there exists the capability to fully strip the ions as they exit the accelerator at higher energies. By removing all the electrons a charge difference is created between magnesium (Mg^{12+}) and aluminum (Al^{13+}) and allowing for charge separation techniques to be used.

As predicted, AlN has demonstrated to be a novel and more efficient way for producing beams of ^{27}Al isotopes, which makes it an optimal source material for ^{26}Al AMS measurements of geological samples. The relative peak intensities of AlN^-/AlO^- and AlN^-/Al^- within a sample change over the course of a day with the current of AlN^-

increasing the most at the beginning of a run. For AlN samples the total beam, AlN^- beam and Al^- beam all grow very quickly and in the first couple of hours of running AlN samples outperform Al_2O_3 samples the most. This observation is important when doing AMS measurements of geological material because there is very little sample material. A fast growing current will shorten the measurement time needed preserving sample material as well as allowing for the rapid switching between samples.

2.8 Suggestions for Future Research

The mixed AlN + Al_2O_3 samples did not perform as well as the pure AlN samples. The mixed samples were prepared so that it was a 50:50 AlN to Al_2O_3 ratio by volume with Ag added so that the mixture to Ag was 3:1 by weight. However, when preparing a geological sample as an AlN it is first precipitated as an Al_2O_3 and then reacted to form AlN. Within the ceramics industry a carbothermal reduction technique is used to convert the Al_2O_3 and reports of a near 98% conversion to AlN have been made (Selvaduray & Sheet, 1993). However, these techniques have yet to be attempted at the scale needed for the AMS measurements of geological material. J. Li *et al*. (2005) demonstrated that AlN powders with a higher oxygen content, such as those produced by the carbothermal reduction of Al_2O_3, have protective oxide layers at the surface of the AlN powder and therefore have a better resistance to hydrolysis in moist air (Li *et al.*, 2005). An excess of oxygen within the mixed sample, which increases the resistance to hydrolysis may be one of the reasons the mixed AlN + Al_2O_3 sample does not perform as well as an AlN sample. To further examine the effects of oxygen on an AlN sample it would prove useful to run multiple mixed samples with differing ratios of AlN:Al_2O_3, in

particular a sample with ~2% Al_2O_3 to simulate a converted AlN sample. Observing how AlN samples with different Al_2O_3 contents react in the ion source may lend information as to the differences in chemical behavior between a converted AlN sample and a decomposed AlN sample.

The samples that were exposed to moist air and allowed to decompose yielded better results than an AlN sample with added Al_2O_3. Therefore, there is some indication that the decomposition of AlN to form an intermediate compound, such as AlOOH and aluminum hydroxide $Al(OH)_3$ is an ideal component in the AlN + Ag sample mixture. Since the "one-hour" AlN sample yielded the most prolific negative ion beams it would appear that there exists an optimal level of decomposition. To further investigate the extent of this claim, multiple AlN samples should be made up and exposed to air for various amounts of time. Each of the exposed AlN samples should then be split into two equal parts. One of the samples should be run from the SIB injector and the production of negative ions for Al species should be observed. The other sample should be examined using X-Ray Powder Diffraction techniques. X-Ray Powder Diffraction is an analytical technique that can provide information about the physical property, chemical composition and crystalline structure of the AlN powder (Dutrow & Clark, 2012). The XRD measurements on the AlN powder would characterize any changes in elemental composition as the sample decomposes and the simultaneous measurements from the SIB injector would characterize the effects on the material's performance in the negative ion source.

When preparing samples of exposed AlN the material was mixed with Ag and left fully exposed to air prior to packing into a cathode. Therefore, most of the material was

in contact with the air and susceptible to decomposition. A previous study by Flarend (2004) prepared similar samples under a nitrogen atmosphere but left the samples exposed to air once already packed into a cathode. This technique ensures that only the surface of the AlN sample would have been exposed to the air. It is unknown whether exposing the entire sample or simply the surface will yield different results. Further experimentation is needed to determine how the decomposition in air affects the sample's chemical and physical properties so that its performance within the ion source is altered. Future work could include preparing two identical samples; one left fully exposed prior to packing into a cathode and the other immediately packed into a cathode so only the surface is exposed. Then the samples should be run for similar lengths of time and the beam intensities for the aluminum species compared.

3. PREPARATION OF NATURAL QUARTZ SAMPLES AS ALN TARGETS FOR EARTH SCIENCE APPLICATIONS

3.1 Overview of ^{26}Al Sample Preparation for AMS Measurements

The low natural abundance of cosmogenic ^{26}Al radionuclides in samples presents a key challenge in the accurate determination of its concentration. Any loss of sample material could result in an insufficient signal during analysis and contamination of the sample during processing could result in an unrepresentative isotopic signature being reported. As such, the preparation of geologic samples for the measurement of ^{26}Al is rather extensive and involved. Numerous investigations have focused on optimizing the sample preparation of ^{26}Al (Hunt, 2008, Flarend *et al.*, 2004, Hunt, 2007, Ochs & Ivy-Ochs, 1997 and Strelow *et al.*, 1972) and each laboratory has developed distinct procedures for its preparation and analysis.

As previously discussed, ^{26}Al measurements are typically made and reported in conjunction with measurements of ^{10}Be. This is because both nuclides can be extracted from the same quartz grains and their common chemical behavior allows them to be prepared simultaneously. Both Al and Be are soluble in a range of acids, amphoteric in nature with respect to the formation of hydrogel precipitates in the presence of ammonium salts and similar in their retention behavior in ion exchange columns. The procedures for extracting both Al and Be are similar and done concurrently to produce the oxides BeO and Al_2O_3. The dual analysis by AMS of these two cosmogenic isotopes therefore ultimately provides two independent assessments for the exposure age and erosion history of a single sample.

There are two main phases involved in the sample preparation of ^{26}Al. The first of these involves the concentration and purification of the selected target material/mineral by physical and chemical preparation (parts A and B). The second phase involves the

chemical enrichment of the cosmogenic isotope and separation from interfering isotopes of other interest (parts C and D). Part A involves physically separating out the quartz from other minerals by crushing the rock and sifting the grains. The grain sizes produced by the rock crusher are dependent on the material and rock type. Most quartz bearing rocks will have similar strengths and the crusher is typically set up so that the grain size of the quartz is 0.250 to 0.500mm (Bookhagen, 2009). If the sample contains a high content of non-quartz minerals (feldspars, micas, garnets, zircons, pyroxenes, etc.) a magnetic separation, heavy-liquid separation or a frothing is applied following the sifting of the sample. The process of producing pure mineral separates is very important as the presence of additional minerals can result in the contamination of the ^{10}Be and ^{26}Al and potentially contain interfering elements (^{26}Mg in the case of ^{26}Al, ^{10}B in the case of ^{10}Be) that will invalidate the later measurements. Even a few grains of an accessory mineral (e.g. Beryl in the case of ^{10}Be) can compromise the measurement results (Dunai, 2010). Part B of the sample preparation involves chemically purifying the quartz through a series of acid baths and density separation techniques. This step will remove more easily soluble impurities as well as meteoric components of ^{10}Be and ^{26}Al within the quartz grains. The density separation can be used to remove acid resistant impurities such as small grains of other minerals (ie. garnet and zircon) (Dunai, 2010).

The cleaned quartz grains that have been stripped of mineral impurities and meteoric components can then undergo the chemical procedure for AMS-target preparation. Part C is the most time intensive of the 4 steps and involves the complete isolation of ^{26}Al from the other elements in the quartz sample. Finally, part D involves

producing a material that is suitable for AMS measurements. The processes involved in parts A to D are summarized in Figure 25 below.

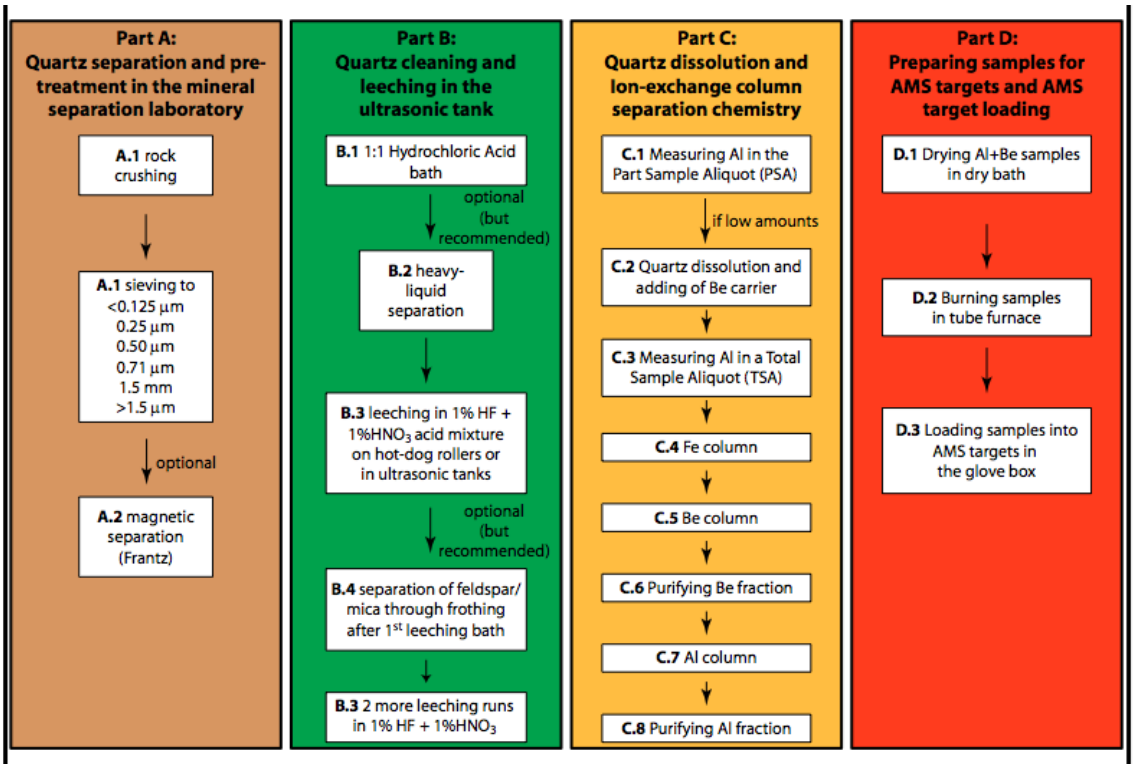

Figure 25: Schematic diagram of the physical and chemical steps used to extract Al and Be from quartz-bearing rocks and the steps that follow in the preparation of BeO and Al_2O_3 for the AMS measurements of ^{10}Be and ^{26}Al. These procedures may differ slightly depending on the laboratory. The figure presented here is taken from the sample preparation manual for UC Santa Barbara (Bookhagen, 2009).

One of the consequences of the mutual chemical separation method used for the extraction of Al and Be nuclides is that both samples must be prepared as oxide cathodes. This is a major limitation in ^{26}Al analysis because Al_2O_3 targets for AMS do not yield a prolific beam of atomic aluminum (Al^-) and because of the presence of molecular isobars, which are ion-optically undesired (i.e. Mg oxide impurities) (Hunt, 2008). A requirement therefore exists for the development of a more suitable target for the AMS measurements of ^{26}Al. This target should produce a prolific beam of atomic and molecular aluminum

negative ions and must not require extensive alteration to the existing sample preparation procedure so that Al can still be prepared alongside Be from a quartz sample. As discussed in chapter 2, aluminum nitride represents a target material that meets these requirements and so a procedure for the preparation of quartz samples as AlN was investigated.

3.2 Conversion of Al_2O_3 to AlN

The chemical synthesis of AlN has been the focus of numerous studies since the early 1990's, with different synthesis methods such as carbothermal reduction, direct nitridation, floating nitridation, chemical vapour deposition, vapour phase and organometallic precursors investigated (Cho & Charles, 1991, Selvaduray & Sheet, 1993, Ercayhan *et al.*, 2004, Tan *et al.*, 1992). As discussed briefly above, for a synthesis method to be applicable to the preparation of an AlN target for AMS analysis it must meet certain criteria. Firstly, the method must include the same raw materials as the existing ^{26}Al sample preparation technique, such that Al and Be targets can still be prepared in unison. The method must not contaminate the sample with outside sources of aluminum or aluminum isobars, which would result in an erroneous measurement. In addition, the method utilized must result in the almost entire conversion for Al_2O_3 to AlN so that isotope fractionation is not introduced. Finally, for the synthesis method to be possible in this study, it must be cost effective and achievable using available equipment. Given these criteria, the synthesis method chosen for the production of AlN in this study is the carbothermal reduction of either Al_2O_3 or $Al(OH)_3$.

The carbothermal reduction process is one of two synthesis methods used to commercially produce AlN powders. The process involves a solid-solid reaction between aluminum oxide and carbon, and the subsequent conversion of aluminum oxide in a nitrogen atmosphere. First the raw materials are selected and the Al_2O_3 powder/graphite powder ratio is defined. In this process, the stoichiometric excess of carbon is essential. The graphite powder serves to increase the reaction rate, complete the transformation, improve powder dispersion and control powder aggregation (Selvaduray & Sheet, 1993). In the next step Al_2O_3 and graphite powder are mixed together at room temperature and atmospheric pressure. The ceramics industry has found that the contact between the two reactants must be improved to protect against large amounts of residual Al_2O_3 (Selvaduray & Sheet, 1993). This improved contact can be achieved through a technique known as wet mixing where the reactants are mixed with a liquid medium and then the material is dried. In the final step the dried mixture is placed within an oven supporting a nitrogen flow or nitrogen atmosphere and fired to a temperature of 1673-2073 K (Selvaduray & Sheet, 1993). This final step results in the conversion of Al_2O_3 powder to an AlN powder. This entire process is presented in a flowchart in Figure 26. The overall reaction is given in reaction 5 below as:

$$Al_2O_3(s) + 3C(s) + N_2(g) \rightarrow 2AlN(s) + 3CO(g) \quad (5)$$

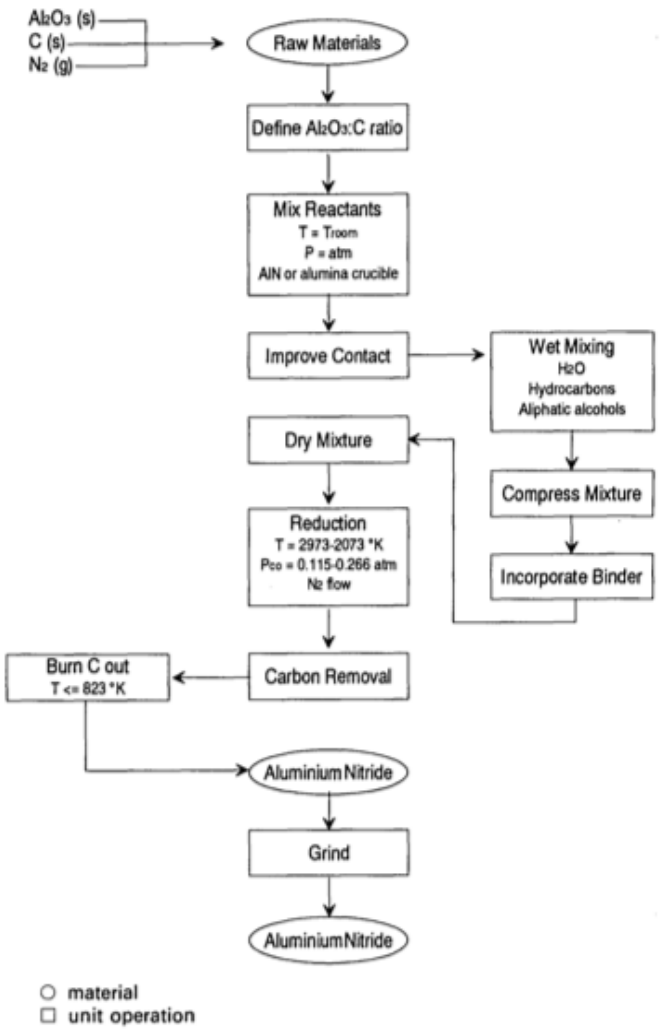

Figure 26: Process flowchart for the carbothermal reduction of Al_2O_3 in the presence of a N_2 flow to produce AlN, as used for industrial purposes. This figure is taken from Selvaduray & Sheet (1993).

3.3 Preparation of Al_2O_3 From Quartz

Two quartz samples (TB0420 and TB0421) were analyzed in this study. These samples were collected in July 2004 from exposed boulders in the Tibetan Plateau of the Himalayas and donated by Dr. Li of the University of Tennessee Department of Geography. The first stage of the sample preparation of AlN and Al_2O_3 AMS targets from the natural quartz samples was conducted at Purdue Rare Isotope Measurement

Laboratory (PRIME Lab). The PRIME AMS facility is built around the Physics Department's tandem accelerator and research focuses on the low-level measurements of ^{14}C, ^{10}Be, ^{26}Al and ^{36}Cl in natural samples.

After purification, samples TB0420 and TB0421 contained approximately 35 g and 12 g of quartz grains respectively, with grain sizes of between 0.250 to 0.500 mm. Before chemical preparation, a sub-fraction of the two samples were analyzed using Inductively Coupled Plasma Optical Emission Spectrometry (ICP-OES) to determine the concentration of Al in each sample. Samples TB0420 and TB0421 had Al concentrations of 17 ppm and 16 ppm, giving a native weight of 0.60 and 0.19 mg respectively. Previous ^{10}Be analysis of these samples reported concentrations that are consistent with the steady state production of Be and Al, with an expected 6.7 times as many ^{26}Al atoms to ^{10}Be atoms (Chmiel, 2012). Based on this production ratio, the measured ^{10}Be concentration and the calculated mass of ^{10}Be per gram of SiO_2 for these samples, an expected mass of ^{26}Al per gram of SiO_2 can be calculated. From this and the measured total concentration of Al provided by ICP-OES, an estimated ratio of $^{26}Al/^{27}Al$ can be determined. These measurements and calculations are presented in Appendix 8.

Following preliminary characterization, samples TB0420 and TB0421were split in to two fractions to allow for the preparation of an Al_2O_3 and an AlN target for each of the samples. Sample TB0420 was split to form samples TB0420 and TB0423, while TB0421 was split to form TB0421 and TB0424. The native Al weight of the split samples was approximately 0.3 mg for TB0420 and TB0423 and 0.1 mg for TB0421 and TB0424. When the Al content in a sample is less than 2 mg, a carrier material containing Al of a known stable aluminum composition is added to ensure sufficient Al is present to

produce at least 4 mg of Al_2O_3 precipitate. Any less material than 4 mg for an AMS target may not be enough to fill a cathode and get a reliable measurement (Chmiel, 2012). Typically 20 g of quartz will contain an excess of ~ 2 mg of Al (Faure & Mensing, 2005). As a result, 1.7 mg of Al carrier had to be added to samples TB0420 and TB0423 following digestion in hydrofluoric acid (HF) and nitric acid (HNO_3), while 1.9 mg of Al carrier had to be added to samples TB0421 and TB0424 to bring the total Al weight up to 2 mg.

The carrier is insensitive to incomplete recovery of Al during the sample preparation process because the ratio of stable to radionuclide isotopes remains fixed. Two additional samples (TB0422 and TB0425) were prepared to characterize the carrier material. An aliquot is taken each sample and digested for analysis by ICP-OES to determine the Al aluminum concentration within the carrier (see Appendix 9). The isotopic signature of Al in a carrier material is then determined by AMS analysis of cathodes prepared solely from a sample of carrier material. This information is then utilized to resolve Al contributions from the carrier material to the sample signature and hence determine the Al signature of the natural sample.

After the sample is dissolved, an Al carrier is added and an Al aliquot is taken the sample goes through a series of steps to remove undesired elements and reduce the volume of the sample. The first step involves the addition of trace-metal grade concentrated sulfuric acid (H_2SO_4) and then the sample is transferred to a platinum crucible and heated to evaporate off any moisture. H_2SO_4 is added a second time to the crucible and then the sample is fumed to remove HF, HNO_3 and silica as H_2SiF_6. Fuming of the residue in an acid with a high boiling point, like H_2SO_4, also destroys fluorides and

drives off boron, a large isobar of ^{10}Be, as BF_3. Once the crucibles have been evaporated to complete dryness, 6M hydrocholic acid (HCl) is added to the residual and then the crucibles are once again evaporated to dryness. The addition of the HCl ensures that the residual solids, mostly fluorides of Be, Al, Fe, Ti and alkali and alkali-earth elements, are converted to chlorides.

The next step involves the removal of the elements of Fe, Ti, Mg, Mn and Ca followed by the precipitation of Al and Be hydroxides. Once again HCl is added to the crucible and the residual sample is dissolved and transferred from the crucible to a Teflon vial. 12.5% Sodium hydroxide (NaOH) is then added to increase the pH so that Al and Be remain trapped as a precipitate, whereas Fe, Ti, Mg, Mn and Ca remain as free ions within the solution. The supernatant containing the Fe, Ti, Mg, Mn and Ca is then siphoned off and discarded while the Al and Be remain within the precipitate. To precipitate the Al and Be as hydroxides an ammonium hydroxide (NH_4OH) is added to the solution to initially increase the pH. HCl is then slowly added until the pH decreases to about 8. A pH of 8 allows for the maximum amount of both Al and Be to precipitate as solid hydroxides of $Al(OH)_3$ and $Be(OH)_2$ (see Figure 27).

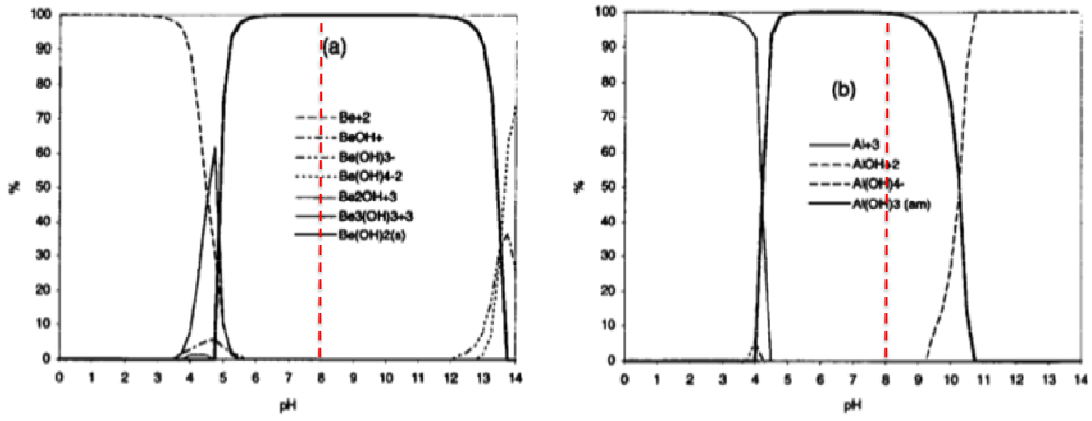

Figure 27: Modeled speciation of Al and Be as a function of pH. At pH ~ 8 almost 100% of the Al and Be will precipitate as a hydroxide phase. This figure is taken from Ochs and Ivy-Ochs (1997).

Once the Al and Be are precipitated as hydroxides the two elements can be separated from one another as well as other cations of the alkali metal (Li, Na, K), alkali-earth metal (Mg, Ca), transition metal (Cu) and alkaline metal (Mg) groups by using a cation-anion exchange resin columns. The aluminum is isolated out using the anion exchange column. Multivalent elements, such as Al^{3+}, form oxalate complexes with stability constants several orders of magnitude larger than Be, Li, K, Na, Cu, Mn, Mg and Ni (Strelow *et al.*, 1972). By rinsing the column with a 0.05M oxalic acid/0.5M HCl mixture the Al remains absorbed within the column resin whereas Cu, Mn and Ni are washed through. Next, a more concentrated 1.2M HCl is added to elute Ti. As shown in Appendix 10 the anion exchange distribution coefficient for aluminum in an oxalic acid-HCl mixture decreases with increasing HCl concentration (Strelow *et al.*, 1972). So the aluminum remains absorbed in the anion resin until a >2.5M HCl is drained through the column, removing Al with it.

Once the Al has been isolated and removed from the anion column it is re-precipitated as an $Al(OH)_3$ amorphous gel. This is achieved by adding 30% NH_4OH to the solution and then slowly adding HCl to bring to pH to as close to 7 as possible. As shown in Figure 27, at a pH of 7 the most stable form of Al will be the hydroxide phase and all the Al will be taken up as $Al(OH)_3$. Once all the $Al(OH)_3$ has precipitated it is transferred to a glass vial and heated at 1600°C for approximately an hour, which thermally decomposes the hydroxide to form a the oxide Al_2O_3. A more detailed version of the sample preparation manual for ^{26}Al and ^{10}Be for AMS measurements by Purdue University is provided in Appendix 13.

All 6 samples (TB0420-TB0425) were prepared as Al_2O_3 and were then brought back to ORNL for the conversion to AlN. Originally all 6 samples were going to be run using an AMS system, however, one was not available during the timeframe needed. Alternatively half of the samples would be run from the SIB injector and the other half of the samples would be kept at HRIBF until they could be run using the AMS system. Three samples were prepared for measurement using the SIB; one Al_2O_3 for comparison and two converted AlN samples. TB0421 was left as an Al_2O_3 whereas its sister sample, TB0424, as well as one the sample with only Al carrier, TB0425, were converted to AlN.

3.4 Preparation of Al_2O_3 Samples as an AlN Target

The conversion of the geological Al_2O_3 samples to AlN was done in a similar fashion to the carbothermal reduction used in the ceramics industry, only on a much smaller scale. A revised version of the procedure was adapted for the small amounts of material used and the limited equipment available. Figure 30 shows a simplified flowchart of the conversion of Al_2O_3 samples to an AlN target for AMS. The most difficult task was working with such small amounts of material. The Al_2O_3 samples were stored in tiny glass vials and removing the sample to weigh the amount of material would have been impractical as there was risk in losing sample material during transfer (see Figure 28). The glass vials were weighed before the sample was added and placed in the oven. The vials were then weighed after the formation of Al_2O_3 in an attempt to weigh the amount of material formed. But during combustion the glass vials de-gassed and so the vials changed in weight making the calculated sample weights erroneous. So the

measurements made were not accurately reflecting the amount of Al_2O_3 material produced.

Figure 28: Image of a glass vial containing Al_2O_3 target material prepared from quartz samples. The $Al(OH)_3$ is placed in the glass vials and then the vials are placed in the oven and heated to 1100°C to form Al_2O_3. Typically enough Ag is added directly to the glass vial to contribute 25% of the mixture weight and then the material is packed into a cathode. A 30 cm rule is provided in the image for scale.

Since the material could not be weighed it had to be assumed that each sample contained about 4 mg of Al_2O_3. This is a reasonable assumption to make as the amount of carrier was calculated and added to each sample so that exactly 2mg of Al was within each sample and 4mg of Al_2O_3 would be formed. Enough graphite powder had to be added to ensure a 1:1 ratio of O:C because as the Al becomes reduced the oxygen is removed as CO. 4 mg of Al_2O_3 yields about $2.36x10^{19}$ atoms of O and so $2.36x10^{19}$ atoms of C were needed, which means about 0.47 mg of graphite powder was needed. It was very difficult to measure out the graphite powder as it was very adhesive and light, but approximately 0.5 mg of graphite powder was added to the TB0424 and TB0425 samples in the glass vial.

To speed up the reduction of the Al_2O_3 powders and convert the Al from an oxide to a nitride the samples were heated in a furnace at a temperature of 1600°C for 1.5 hours

under a nitrogen atmosphere. However, the samples had to be contained within a material that could survive 1600°C temperatures and would not contaminate the sample with any outside source of aluminum. A graphite crucible was chosen to contain the samples while they reacted in the furnace. To ensure that none of the sample was lost a small holder was fashioned out of graphite paper to separately contain each sample within the crucible (see Figure 29).

a) 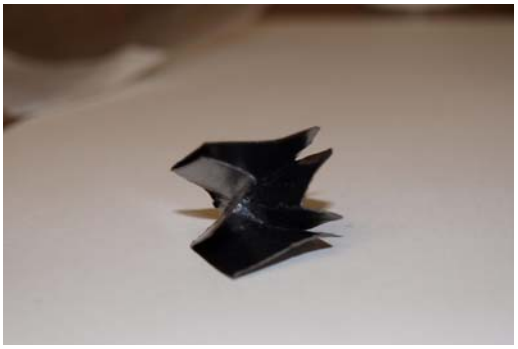 b) 

Figure 29: Photo a) is an example of the container fashioned out of graphite paper in which the Al_2O_3-C mixture was placed. Samples TB0421 and TB0425 both were placed in separate containers. Photo b) shows both samples within graphite paper and then placed into the graphite crucible.

After the graphite crucible containing samples TB0424 and TB0425 was removed from the oven, the samples were immediately mixed with Ag powder and pressed into cathodes. Again because of the extremely small sample size, weighing the sample material was impractical and the amount of Ag added had to be estimated. However, previous studies have found that the ratio of metal matrix to sample material needs not be exact and if the ratio differs anywhere from 1:2-1:4 the performance of the sample in the negative ion source is not drastically affected (Flarend *et al.*, 2004, Hunt, 2007 and Flarend, 2011). A typical cathode used for the SIB injector at HRIBF holds a sample size up to 100 mg, which is far too large for the geological samples. New cathodes had to be drilled out of existing solid copper cathodes and were made to the specifications provided

by the PRIME Lab. A small hole was drilled into solid copper cathodes to accommodate the smaller sample size. Appendix 14 shows the specifications for cathodes used for the AMS measurements of geological material provided by the PRIME Lab.

After the cathodes were prepared they had to be stored for a couple days prior to loading into the source. The samples were handled in such a way so as to minimize their exposure to air so that they were not exposed to an air atmosphere for more than one hour. To avoid decomposition of the AlN the cathodes were stored in argon filled glass vials and wrapped in parafilm multiple times. When it came time to run the samples from the SIB injector each sample was loaded into the source and run for approximately 6 hours. After 6 hours of running the negative ion currents for molecular and atomic aluminum species decreased and there was an increase in the currents of copper ions (mass 63 and 65 amu). This was an indication that the cathode had run out of sample material and that the cathode was being sputtered away instead, which was confirmed upon removing the cathode from the source. During the 6-hour running period mass scans were done as often as possible so that the relative peak intensities could be observed and any unknown peaks could be identified.

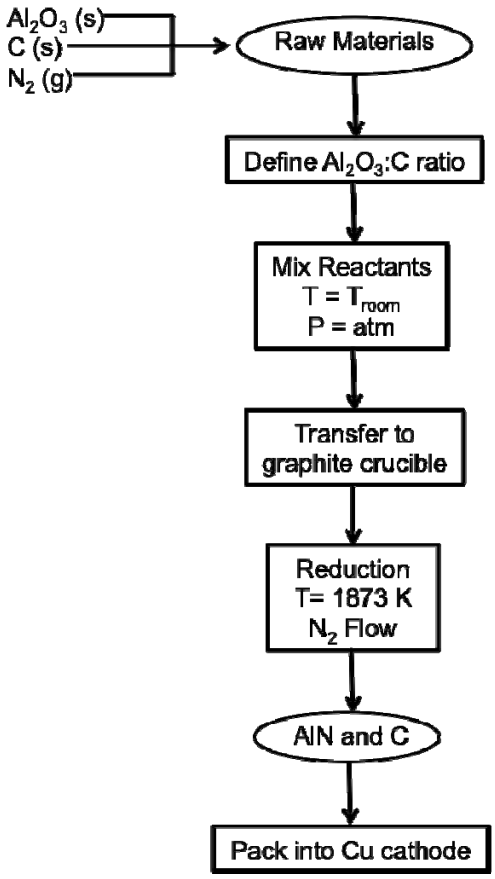

Figure 30: Revised flowchart for the carbothermal reduction of geological Al_2O_3 samples in the presence of N_2 flow to produce AlN for the creation of an AMS target material. This figure is revised from Ochs & Ivy-Ochs (1997).

3.5 Results and Discussion

The converted AlN samples (TB0424 and TB0425) were run from the SIB injector before the Al_2O_3 sample (TB0421). Like the commercial AlN samples, the currents for both TB0424 and TB0425 increased quickly in the beginning and, within the first hour of running, they had almost reached their maximum current. TB0424 performed better than TB0425 as it had a higher total beam current as well as higher beam currents for each individual mass peak observed. There are several reasons that TB0424 may have performed better than TB0425 despite the fact that there preparations were identical. First

of all, TB0425 may have had a higher graphite powder to AlN powder ratio within the sample. If TB0425 had a higher volume percentage of graphite powder than less AlN powder would have been able to sputter away. Secondly, it may be that less Al_2O_3 was able to convert to AlN.

Unlike the commercial AlN samples previously run, the converted AlN samples yielded a higher atomic Al^- current than a molecular AlN^- current. TB0424 yielded a maximum AlN^- current of 123 nA and a maximum Al^- current of 205 nA (see Table 3). Whereas TB0425 only yielded a maximum AlN^- current of 49 nA and a maximum Al^- current of 58 nA (see Figures 31 and 32). Therefore, the ratio of AlN^-/Al^- within a run was always <1. However, the ratio of AlN^-/AlO^- within a sample was similar to that observed for the commercial AlN samples and ranged from about 2-5. In addition, both TB0424 and TB0425 produced substantial beams of aluminum carbide (AlC_2^-) with maximum currents of 1830 nA and 486 nA respectively.

Both TB0424 and TB0425 performed better than TB0421 in producing a beam of atomic aluminum. TB0421 actually yielded results that were comparable to the commercially produced Al_2O_3 samples. TB0421 had a maximum AlO^- negative ion current of 1050 nA and a maximum Al^- negative ion current of 32 nA (see Figure 33). However, these currents were not observed at the same time. The highest AlO^- currents were observed after 6.5 hours of running whereas the highest Al^- current was observed after 1.5 hours of running.

An ANOVA test in SAS was run to analyze the variance between the geological samples. As shown in Appendix 11 the variance in the Al^- currents due to the difference in sample is significant. As shown in Figure 34 the distribution of Al^- currents for the

geological samples are statistically different from one another. Both of the AlN samples have statistically higher Al^- currents than the Al_2O_3 sample. However, the two AlN samples are also statistically different.

Table 3: Highest currents achieved for the geological samples TB0421, which remained as Al_2O_3 and TBO424, TB0425, which were converted to AlN.

Sample	Species	Current (nA)
TB0424	Al^-	205
	AlN^-	123
	AlC_2^-	1830
TB0425	Al^-	58
	AlN^-	49
	AlC_2^-	486
TB0421	Al^-	32
	AlO^-	1050

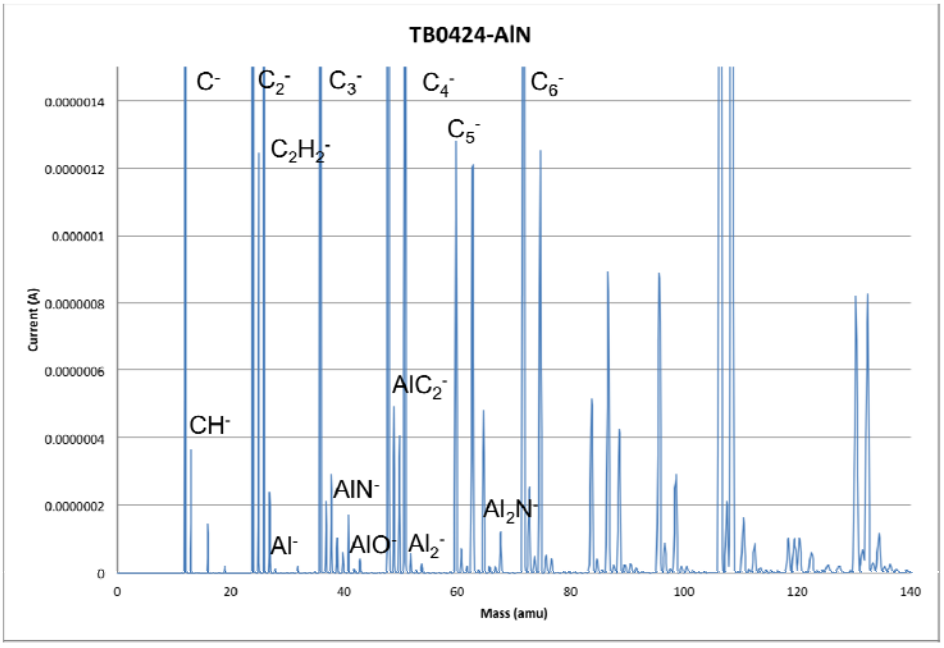

Figure 31: Mass scan displaying the maximum currents observed for sample TB0424 prepared as AlN. The largest peaks observed in the mass scan are attributed to negative ions of carbon species. The scale of the y-axis (current in Amperes) was altered so that the Al-bearing species could be observed. This process prevents the maximum current for the large carbon-bearing species being observed.

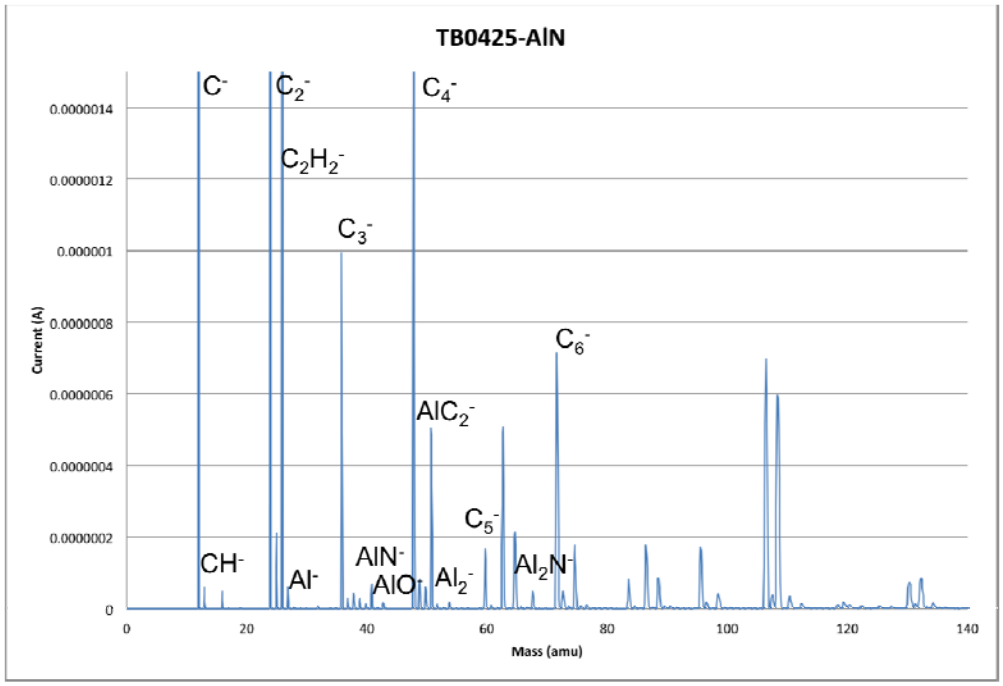

Figure 32: Mass scan displaying the maximum currents observed for sample TB0425 prepared as AlN. The largest peaks observed in the mass scan are attributed to negative ions of carbon species. The scale of the y-axis (current in Amperes) was altered so that the Al-bearing species could be observed. This process prevents the maximum current for the large carbon-bearing species being observed. Sample TB0425 did not yield current intensities as high as those observed for TB0424.

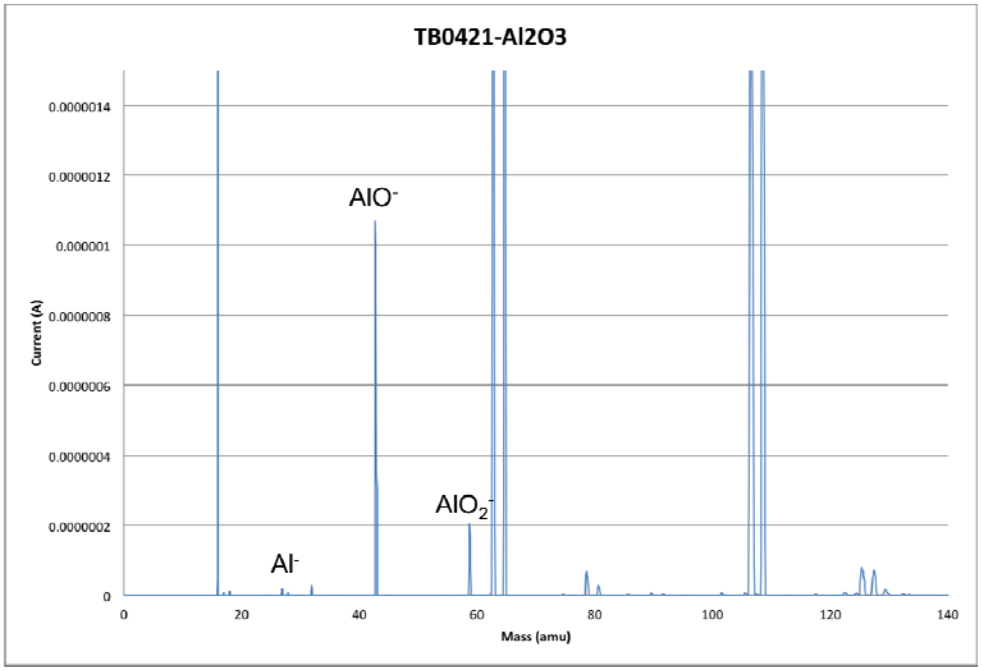

Figure 33: Mass scan displaying the maximum currents observed for sample TB0421 prepared as Al_2O_3. The large peak at mass 16 amu is oxygen, while the large peaks at masses 63 and 65 amu are copper and masses 107 and 109 are silver. The AlO^-, AlO_2^- and Al^- aluminum species all yielded reasonable negative ion currents.

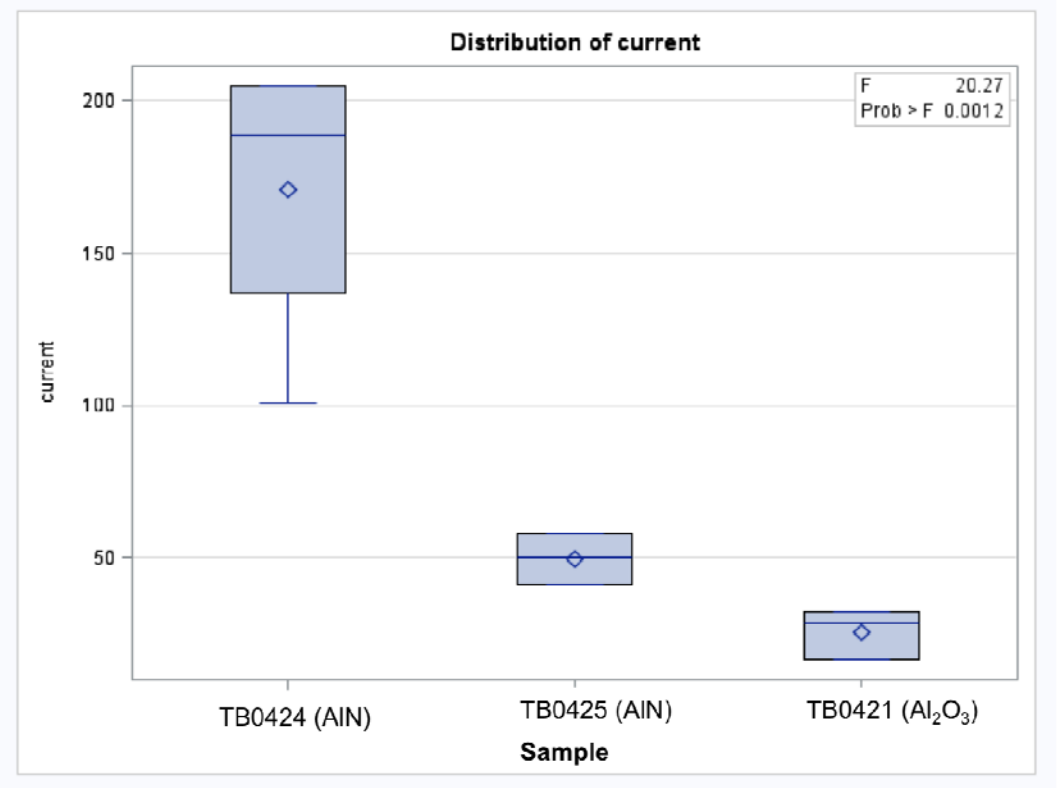

Figure 34: The distribution of Al^- currents for the geological samples. As depicted there is a statistical difference between all of the geological samples, both AlN and Al_2O_3 alike. However, both AlN samples have statistically higher Al^- currents than the Al_2O_3 sample.

One of the concerns when running the geological samples from the SIB injector platform is that the difference in sample size and cathode geometry may have an effect on the negative ion production. Figure 35 shows the two cathode geometries used to measure the commercial samples (photo a) as well as the geological samples (photo b). The concern was that the larger cathodes that are typically used for the SIB injector have the sample material flush with the surface, however, the drilled cathodes for the geological material have a conical indentation. The specifications for the drilled cathode are given in Appendix 14.To observe the effects of differing cathode geometries, three commercial "one-hour" AlN samples were run. Two of the samples were run using the larger sample cathodes and one sample was run using the smaller sample cathode as was used for the

geological samples. The larger cathode samples were run for 8 hours and the smaller cathode sample was run for 6 hours until the source material ran out.

a)  b) 

Figure 35: Photo a) shows a typical cathode used in the SIB injector, which was the standard for the commercial AlN and Al_2O_3 samples run on the source. Picture b) shows the cathode machined especially for geological samples of AlN and Al_2O_3. Note the larger sample size in cathode a) as well the sample material lies almost flush with the cathode surface. Cathode b) contains a smaller sample and has a conical indentation so that the sample is not flush with the surface of the cathode.

An ANOVA test in SAS was run to analyze the variance between the samples with different cathode geometries. As shown in Appendix 12 the variance in the Al^- currents due to the difference in sample is not significant. Statistically there was no difference between the negative ion currents for the larger or smaller cathode samples (see Figure 36). Therefore, the smaller sample size does not hinder the performance of the source material and the cesium beam was well focused and striking the center of the sample.

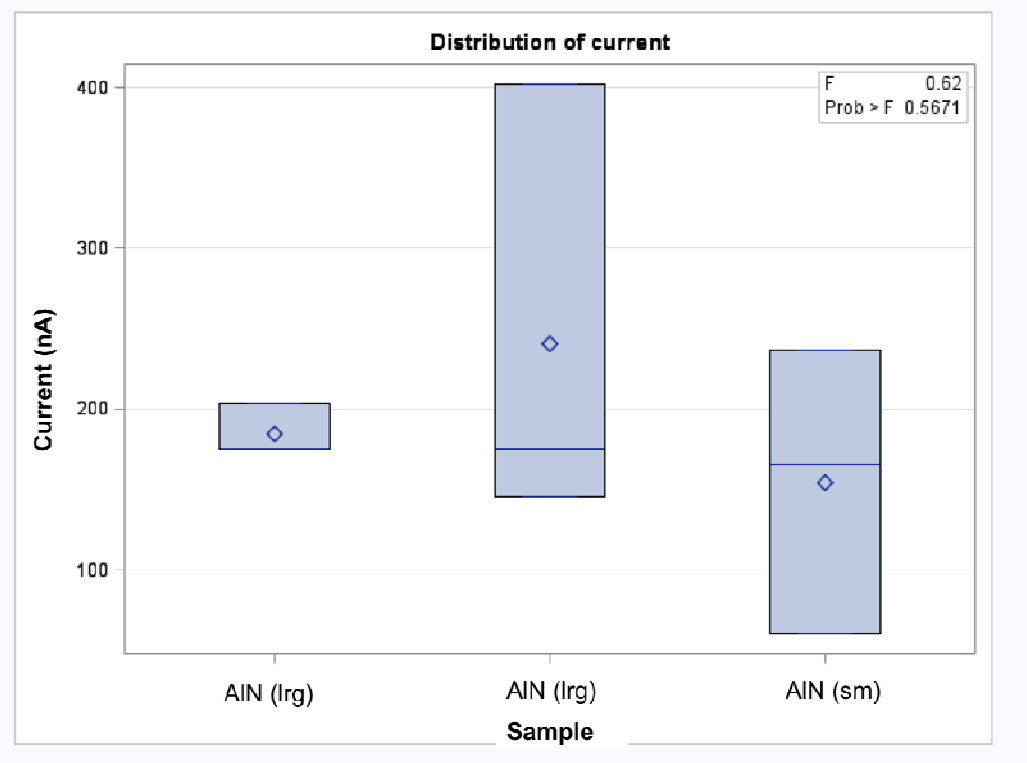

Figure 36: The distribution of Al^- currents for three of the "one-hour" AlN samples that were run using two different cathode geometries. There is no statistical difference between samples run using the larger sample cathode (lrg) and sample run using the smaller sample cathode (sm).

3.6 Conclusions and Suggestions for Future Research

Using a carbothermal reduction process for the synthesis of AlN from Al_2O_3 prepared geological samples did produce promising results. The samples converted to AlN from Al_2O_3 yielded a significantly higher beam of atomic Al^-, however, the two AlN samples are statistically different from one another. A few reasons that the two AlN samples performed differently may be that one sample received more graphite powder, or one sample received more Ag powder or one sample was exposed to air longer than the other or one sample was slightly shielded and wasn't fully exposed to the nitrogen flow and therefore the conversion to AlN wasn't completed. It is difficult to tell if the entire

sample was converted from Al_2O_3, as oxygen was present in every sample and a beam of AlO^- negative ions is always a significant component to AlN samples as well.

While most of the sample converted from Al_2O_3 it definitely did not produce a pure AlN sample. Comparatively, the overall currents for the aluminum species were depressed and the system appeared to be overwhelmed with carbon. It was thought that most of the carbon would be removed with the oxygen as CO or CO_2, however, the graphite powder in the Al_2O_3 + C mixture was very much in excess of the oxygen provided by the Al_2O_3. It may be that the carbon within the graphite paper and graphite crucible were reacting with the Al_2O_3 material as well. The highest current for any aluminum species was seen for the aluminum carbide (AlC_2). Carbon has the ability to form long chains of interconnecting C-C bonds allowing it to form an infinite number of compounds, such as was seen in the mass scans. Like fluorine, carbon is a very reactive element and also readily attaches itself to other elements within the source. The carbon appears to be taking up the Al in the sample and hindering the production of AlN and ultimately Al^- and AlN^- negative ions. Therefore, aluminum carbide is not an ideal source material and a mechanism for removing the excess carbon prior to loading the sample into a cathode is desired.

While the results of samples TB0424 and TB0425 seem promising there are many improvements to the methods that need to be done to optimize the conversion of Al_2O_3 samples to AlN for geological samples. Ercayhan *et al*. (2004) has suggested that better results can be achieved for the carbothermal reduction of $Al(OH)_3$ as opposed to Al_2O_3 to synthesis AlN. It has been discovered that the overall reaction rate between alumina and carbon in nitrogen can be considerably increased by using an $Al(OH)_3$-C mixture instead

of a Al_2O_3-C mixture (Selvaduray & Sheet, 1993). Ercayhan *et al.* (2004) reported producing AIN powders containing 1.0 wt-% oxygen and 0.1 wt-% carbon could be produced from $AI(OH)_3$-C mixtures reacted in nitrogen at 1550°C for 3 hours. It would be worth investigating the use of $Al(OH)_3$ as a raw material as opposed to Al_2O_3. $Al(OH)_3$ is an intermediate step in the sample preparation procedure before the combustion to form Al_2O_3 and so therefore would not require extensive alterations to existing procedures and may even shorten the sample preparation time.

In addition, while outside the scope of this thesis, it would be interesting to further investigate a conversion of Al_2O_3 to AlN which includes steps for the removal of carbon, as is done in the ceramics industry. For the industrial synthesis of AlN the carbon is removed in a couple different ways. One method for the removal of C is through the oxidization and heating of the sample to 599-800°C. The idea being that the oxidization temperature for AlN is 800°C and so as long as the sample is kept at reasonable temperature the material will not oxidize back to Al_2O_3 (Selvaduray & Sheet, 1993). This process may be possible for the geological samples as long as the combustion took place in a dry environment to avoid the decomposition of AlN to $Al(OH)_3$. Another method for the removal of carbon is through reacting the sample with boric oxide in a nitrogen atmosphere at temperatures anywhere from 200-2059°C (Selvaduray & Sheet, 1993). However, since boron is such a large isobar for ^{10}Be the introduction of boron to the sample may be undesirable is simultaneous measurement of ^{26}Al and ^{10}Be are being done.

While the sample preparation of AlN still needs revising one key finding, when preparing and running the geological samples from the SIB injector, is that the cathode geometry appears to make a slight difference in the production of negative ions. The fact

that the smaller sample size does not hinder the beam focus and increases the production of negative ions indicates that smaller sample size can now be used at HRIBF. This is important to note if geological samples will continue to be run at HRIBF. Commonly only a couple milligrams of material are produced from geological materials for cosmogenic nuclide AMS measurements. The system at HRIBF appears to be ideal for handling geological samples.

4. CONCLUDING REMARKS

Negative ions are formed through exoergic attachment processes in which an electron attaches itself to a neutral atom or molecule. The production of negative ion beams in a source is not well understood, with an entire field dedicated to examining how they are produced and subsequently behave. Negative ion source operations can vary substantially and there are many unknown variables associated with the production of a negative ion beam. Despite these uncertainties associated with the mechanisms of negative ion beam production and the subsequent controls on their stability, negative ion beams are an interdisciplinary tool and utilized in many different fields of research. The materials sciences utilize negative ion beams to investigate material properties using ion implantation, ion beam etching and ion beam deposition (Ishikawa, 1992 and Ishikawa, 2000). Negative ion beams are also used within atomic and nuclear structure physics research to examine solid-state and atomic-collision applications (Tykesson *et al.*, 1976), as well as nuclear astrophysics research (Alton, 2002). A more recent application involves the use of negative ion sources for fusion applications (Takeiri, 2010, Humphries, 1980, Fantz, 2008 and Hemsworth & Inoue, 2005). The main application for negative ion beams within medical and Earth sciences is as a tool for measuring the concentrations of low-level, rare radioisotopes in samples of interest by AMS.

For cosmogenic radionuclides such as ^{36}Cl, ^{129}I, ^{10}Be and ^{26}Al, with half-lives in the intermediate range (10^5-10^6 years), AMS is the only practical technique for measuring isotopic concentrations. In this thesis, the production of negative ion beams of Al was compared for four different target materials (Al_2O_3, AlN, AlF, and mixed AlN + Al_2O_3) with the aim of identifying which source target provided the most prolific ion beam. The efficiency of the carbothermal reduction technique for the preparation of AlN from two

natural quartz samples was then investigated to assess the fidelity of the technique in producing AlN targets. Successful processing of natural quartz samples would allow for the analysis of cosmogenic ^{26}Al that could be utilized in numerous applications in the Earth sciences.

It is well known that Al target materials do not form a prolific negative ion beam (Flarend, 2004). The production of negative ion beams is further hindered in the Earth sciences by the fact that in-situ cosmogenic ^{26}Al from quartz samples must be prepared as an Al_2O_3. In this thesis it is shown that Al_2O_3 does not perform well within a negative ion source, with experimental results demonstrating that AlN is a much more effective source material. AlN source material run using the SIB injector and the test stand at HRIBF repeatedly showed an increase in Al^- negative ion production. This was particularly pronounced after one hour of exposure of the target in moist air, with the Al^- ion for this particular sample yielding currents 7 times greater that of the Al_2O_3 sample. This is thought to be associated with partial oxidation and crystallization of amorphous AlN to $Al(OH)_3$. Partial decomposition of AlN is suggested here to be favorable for the production of negative ions. However, further work is required to determine the precise chemical and physical controls for the increased productivity associated with this decomposition.

Cosmogenic ^{26}Al produced *in situ* in exposed quartz is observed at levels 10^{-14} times lower than that of ^{27}Al and as such can only be observed when using accelerator mass spectrometry techniques (Faure & Mensing, 2005). As described above, using ^{27}Al as a proxy for ^{26}Al measurements, the AlN source material was shown to be a promising target material for the preparation of quartz samples for AMS measurements. In this

thesis it was demonstrated that, with minimal alteration to common sample preparation procedures it could be possible to prepare quartz samples as an Al_2O_3 target material and then convert the samples to AlN using a carbothermal reduction process. The converted AlN targets yielded higher currents of atomic Al^- than the Al_2O_3, however, the molecular Al^- currents were much lower. The carbothermal reduction process introduces an excess of carbon in to the produced sample, which is manifested by the presence of an abundant source of AlC_2, and this carbon excess also appears to somewhat inhibit the production of AlN^- negative ion currents. Most likely not all of the sample material is being converted to AlN and the aluminum is binding with the carbon to form AlC_2. This material should be removed before loading the sample into a cathode as it produces a current greater than that of the target AlN. This sample preparation procedure therefore requires modification to obtain the maximum yield of AlN for the characterization of ^{26}Al in natural quartz samples for Earth science related research.

Any process that increases the yield for Al by multiple orders of magnitude will have large impacts on the amount of detectable ^{26}Al within natural samples. With improved sensitivity and precision, low-level AMS measurements become more cost-effective with less time needed per sample. The sharp rise in the negative ion beam current for AlN samples at the beginning of a run as documented here is crucial for the measurement of cosmogenic nuclides when dealing with very small sample sizes. The high currents of Al^- for ^{26}Al AMS measurements provided by AlN targets means that analysis may now be achievable on a lower voltage machine. Indeed, it is conceivable that a low voltage machine using an AlN target could achieve better results than a large 4-8MV machine using an Al_2O_3 target (Flarend *et al.*, 2004). While the use of AlN as a

target material provides a new opportunity for applications in the earth sciences, the increased intensity of ^{26}Al ion beams also represents a potential breakthrough for use in other fields of research. Indeed, fields such as nuclear physics, astrophysics, biology and toxicology may utilize this prolific ^{26}Al ion beam to more comprehensively investigate phenomena such as intergalactic ^{26}Al destruction as well as improved AMS measurements for trace amount of ^{26}Al used in the investigation of life threatening diseases, which may otherwise not be possible.

LIST OF REFERENCES

Aardsma, G. (1984) *Accelerator Mass Spectrometry of ^{26}Al*. Unpublished manuscript, Ph.D. Thesis, University of Toronto.

Alton, G. D., Liu, Y., Murray, S. N., Mills, G. D. & Zaim, H. (2002). Efficient negative ion sources for radioactive ion beam applications. *Review of Scientific Instruments, 73,* 796-796

Alvarez, L. W. and Cornog, R. (1939). Helium and Hydrogen of Mass 3. *Physical Review, 56,* 613-613

Ajormand, A. (2010) Accelerator mass spectrometry-enabled studies: current status and future prospects. *Bioanalysis, 2*, 519-541

Argento, D.C., Stone, J.O., Fifield L.K. & Tims, S.G. (2010). Chlorine-36 in seawater. *Nuclear Instruments and Methods in Physics Research B, 268*, 1226-1228

Arnold, J. & Libby, W. (1949). Age determinations by radiocarbon content: checks with samples of known age. *Science, 110*, 678-680

Balco, G., Stone, J. O., Lifton, N. A. & Dunai, T. J. (2008). A complete and easily accessible means of calculating surface exposure ages or erosion rates from ^{10}Be and ^{26}Al measurements. *Quaternary Geochronology. 3,* 174-195

Barker, J. & Day, J. P. (1990). Development of ^{26}Al Accelerator Mass Spectrometry for biological and toxicological applications. *Nuclear Instruments and Methods in Physics Research B, 52*, 540-543

Beene, J. (2011). ISOL science at the Holifield Radioactive Ion Beam Facility. Journal of Physics G: Nuclear and Particle Physics [On-line serial], 38. Downloaded from IOP Publishing

Belchenko, Y. (1993). Surface negative ion production in ion sources. *Review of Scientific Instruments, 64,* 1385-1393

Bennett, C. L., Beukens, R. P., Clover, M. R., Gove, H. E., Liebert, R. B., Litherland, A. E., Purser, K. H. and Sondheim, W. (1977). Radiocarbon dating using electrostatic accelerators: negative ions provide the key. *Science, 198*, 508–510

Bookhagen, B. (2009). Sample Preparation Manual. Unpublished manuscript. Cosmogenic Nuclide Preparation Facility, University of California, Santa Barbara.

Chmiel, G. (2012). Personal Communications. Purdue University, PRIME Lab

Cho, Y. & Charles, J. (1991) Synthesis of nitrogen ceramic powders by carbothermal reduction and nitridation Part 3 Aluminium nitride. *Materials Science and Technology, 7,* 495-504

Clouthier, C. M., Grien, F. & Bruna, P. J. (2003). MRCI studies on the electronic structure of AlN and AlN^- and the electron affinity of AlN. *Journal of Molecular Spectroscopy, 219,* 58-64

Craig, H. & R. Poreda, R. (1986) Cosmogenic ^{3}He in terrestrial rocks: The summit lavas of Maui. *Proceedings of the National Academy of Sciences of the United States of America, 83*, 1970-1974

Davis, R. & Schaeffer, O. (1955) Chlorine-36 in nature. *Annals of the New York Academy of Sciences, 62,* 107-121

Day, J., Barker, J., Evans, L. J. A., Perks, J., Seabright, P. J., Ackrill, P., Lilley, J. S., Drumm, P. V. & Newton, G. W. A. (1991). Aluminum absorption studied by ^{26}Al tracer. *The Lancet, 337,* 1345

Dunai, T. J. (2010). *Cosmogenic Nuclides: Principles, Concepts and Applications in the Earth Surface Sciences.* The United Kingdom: Cambridge University Press.

Dutrow, B. & Clark, C. (2012). X-Ray Powder Diffraction. Unpublished manuscript. Geochemical Instrumentation and Analysis, Science Education Resource Center at Carleton College.

Ercayhan, S., Derin, B., Sahin, F. C. & Yucel, O. (2004). Production of Aluminum Nitride Powders from Seydisehir Aluminum Hydroxide. *Key Engineering Materials, 264-268*, 105-108

Fantz, U, Franzen, P., Kraus, W., Falter, H. D., Berger, M., Christ-Koch, S., Froschle, M., Gutser, R., Heinemann, B., Martens, C., McNeely, P., Riedl, R., Speth, E. & Wunderlich, D. (2008). Low pressure and high power rf sources for negative hydrogen ions for fusion applications (ITER neutral beam injection). *Review of Scientific Instruments, 79*, 02A511

Faure, G. & Mensing, T. M. (2005). *Isotopes Principles and Applications* (Third Edition). Hoboken, New Jersey: John Wiley & Sons, INC.

Flarend, R. (2011). Personal communications. Pennsylvania State University, Physics Department

Flarend, R., Hasan, M. E. & Redd, C. S. (2004) Aluminum nitride as a novel aluminum-26 ion source material for accelerator mass spectrometry. *Nuclear Instruments and Methods in Physics Research B, 223-224*, 263-266

Fogwill, C., Bentley, M. J., Sugden, D. E., Kerr, A. R. & Kubik, P. W (2004). Cosmogenic Nuclides ^{10}Be and ^{26}Al Imply limited Antarctic Ice Sheet Thickening and Low Erosion in the Shackleton Range <1m.y. *Geology, 32*, 265-268

Galindo-Uribarri, A. (2012). Personal Communications. Oak Ridge National Laboratory, Holifield Radioactive Ion Beam Facility.

Galindo-Uribarri, A., Beene, J. R., Danchev, M., Doupe, J., Fuentes, B., Gomez Del Campo, J., Hausladen, P. A., Juras, R. C., Liang, J. F., Litherland, A. E., Liu, Y., Meigs, M. J., Mills, G. D., Mueller, P. E., Padilla-Rodal, E., Pavan, J., Sinclair, J. W. & Stracener, D. W. (2007) Pushing the limits for accelerator mass spectrometry. *Nuclear Instruments and Methods in Physics Research B, 259* 123-130

Globus, R., NASA (2010). Chapter 2: The Physical Properties of Space. [www page] http://settlement.arc.nasa.gov/75SummerStudy/Chapt.2.html

Gosse, J.C. (2007). Cosmogenic nuclide dating; overview. In S.A. Elias (Eds). Encyclopedia of Quaternary science. (pp. 409-411) Elsevier, Amsterdam, Netherlands.

Granger, D. (2012). Personal communications. Purdue University, Earth and Atmospheric Sciences Department

Heisinger, B., Lal, D., Jull, A. J. T., Kublik, P., Ivy-Ochs, S., Neumaier, S., Knie, K., Lazarev, V. & Nolte, E. (2002). Production of selected cosmogenic radionuclides by muons: 1. Fast muons. *Earth and Planetary Science Letters, 200,* 345-355

Hellborg, R. & Skog, G. (2008). Accelerator Mass Spectrometry. *Mass Spectrometry Reviews, 27*, 398-427

Hemsworth, R. S. & Inoue, T. (2005). Positive and Negative Ion Sources for Magnetic Fusion. *IEEE Transactions for Plasma Science, 33*, 1799-1813

Humphries, S. Jr. (1980). Intense pulsed ion beams for fusion applications. *Nuclear fusion, 20,* 1549-1553

Hunt, A. (2008). *Analysis of Factors that Affect Ion Beam Currents for Cosmogenic ^{10}Be and ^{26}Al Analysis by Acceleration Mass Spectrometry (AMS)*. Unpublished Manuscript, Ph.D. Thesis, University of Vermont.

Hunt, A. (2007) Investigation of Metal Matrix Systems for Cosmogenic ^{26}Al Analysis by Accelerator Mass Spectrometry. *Nuclear Instruments and Methods in Physcis Research B, 260,* 633-636

Ishikawa, J. (1992). Negative ion beam technology for materials science. *Review of Scientific Instruments, 63*, 2368-2374

Ishikawa, J. (2000). Applications of heavy-negative-ion sources for material sciences. *Review of Scientific Instruments, 71,* 1036-1041

Jull, A. & Burr, G. (2006) Accelerator mass spectrometry: Is the future bigger or smaller? *Earth and Planetary Science Letters, 243(3-4)*, 305-325

Kameshima, Y., Kuramochi, S., Yasumori, A. & Okada, K. (1998) Analysis of Surface State and Stability during Storage of AlN Powders by X-ray Photoelectron Spectroscopy. *Journal of the Ceramic Society of Japan, 106*, 749-753

Kieser, W. E., Zhao, X.-L., Eliades, J. & Litherland, A. E. (2012) Fluoride sample matrices and reaction cells — new capabilities for isotope measurements in accelerator mass spectrometry. EPJ Web of Conferences [On-line serial], 24.

Kilius, L., Beukens, R. P., Chang, K. H., Lee, H. W., Litherland, A. E., Elmore, D., Ferraro, R. & Gove, H. E. (1979). Separation of ^{26}Al and ^{26}Mg Isobars by Negative Ion Mass Spectrometry. *Nature, 282*, 488-489

Kurz, M. (1986). Cosmogenic helium in a terrestrial igneous rock. *Nature, 320*, 435-439

Kutschera, W. (2005). Progress in isotope analysis at ultra-trace level by AMS. *International Journal of Mass Spectrometry, 242,* 145-160

Lal, D. (1988). In-situ produced cosmogenic isotopes in terrestrial rocks. *Annual Review of Earth and Planetary Sciences, 16,* 355-388

Lal, D., Nishiizumi, K. & Arnold, J. R. (1987). *In situ* cosmogenic ^{3}H, ^{14}C, and ^{10}Be for determining the net accumulation and ablation rates of ice sheets. *Journal of Geophysical Research, 92*, 4947-4952

Li, J., Nakamura, M., Shirai, T., Matsumaru, K. & Ishizaki, K. (2005). Hyrolysis of Aluminum Nitride Powders in Moist Air. *Advances in Technology of Materials and Materials Processing, 7*, 37-42

Li, Y., & Harbor, J. (2009). Cosmogenic nuclides and geomorphology: Theory, limitations and applications. In D. M. Ferrari & A. R. Guiseppi (Eds), *Geomorphology and Plate Tectonics* (pp. 1-33) Nova Science Plublishers, Inc.

Masarik, J. & J. Beer, J. (1999). Simulation of particle fluxes and cosmogenic nuclide production in the Earth's atmosphere. *Journal of Geophysical Research, 104,* 12099-13012

Middleton, R. (1977). A survey of negative ions from a sputter source. *Nuclear Instruments and Methods, 144,* 373-399

Middleton, R. (1990). A Negative-Ion Cookbook. Unpublished manuscript. University of Pennsylvania.

Mills, G. (2012) Personal communications. Oak Ridge National Laboratory, Holifield Radioactive Ion Beam Facility

National Electrostatics Coorporation. (2007). Negative Ion Beam Sources [www page] http://www.pelletron.com/negion.htm

Nelson, D. E., Korteling, R. G. and Stott, W. R. (1977). Carbon-14 direct detection at natural concentrations. *Science, 198*, 507–508.

Nishiizumi, K., Kohl, C. P., Arnold, J. R., Dorn, R., Klein, I., Fink, D., Middleton, R. & Lal, D. (1993) Role of *in situ* cosmogenic nuclides ^{10}Be and ^{26}Al in the study of diverse geomorphic processes. *Earth Surface Processes and Landforms*, *18*, 407-425

Nishiizumi, K., Lal, D., Klein, J., Middleton, R. & Arnold, J. R. (1986) Production of 10Be and 26Al by cosmic rays in terrestrial quartz *in situ* and implications for erosion rates. *Nature, 319*, 134-136

Ochs, M. & Ivy-Ochs, S. (1997). The chemical behavior of Be, Al, Fe, Ca and Mg during AMS target preparation from terrestrial silicates modeled with chemical speciation calculations. *Nuclear Instruments and Methods in Physics Research B, 123*, 235-240

Pegg, D. (2004). Structure and dynamics of negative ions. *Reports on Progress in Physics, 67,* 857-905

Phillips, F., Leavy, B. D., Jannik, N. O., Elmore, D. & Kubik, P. W. (1986) The accumulation of cosmogenic chlorine-36 in rocks: A method for surface exposure dating. *Science, 231*, 41-43

Raisbeck, G., Yiou, F., Fruneau, M., Loiseaux, J. M., Lieuvin & M., Ravel, J. C. (1979) Deposition rate and seasonal variations in precipitation of cosmogenic ^{10}Be. *Nature, 282*, 279-280

Rienstra-Kiracofe, J. C., Tschumper, G. S. & Schaefer, H. F. (2002). Atomic and molecular electron affinities: Photoelectron experiments and theoretical computation. *Chemical Reviews, 102,* 231-282

Selvaduray, G. & Sheet, L. (1993). Aluminum Nitride: Reviews of Synthesis Methods. *Materials Science and Technology, 9*, 463-473

Schaefer, J.M., and Lifton, N. (2007). Cosmogenic nuclide dating; methods. In S.A. Elias (Eds). Encyclopedia of Quaternary science. (pp. 412-419). Elsevier, Amsterdam, Netherlands.

Strelow, F. W. E., Weinert, C. H. S. W. & Eloff, C. (1972). Distribution Coefficients and Anion Exchange Behavior of Elements in Oxalic Acid-Hydrochloric Acid Mixtures. *Analytical Chemistry, 44*, 2352-2356

Takeiri, Y. (2010). Negative ion source development for fusion applications. *Review of Scientific Instruments, 81,* 02B114

Tan, B. J., Xiao, Y. & Suib, S. L. (1992). Thermodynamic Analysis of the Thermal Nitridation of Aluminum Oxide by Ammonia and Methane. *Chemical Materials, 4*, 648-657

Tuniz, C., Kutschera, W., Fink, D., & Herzog, G. F. (1998) *Accelerator Mass Spectrometry: Ultrasensitive Analysis for Global Science.* New York: CRC Press.

Tykesson, P., Andersen, H. H. & Heinemeier, J. (1976). Further investigations of ANIS (The Aarhus Negative Ion Source). *IEEE Transactions on Nuclear Science, 23,* 1104-1108

Weiler, R. (2002). Cosmic-Ray- Produced Noble Gases in Meteorites. *Reviews in Mineralogy and Geochemistry, 47*, 125-170

Yu, M. L. (1978). Work-Function Dependence of Negative Ion Production during Sputtering. *Physical Review Letters, 40,* 574-577

Zhao, X.-L., Litherland, A. E., Doupe, J. P. & Kieser, W. E. (2004). The Potential for AMS Analysis of ^{10}Be using BeF^-. *Nuclear Instruments and Methods in Physics Research B, 223-224,*199-204

APPENDIX

Appendix 1: The following table contains the raw data collected from the stable injector after each mass scan. After running a mass scan the peaks of interest were identified and the bending magnet was tuned to examine the peak current for each mass and the results are recorded in the table shown. The currents reported below were rounded to the nearest nA.

Table 4: Raw data collected from mass scans taken using the stable injector.

Date	Time	Sample	Molecule	Mass	Current (nA)	% of Total Beam
5/31/12	10:10	Al2O3	total beam		57000	100
			O	16	6200	10.87719298
			OH	17	145	0.254385965
			Al	27	58	0.101754386
			AlO	43	1070	1.877192982
			AlO2	59	360	0.631578947
5/31/12	14:50	Al2O3	total beam		82000	100
			O	16	12600	15.36585366
			OH	17	170	0.207317073
			Al	27	100	0.12195122
			AlO	43	1800	2.195121951
			AlO2	59	520	0.634146341
6/4/12	12:15	AlN (1 hr)	total beam		33000	100
			O	16	6200	18.78787879
			OH	17	58	0.175757576
			Al	27	820	2.484848485
			AlN	41	4400	13.33333333
			AlO	43	2600	7.878787879
			Al2	54	1000	3.03030303
			AlO2	59	57	0.172727273
			Al2N	68	3700	11.21212121
			Ag	107	620	1.878787879
			Ag	109	740	2.242424242
6/4/12	15:30	AlN (1 hr)	total beam		30000	100
			O	16	7400	24.66666667
			OH	17	28	0.093333333
			Al	27	1000	3.333333333
			AlN	41	7100	23.66666667
			AlO	43	3000	10
			Al2	54	1700	5.666666667
			AlO2	59	57	0.19
			Al2N	68	5200	17.33333333
			Ag	107	1800	6

Table 4: Continued

Date	Time	Sample	Molecule	Mass	Current (nA)	% of Total Beam
			Ag	109	2080	6.933333333
6/5/12	10:15	AlN (1 hr)	total beam		25000	100
			O	16	7600	30.4
			OH	17	28	0.112
			Al	27	890	3.56
			AlN	41	6400	25.6
			AlO	43	3100	12.4
			Al2	54	1800	7.2
			AlO2	59	55	0.22
			Al2N	68	5200	20.8
			Ag	107	2100	8.4
			Ag	109	2100	8.4
6/5/12	15:30	AlN (1 hr)	total beam		23100	100
			O	16	9200	39.82683983
			OH	17	19	0.082251082
			Al	27	1000	4.329004329
			AlN	41	7600	32.9004329
			AlO	43	3100	13.41991342
			Al2	54	2500	10.82251082
			AlO2	59	50	0.216450216
			Al2N	68	5400	23.37662338
			Ag	107	2600	11.25541126
			Ag	109	2900	12.55411255
6/6/12	10:20	AlN (2 days)	total beam		30000	100
			O	16	1800	6
			OH	17	8.3	0.027666667
			Al	27	300	1
			AlN	41	2040	6.8
			AlO	43	880	2.933333333
			Al2	54	500	1.666666667
			AlO2	59	24	0.08
			Cu	63	520	1.733333333
			Cu	65	245	0.816666667
			Al2N	68	1700	5.666666667
			Ag	107	250	0.833333333
			Ag	109	300	1
6/6/12	15:30	AlN (2 days)	total beam		28000	100

Table 4: Continued

Date	Time	Sample	Molecule	Mass	Current (nA)	% of Total Beam
			O	16	1740	6.214285714
			OH	17	4.7	0.016785714
			Al	27	290	1.035714286
			AlN	41	2050	7.321428571
			AlO	43	725	2.589285714
			Al2	54	620	2.214285714
			AlO2	59	11	0.039285714
			Cu	63	592	2.114285714
			Cu	65	280	1
			Al2N	68	1800	6.428571429
			Ag	107	1000	3.571428571
			Ag	109	1050	3.75
6/7/12	12:30	AlN + Al2O3	total beam		25000	100
			O	16	1740	6.96
			OH	17	20	0.08
			Al	27	28	0.112
			AlN	41	72	0.288
			AlO	43	360	1.44
			Al2	54	20	0.08
			AlO2	59	71	0.284
			Cu	63	175	0.7
			Cu	65	83	0.332
			Al2N	68	48	0.192
			Ag	107	85	0.34
			Ag	109	80	0.32
6/7/12	15:25	AlN + Al2O3	total beam		28000	100
			O	16	1700	6.071428571
			OH	17	18	0.064285714
			Al	27	23	0.082142857
			AlN	41	35	0.125
			AlO	43	350	1.25
			Al2	54	11	0.039285714
			AlO2	59	71	0.253571429
			Cu	63	210	0.75
			Cu	65	82	0.292857143
			Al2N	68	28	0.1
			Ag	107	50	0.178571429
			Ag	109	50	0.178571429

Table 4: Continued

Date	Time	Sample	Molecule	Mass	Current (nA)	% of Total Beam
6/14/12	11:15	Al2O3	total beam		73600	100
			O	16	12000	16.30434783
			OH	17	1250	1.698369565
			Al	27	81	0.110054348
			AlO	43	1000	1.358695652
			AlO2	59	347	0.471467391
			Cu	63	100	0.135869565
			Cu	65	46	0.0625
			Ag	107	700	0.951086957
			Ag	109	700	0.951086957
	16:05	Al2O3	total beam		106000	100
			O	16	13000	12.26415094
			OH	17	404	0.381132075
			Al	27	147	0.138679245
			AlO	43	1830	1.726415094
			AlO2	59	515	0.485849057
			Cu	63	200	0.188679245
			Cu	65	95	0.089622642
			Ag	107	1800	1.698113208
			Ag	109	1500	1.41509434
6/15/12	10:30	AlN-no exposure	total beam		30000	100
			O	16	1450	4.833333333
			OH	17	6	0.018666667
			Al	27	200	0.666666667
			AlN	41	1210	4.033333333
			AlO	43	620	2.066666667
			Al2	54	400	1.333333333
			AlO2	59	12	0.04
			Cu	63	300	1
			Cu	65	140	0.466666667
			Al2N	68	1050	3.5
			Ag	107	430	1.433333333
			Ag	109	490	1.633333333
	15:30		total beam		27700	100
			O	16	1530	5.523465704
			OH	17	5	0.016967509

Table 4: Continued

Date	Time	Sample	Molecule	Mass	Current (nA)	% of Total Beam
			Al	27	234	0.844765343
			AlN	41	1260	4.548736462
			AlO	43	600	2.166064982
			Al2	54	500	1.805054152
			AlO2	59	7	0.024548736
			Cu	63	515	1.859205776
			Cu	65	205	0.740072202
			Al2N	68	1050	3.790613718
			Ag	107	1020	3.682310469
			Ag	109	880	3.176895307
6/18/12	11:00	AlF3	total beam		16000	100
			O	16	210	1.3125
			OH	17	2	0.014375
			F	19	1700	10.625
			Al	27	1	0.005
			F2	38	4	0.025
			AlN	41	None	0
			AlO	43	13	0.08125
			AlF	46	None	0
			Al2	54	0	0
			AlO2	59	11	0.06875
			Cu	63	4	0.02375
			AlF2/Cu	65	16	0.1
			Al2N	68	None	0
			Al2F	73	None	0
			Al2F2	92	None	0
			Ag	107	14	0.0875
			Ag	109	13	0.08125
	15:10		total beam		16000	100
			O	16	160	1
			OH	17	3	0.016875
			F	19	2500	15.625
			Al	27	1	0.005625
			F2	38	6	0.0375
			AlN	41	None	0
			AlO	43	10	0.06125
			AlF	46	None	0
			Al2	54	0	0

Table 4: Continued

Date	Time	Sample	Molecule	Mass	Current (nA)	% of Total Beam
			AlO2	59	8	0.04875
			Cu	63	8	0.05125
			AlF2/Cu	65	20	0.125
			Al2N	68	None	0
			Al2F	73	None	0
			Al2F2	92	None	0
			AlF4	103	145	0.90625
			Ag	107	10	0.06
			Ag	109	9	0.0575
7/17/12	12:00	AlF3	total beam		30300	100
			O	16	16	0.053135314
			OH	17	0	0
			F	19	2	0.006765677
			Al	27	1	0.004290429
			F2	38	5	0.015841584
			AlN	41	0	0
			AlO	43	2	0.007590759
			AlF	46	0	0
			Al2	54	6	0.018481848
			AlO2	59	0	0
			Cu	63	86	0.283828383
			AlF2/Cu	65	85	0.280528053
			Al2N	68	0	0
			Al2F	73	0	0
			Al2F2	92	0	0
			AlF4	103	500	1.650165017
			Ag	107	68	0.224422442
			Ag	109	58	0.191419142
	15:30		total beam		22000	100
			O	16	3	0.015454545
			OH	17	0	0
			F	19	800	3.636363636
			Al	27	1	0.004318182
			F2	38	2	0.009090909
			AlN	41	0	0
			AlO	43	1	0.002045455
			AlF	46	0	0
			Al2	54	4	0.017727273

Table 4: Continued

Date	Time	Sample	Molecule	Mass	Current (nA)	% of Total Beam
			AlO2	59	0	0
			Cu	63	41	0.186363636
			AlF2/Cu	65	34	0.154545455
			Al2N	68	0	0
			Al2F	73	0	0
			Al2F2	92	0	0
			AlF4	103	190	0.863636364
			Ag	107	24	0.109090909
			Ag	109	20	0.090909091
8/1/12	11:30	AlN (1 hr)	total beam		33700	100
			O	16	1020	3.026706231
			OH	17	7	0.019881306
			Al	27	143	0.424332344
			AlN	41	1020	3.026706231
			AlO	43	515	1.528189911
			Al2	54	205	0.608308605
			AlO2	59	19	0.056379822
			Cu	63	580	1.721068249
			Cu	65	285	0.845697329
			Al2N	68	825	2.448071217
			Ag	107	145	0.430267062
			Ag	109	170	0.504451039
	15:00		total beam		31300	100
			O	16	740	2.364217252
			OH	17	3	0.008626198
			Al	27	140	0.447284345
			AlN	41	1020	3.258785942
			AlO	43	350	1.118210863
			Al2	54	240	0.766773163
			AlO2	59	8	0.025878594
			Cu	63	613	1.958466454
			Cu	65	284	0.907348243
			Al2N	68	880	2.811501597
			Ag	107	340	1.086261981
			Ag	109	336	1.073482428
8/2/12	11:15	Al2O3 + AlN	total beam		15500	100
			O	16	1410	9.096774194

Table 4: Continued

Date	Time	Sample	Molecule	Mass	Current (nA)	% of Total Beam
			OH	17	16	0.10516129
			Al	27	19	0.124516129
			AlN	41	20	0.129677419
			AlO	43	146	0.941935484
			Al2	54	6	0.036129032
			AlO2	59	29	0.187741935
			Cu	63	59	0.379354839
			Cu	65	24	0.156129032
			Al2N	68	11	0.072258065
			Ag	107	14	0.091612903
			Ag	109	13	0.085806452
	15:15		total beam		30300	100
			O	16	1500	4.95049505
			OH	17	10	0.031353135
			Al	27	20	0.066336634
			AlN	41	20	0.0669967
			AlO	43	212	0.699669967
			Al2	54	8	0.027062706
			AlO2	59	42	0.136963696
			Cu	63	80	0.264026403
			Cu	65	35	0.115511551
			Al2N	68	14	0.045874587
			Ag	107	20	0.067326733
			Ag	109	20	0.064356436
8/3/12	9:30	AlN (2 days)	total beam		31800	100
			O	16	1260	3.962264151
			OH	17	11800	37.10691824
			Al	27	120	0.377358491
			AlN	41	858	2.698113208
			AlO	43	520	1.635220126
			Al2	54	200	0.628930818
			AlO2	59	19	0.059433962
			Cu	63	416	1.308176101
			Cu	65	198	0.622641509
			Al2N	68	620	1.949685535
			Ag	107	212	0.666666667
			Ag	109	242	0.761006289
	15:00		total beam		33500	100

Table 4: Continued

Date	Time	Sample	Molecule	Mass	Current (nA)	% of Total Beam
			O	16	1280	3.820895522
			OH	17	5	0.014328358
			Al	27	148	0.441791045
			AlN	41	1200	3.582089552
			AlO	43	613	1.829850746
			Al2	54	340	1.014925373
			AlO2	59	9	0.028059701
			Cu	63	517	1.543283582
			Cu	65	242	0.72238806
			Al2N	68	1060	3.164179104
			Ag	107	1070	3.194029851
			Ag	109	870	2.597014925
9/6/12	15:00	Al2O3	total beam		22200	100
			O	16	1500	6.756756757
			OH	17	60	0.27027027
			Al	27	10	0.043243243
			AlO	43	250	1.126126126
			AlO2	59	82	0.370720721
			Cu	63	117	0.527027027
			Cu	65	49	0.220720721
			Ag	107	6	0.025225225
			Ag	109	6	0.02509009
9/7/12	10:30	Al2O3	total beam		25400	100
			O	16	2150	8.464566929
			OH	17	29	0.112598425
			Al	27	14	0.053543307
			AlO	43	334	1.31496063
			AlO2	59	122	0.480314961
			Cu	63	207	0.81496063
			Cu	65	84	0.329527559
			Ag	107	12	0.046456693
			Ag	109	11	0.043307087
	15:00		total beam		23200	100
			O	16	3130	13.49137931
			OH	17	17	0.073706897
			Al	27	24	0.101724138
			AlO	43	486	2.094827586

Table 4: Continued

Date	Time	Sample	Molecule	Mass	Current (nA)	% of Total Beam
			AlO2	59	163	0.702586207
			Cu	63	252	1.086206897
			Cu	65	97	0.419827586
			Ag	107	17	0.072844828
			Ag	109	13	0.057327586
9/10/12	9:50	Al2O3	total beam		47500	100
			O	16	4200	8.842105263
			OH	17	29	0.060210526
			Al	27	28	0.058315789
			AlO	43	596	1.254736842
			AlO2	59	205	0.431578947
			Cu	63	208	0.437894737
			Cu	65	80	0.168421053
			Ag	107	14	0.028421053
			Ag	109	11	0.023368421
	15:00		total beam		69200	100
			O	16	7310	10.56358382
			OH	17	66	0.095520231
			Al	27	72	0.103901734
			AlO	43	742	1.072254335
			AlO2	59	253	0.365606936
			Cu	63	103	0.148843931
			Cu	65	48	0.069364162
			Ag	107	28	0.040028902
			Ag	109	23	0.033236994
9/11/12	9:00	AlN TB0424	total beam		67200	100
			C	12	11000	16.36904762
			O	16	84	0.125297619
			OH	17	1	0.00171131
			C2	24	18000	26.78571429
			Al	27	101	0.150297619
			AlN	41	81	0.119791667
			AlO	43	20	0.029910714
			Al2	54	11	0.016964286
			AlO2	59	1	0.002008929
			Cu	63	400	0.595238095
			Cu	65	177	0.263392857

Table 4: Continued

Date	Time	Sample	Molecule	Mass	Current (nA)	% of Total Beam
			Al2N	68	49	0.073065476
			Ag	107	1460	2.172619048
			Ag	109	1430	2.12797619
	13:15		total beam		67200	100
			C	12	17200	25.5952381
			O	16	334	0.49702381
			OH	17	2	0.002872024
			C2	24	20100	29.91071429
			CN	26	9250	13.76488095
			Al	27	205	0.305059524
			AlN	41	123	0.183035714
			AlO	43	57	0.084970238
			C2Al	51	1830	2.723214286
			Al2	54	17	0.025297619
			AlO2	59	4	0.005982143
			Cu	63	1100	1.636904762
			Cu	65	509	0.757440476
			Al2N	68	71	0.105803571
			C4Al	75	830	1.235119048
			Ag	107	3740	5.56547619
			Ag	109	3760	5.595238095
	14:15		total beam		67200	100
			C	12	15200	22.61904762
			O	16	208	0.30952381
			OH	17	3	0.004627976
			C2	24	19000	28.27380952
			CN	26	8800	13.0952381
			Al	27	205	0.305059524
			AlN	41	99	0.147470238
			AlO	43	41	0.060267857
			C2Al	51	1740	2.589285714
			Al2	54	13	0.019940476
			AlO2	59	3	0.0040625
			Cu	63	1260	1.875
			Cu	65	582	0.866071429
			Al2N	68	60	0.089434524
			C4Al	75	725	1.078869048
			Ag	107	3060	4.553571429
			Ag	109	3140	4.672619048

Table 4: Continued

Date	Time	Sample	Molecule	Mass	Current (nA)	% of Total Beam
	15:05		total beam		69200	100
			C	12	16000	23.12138728
			O	16	96	0.138439306
			OH	17	2	0.002312139
			C2	24	18600	26.87861272
			CN	26	7600	10.98265896
			Al	27	173	0.25
			AlN	41	82	0.118930636
			AlO	43	20	0.028901734
			C2Al	51	1510	2.182080925
			Al2	54	13	0.018930636
			AlO2	59	1	0.001936416
			Cu	63	1240	1.791907514
			Cu	65	609	0.880057803
			Al2N	68	59	0.085404624
			C4Al	75	616	0.89017341
			Ag	107	3040	4.393063584
			Ag	109	2600	3.757225434
9/12/12	9:20	AlN TB0425	total beam		63200	100
			C	12	5240	8.291139241
			O	16	35	0.055063291
			OH	17	1	0.000822785
			C2	24	9100	14.39873418
			CN	26	2530	4.003164557
			Al	27	50	0.07943038
			AlN	41	49	0.076740506
			AlO	43	12	0.018829114
			C2Al	51	486	0.768987342
			Al2	54	14	0.021360759
			AlO2	59	1	0.001202532
			Cu	63	500	0.791139241
			Cu	65	237	0.375
			Al2N	68	41	0.064082278
			C4Al	75	197	0.311708861
			Ag	107	613	0.969936709
			Ag	109	609	0.963607595
	11:00		total beam		74400	100
			C	12	6240	8.387096774

Table 4: Continued

Date	Time	Sample	Molecule	Mass	Current (nA)	% of Total Beam
			O	16	33	0.043951613
			OH	17	0	0
			C2	24	8600	11.55913978
			CN	26	2940	3.951612903
			Al	27	58	0.078091398
			AlN	41	42	0.056317204
			AlO	43	8	0.011034946
			C2Al	51	486	0.653225806
			Al2	54	10	0.012916667
			AlO2	59	1	0.000725806
			Cu	63	573	0.77016129
			Cu	65	251	0.337365591
			Al2N	68	29	0.038306452
			C4Al	75	177	0.237903226
			Ag	107	742	0.997311828
			Ag	109	725	0.974462366
	14:00		total beam		73600	100
			C	12	5220	7.092391304
			O	16	17	0.022961957
			OH	17	0	0
			C2	24	6040	8.206521739
			CN	26	2050	2.785326087
			Al	27	42	0.05638587
			AlN	41	2	0.00326087
			AlO	43	5	0.00642663
			C2Al	51	302	0.410326087
			Al2	54	6	0.007785326
			AlO2	59	0	0
			Cu	63	503	0.683423913
			Cu	65	242	0.328804348
			Al2N	68	16	0.02173913
			C4Al	75	70	0.095516304
			Ag	107	713	0.96875
			Ag	109	606	0.823369565
9/14/12	9:30	Al2O3 TB0421	total beam		43400	100
			C	12	1	0.003041475
			O	16	6210	14.30875576

Table 4: Continued

Date	Time	Sample	Molecule	Mass	Current (nA)	% of Total Beam
			OH	17	12	0.026728111
			Al	27	32	0.074654378
			AlO	43	893	2.057603687
			AlO2	59	174	0.400921659
			Cu	63	302	0.695852535
			Cu	65	122	0.281105991
			Ag	107	2090	4.815668203
			Ag	109	1820	4.193548387
	11:15		total beam		45600	100
			C	12	1	0.001754386
			O	16	7150	15.67982456
			OH	17	11	0.025
			Al	27	29	0.062719298
			AlO	43	1000	2.192982456
			AlO2	59	174	0.381578947
			Cu	63	873	1.914473684
			Cu	65	363	0.796052632
			Ag	107	2150	4.714912281
			Ag	109	2170	4.75877193
	14:40		total beam		48300	100
			C	12	1	0.001614907
			O	16	6240	12.91925466
			OH	17	10	0.019875776
			Al	27	17	0.034575569
			AlO	43	1050	2.173913043
			AlO2	59	20	0.041407867
			Cu	63	3720	7.701863354
			Cu	65	1800	3.726708075
			Ag	107	1800	3.726708075
			Ag	109	1680	3.47826087
9/17/12	10:05	AlN-1hr	total beam		25600	100
			O	16	1060	4.140625
			OH	17	2	0.008671875
			Al	27	204	0.796875
			AlN	41	1280	5
			AlO	43	500	1.953125
			Al2	54	430	1.6796875
			AlO2	59	8	0.03171875

Table 4: Continued

Date	Time	Sample	Molecule	Mass	Current (nA)	% of Total Beam
			Cu	63	249	0.97265625
			Cu	65	102	0.3984375
			Al2N	68	1240	4.84375
			Ag	107	343	1.33984375
			Ag	109	416	1.625
	12:30		total beam		21100	100
			O	16	1280	6.066350711
			OH	17	3	0.013364929
			Al	27	175	0.829383886
			AlN	41	1280	6.066350711
			AlO	43	573	2.71563981
			Al2	54	586	2.777251185
			AlO2	59	7	0.032890995
			Cu	63	361	1.710900474
			Cu	65	145	0.687203791
			Al2N	68	1060	5.023696682
			Ag	107	873	4.137440758
			Ag	109	888	4.208530806
	15:00		total beam		21100	100
			O	16	1220	5.781990521
			OH	17	2590	12.27488152
			Al	27	175	0.829383886
			AlN	41	1250	5.924170616
			AlO	43	520	2.464454976
			Al2	54	602	2.853080569
			AlO2	59	6	0.027014218
			Cu	63	427	2.023696682
			Cu	65	173	0.819905213
			Al2N	68	1030	4.881516588
			Ag	107	853	4.042654028
			Ag	109	863	4.090047393
9/18/12	10:15	AlN-1hr (sm)	total beam		25000	100
			O	16	1250	5
			OH	17	5	0.01864
			Al	27	237	0.948
			AlN	41	2120	8.48
			AlO	43	613	2.452
			Al2	54	503	2.012

Table 4: Continued

Date	Time	Sample	Molecule	Mass	Current (nA)	% of Total Beam
			AlO2	59	10	0.03932
			Cu	63	1280	5.12
			Cu	65	520	2.08
			Al2N	68	2050	8.2
			Ag	107	633	2.532
			Ag	109	623	2.492
	13:00		total beam		30300	100
			O	16	1060	3.498349835
			OH	17	4	0.012607261
			Al	27	166	0.547854785
			AlN	41	1530	5.04950495
			AlO	43	506	1.669966997
			Al2	54	411	1.356435644
			AlO2	59	6	0.019141914
			Cu	63	2190	7.227722772
			Cu	65	888	2.930693069
			Al2N	68	1250	4.125412541
			Ag	107	1030	3.399339934
			Ag	109	1060	3.498349835
	15:20		total beam		30800	100
			O	16	413	1.340909091
			OH	17	2	0.006136364
			Al	27	60.1	0.19512987
			AlN	41	873	2.834415584
			AlO	43	245	0.795454545
			Al2	54	103	0.334415584
			AlO2	59	4	0.013149351
			Cu	63	5	0.014642857
			Cu	65	2020	6.558441558
			Al2N	68	888	2.883116883
			Ag	107	238	0.772727273
			Ag	109	242	0.785714286
9/19/12	10:00	AlN-1hr	total beam		23500	100
			O	16	982	4.178723404
			OH	17	2	0.008255319
			Al	27	175	0.744680851
			AlN	41	1240	5.276595745
			AlO	43	435	1.85106383

Table 4: Continued

Date	Time	Sample	Molecule	Mass	Current (nA)	% of Total Beam
			Al2	54	425	1.808510638
			AlO2	59	9	0.040212766
			Cu	63	252	1.072340426
			Cu	65	115	0.489361702
			Al2N	68	1030	4.382978723
			Ag	107	345	1.468085106
			Ag	109	425	1.808510638
	12:10		total beam		21800	100
			O	16	1050	4.816513761
			OH	17	2	0.010229358
			Al	27	146	0.669724771
			AlN	41	1070	4.908256881
			AlO	43	430	1.972477064
			Al2	54	478	2.19266055
			AlO2	59	6	0.026605505
			Cu	63	285	1.30733945
			Cu	65	121	0.555045872
			Al2N	68	1060	4.862385321
			Ag	107	853	3.912844037
			Ag	109	853	3.912844037
	14:45		total beam		21100	100
			O	16	2150	10.18957346
			OH	17	4	0.018246445
			Al	27	402	1.90521327
			AlN	41	2170	10.28436019
			AlO	43	873	4.137440758
			Al2	54	883	4.184834123
			AlO2	59	12	0.05450237
			Cu	63	982	4.654028436
			Cu	65	430	2.037914692
			Al2N	68	2160	10.23696682
			Ag	107	1260	5.971563981
			Ag	109	1060	5.023696682

Appendix 2: Results from ANOVA test run in SAS for the "one-hour" AlN, Al_2O_3 and mixed AlN + Al_2O_3 samples. Because the data set was not balanced the Type III SS ANOVA table should be observed. An alpha value of 0.05 was used. These figures were taken directly from the SAS software.

Source	DF	Sum of Squares	Mean Square	F Value	Pr > F
Model	5	2451576.150	490315.230	120.69	<.0001
Error	21	85315.640	4062.650		
Corrected Total	26	2536891.790			

R-Square	Coeff Var	Root MSE	current Mean
0.966370	28.11644	63.73892	226.6963

Source	DF	Type I SS	Mean Square	F Value	Pr > F
sample	2	968056.4026	484028.2013	119.14	<.0001
source	1	782505.6579	782505.6579	192.61	<.0001
sample*source	2	701014.0892	350507.0446	86.28	<.0001

Source	DF	Type III SS	Mean Square	F Value	Pr > F
sample	2	1615422.313	807711.156	198.81	<.0001
source	1	366085.502	366085.502	90.11	<.0001
sample*source	2	701014.089	350507.045	86.28	<.0001

Means with the same letter are not significantly different.			
t Grouping	Mean	N	sample
A	422.92	13	1
B	53.24	10	2
B			
B	22.60	4	3

Appendix 3: Table displaying the ratios of AlN^-/AlO^- and AlN^-/Al^- negative ion currents within a single AlN sample using the stable injector platform.

Table 5: Ratio of AlN^-/AlO^- and AlN^-/Al^- within a single sample using the stable injector platform.

Description	Sample	Hours after run began	AlN^-/AlO^-	AlN^-/Al^-
6/4/12	AlN (1hr)	1.5	1.692307692	5.365853659
		6.5	2.366666667	7.1
6/5/12	AlN (1hr)	1.5	2.064516129	7.191011236
		6.5	2.451612903	7.6
8/1/12	AlN (1hr)	1.5	1.980582524	7.132867133
		6.5	2.914285714	7.285714286
9/17/12	AlN (1hr)	1.5	2.56	6.274509804
		3.5	2.233856894	7.314285714
		6.5	2.403846154	7.142857143
9/18/12	AlN (1hr)	1.5	3.458401305	8.945147679
		3.5	3.023715415	9.21686747
		6.5	3.563265306	14.52579035
9/19/12	AlN (1hr)	1.5	2.850574713	7.085714286
		3.5	2.488372093	7.328767123
		6.5	2.485681558	5.39800995
Total Average	AlN (1hr)		2.569179004	7.660493055
Standard Deviation			0.518379197	2.086390625
Average 1.5 hours	AlN (1hr)		2.434397061	6.999183966
Standard Deviation			0.652843135	1.186747799
Average 6.5 hours	AlN (1hr)		2.659033634	8.101365782
Standard Deviation			0.425640012	2.595193605
6.5-1.5	AlN (1hr)		0.224636573	1.102181816
6/6/12	AlN (2 days)	1.5	2.318181818	6.8
		6.5	2.827586207	7.068965517
8/3/12	AlN (2 days)	1.5	1.65	7.15
		6.5	1.957585644	8.108108108
Total Average	AlN (2 days)		2.188338417	7.281768406

Table 5: Continued

Description	Sample	Hours after run began	AlN^-/AlO^-	AlN^-/Al^-
Standard Deviation			0.50614627	0.57084326
Average 1.5 hours	AlN (2 days)		1.984090909	6.975
Average 6.5 hours	AlN (2 days)		2.392585926	7.588536813
6.5-1.5	AlN (2 days)		0.408495017	0.613536813
6/15/12	AlN (no exposure)	1.5	1.951612903	6.05
		6.5	2.1	5.384615385
6.5-1.5	AlN (no exposure)		0.148387097	-0.665384615
6/7/12	AlN + Al2O3	1.5	0.2	2.571428571
		6.5	0.1	1.52173913
8/2/12	AlN + Al2O3	1.5	0.137671233	1.041450777
		6.5	0.095754717	1.009950249
Total Average	AlN + Al2O3		0.133356487	1.536142182
Standard Deviation			0.048258067	0.728839921
Average 1.5 hours	AlN + Al2O3		0.168835616	1.806439674
Average 6.5 hours	AlN + Al2O3		0.097877358	1.26584469
6.5-1.5	AlN + Al2O3		-0.070958258	-0.540594985

Appendix 4: Currents of Al^- and AlN^- as well as ratios of AlN^-/AlO^- and AlN^-/Al^- for "one-hour" AlN, "14 day" AlN and AlN + Al_2O_3 samples as measured during mass scans using the test stand. There are numerous mass scans that have not been included in the following table because there measurements do not reflect typical source operations. Data collected during a mass scan is not included if there were abnormalities in the source operation (ie. source was shut down for extended periods, overload in cesium oven, sparking etc.) or source parameters were not held constant.

Table 6: Currents of Al^- and AlN^- as well as ratios of AlN/AlO and AlN/Al for AlN (1hr), AlN (14 days) and AlN + Al_2O_3 samples as measured during mass scans using the test stand.

Date	Sample	Mass Scan	AlN^-/AlO^-	AlN^-/Al^-	AlN^-	Al^-
11/15/11	AlN (1 hr)	4	0.0478021	0.148698885	0.2686	0.0538
		5	1.851178123	4.562471235	139.7745	30.6357
		6	2.092156376	4.805480118	176.0627	36.6379
		7	3.066479476	4.554111323	248.2355	54.508
11/17/11	AlN (1 hr)	1	0.029493719	0.150736182	0.3747	2.4858
		2	1.851178123	4.562471235	139.7745	30.6357
		3	2.092156376	4.075506595	176.0627	43.2002
		4	3.066479476	4.554111323	248.2355	54.508
		5	3.30131197	4.758352273	506.0284	106.3453
		6	3.268253352	5.240975977	698.011	133.1834
11/18/11	AlN (1 hr)	1	3.093362802	5.150215871	667.0642	129.5216
		2	2.209812078	4.291391875	907.4706	211.463
		3	1.676339175	4.034683693	1127.1599	279.3676
		4	2.817035549	5.676179905	684.7681	120.6389
12/2/11	AlN (14 days)	1	0.053579197	1.228258017	2.3402	1.9053
		2	1.849222152	3.870501912	242.8589	62.7461
		3	2.221509884	3.66107297	267.0577	72.9452
		4	1.761152234	2.062464238	178.4211	86.5087
		5	2.339003119	4.008347911	425.5194	106.1583
		6	2.910593041	4.591479896	544.9352	118.684
		7	2.735913286	3.909941691	529.8014	135.5011
		8	2.852160937	4.936492471	428.1336	86.7283
12/5/11	AlN (14 days)	1	1.079775231	6.129837591	41.1024	6.7053
		2	3.003027796	5.242812216	239.2269	45.6295
		3	3.120722147	5.380048425	340.634	63.3143
		4	2.624946058	5.173137037	545.6268	105.4731
		5	2.650206951	4.064329646	593.94	146.1348

Table 5: Continued

Date	Sample	Mass Scan	AlN^-/AlO^-	AlN^-/Al^-	AlN^-	Al^-
12/8/11	AlN (14 days)	1	0.002997256	0.120147874	0.013	0.1082
		2	0.169262176	0.97634095	1.8075	1.8513
12/12/11	AlN (14 days)	1	0.625883676	4.472171223	27.0383	6.0459
		2	2.08598621	4.741967861	140.3172	29.5905
		3	2.53700494	5.519341904	501.0293	90.777
		4	2.547380179	4.458922329	579.4811	129.9599
		6	2.280782178	6.067577668	169.661	27.9619
12/13/11	AlN (14 days)	1	2.456670345	4.944143919	59.2259	11.979
		2	3.052470158	4.727287477	233.0912	49.3076
		3	3.018970546	5.39645231	399.5366	74.0369
		4	2.828766196	4.381126515	470.363	107.3612
		5	2.336212535	4.921212005	539.3983	109.6068
12/14/11	AlN + Al2O3	1	0.016097809	0.93768546	0.0316	0.0337
		2	0.002319468	0.0625	0.012	0.192
12/15/11	AlN + Al2O3	1	0.047504215	0.36048583	0.4452	1.235
		2	0.13081386	1.585188226	16.216	10.2297
		3	0.120316884	1.588658623	41.8324	26.3319
		4	0.124452388	1.379583017	65.6338	47.5751
		5	0.099303477	1.342590705	47.4246	35.3232
		6	0.10222676	1.464977175	44.9915	30.7114
12/20/11	AlN (1 hr)	1	0.114476023	1.119137353	0.5345	0.4776
		2	2.17691138	3.762479291	159.1984	42.3121
		3	2.389956625	4.234616618	282.5531	66.7246
		4	2.358022319	3.50147868	374.2587	106.8859
		5	2.264304602	3.447180106	455.5645	132.1557
		6	2.497652363	4.991719934	374.9186	75.1081

Appendix 5: Currents of AlO^- and Al^- for Al_2O_3 samples as measured by mass scans using the test stand. There are numerous mass scans that have not been included in the following table because there measurements do not reflect typical source operations. Data collected during a mass scan is not included if there were abnormalities in the source operation (ie. source was shut down for extended periods, overload in cesium oven, sparking etc.) or source parameters were not held constant.

Table 7: Currents of AlO^- and Al^- for Al_2O_3 samples as measured by mass scans using the test stand.

Date	Sample	Mass Scan	AlO^-	Al^-
11/22/11	Al2O3	1	7.4438	0.2331
		2	184.3986	15.1710
		3	461.4403	30.1118
11/28/11	Al2O3	1	74.0772	6.7934
		2	54.1836	7.1823
		3	274.6530	10.7814
		4	288.8090	15.7293
		5	363.4053	21.1569
11/29/11	Al2O3	1	141.1494	17.4676
		2	229.3467	19.1340
		3	324.0695	19.7735
		4	303.0794	18.7050

Appendix 6: Graphical representations of AlN^-, Al^- and AlO^- currents for AlN (1 hr) and (14 days) exposure times as well as Al_2O_3 sample. Currents are recorded during mass scans taken over the course of a run typically lasting 8 hours using the test stand. There are numerous mass scans that have not been included in the following table because there measurements do not reflect typical source operations. Data collected during a mass scan is not included if there were abnormalities in the source operation (ie. source was shut down for extended periods, overload in cesium oven, sparking etc.) or source parameters were not held constant.

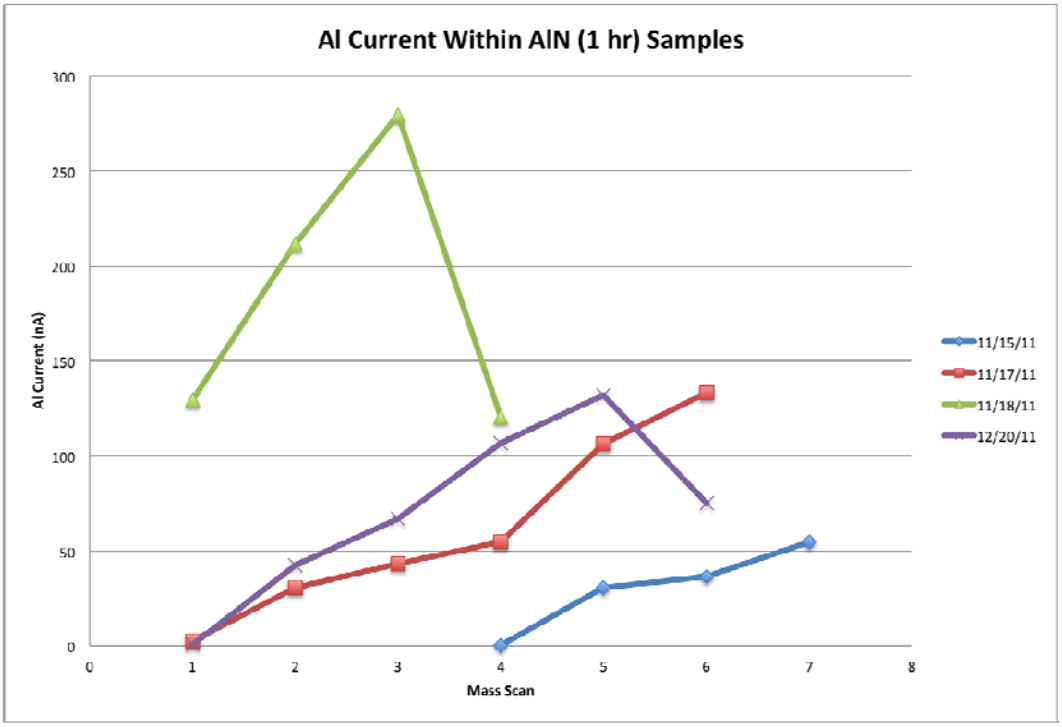

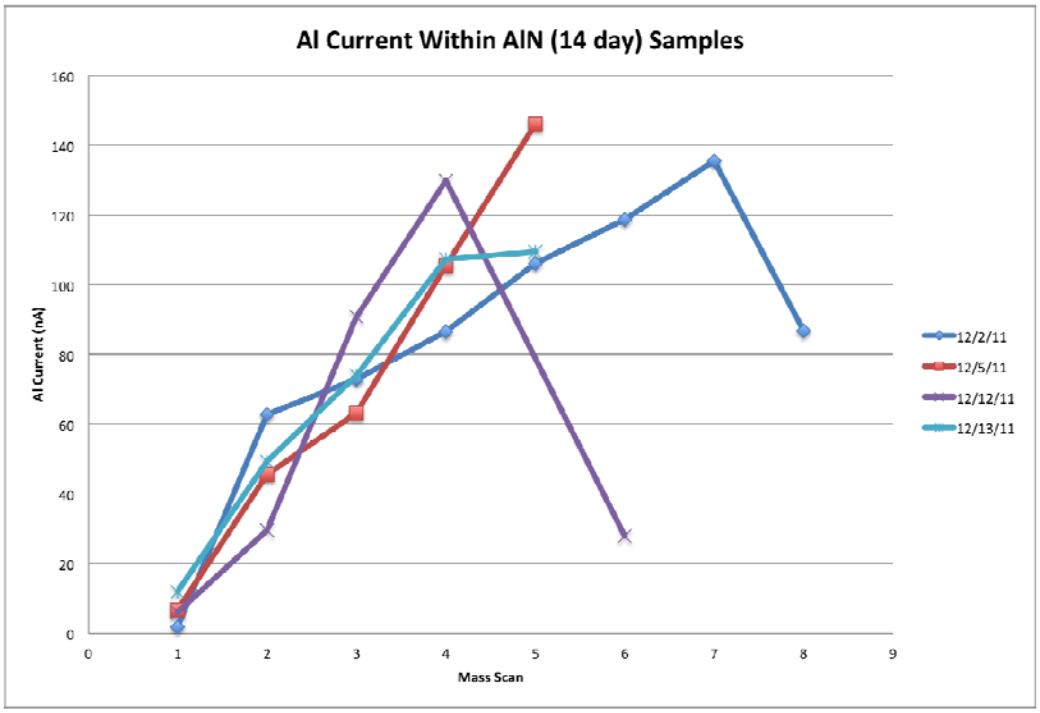
Al Current Within AlN (14 day) Samples
Al Current (nA)
Mass Scan
12/2/11
12/5/11
12/12/11
12/13/11

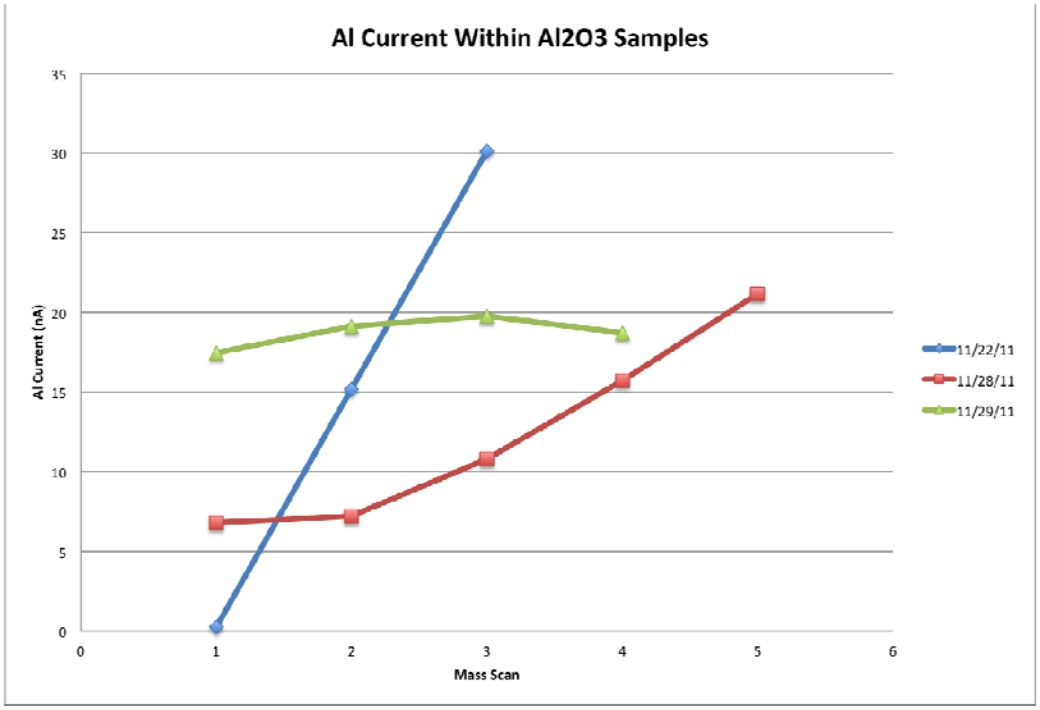
Al Current Within Al2O3 Samples
Al Current (nA)
Mass Scan
11/22/11
11/28/11
11/29/11

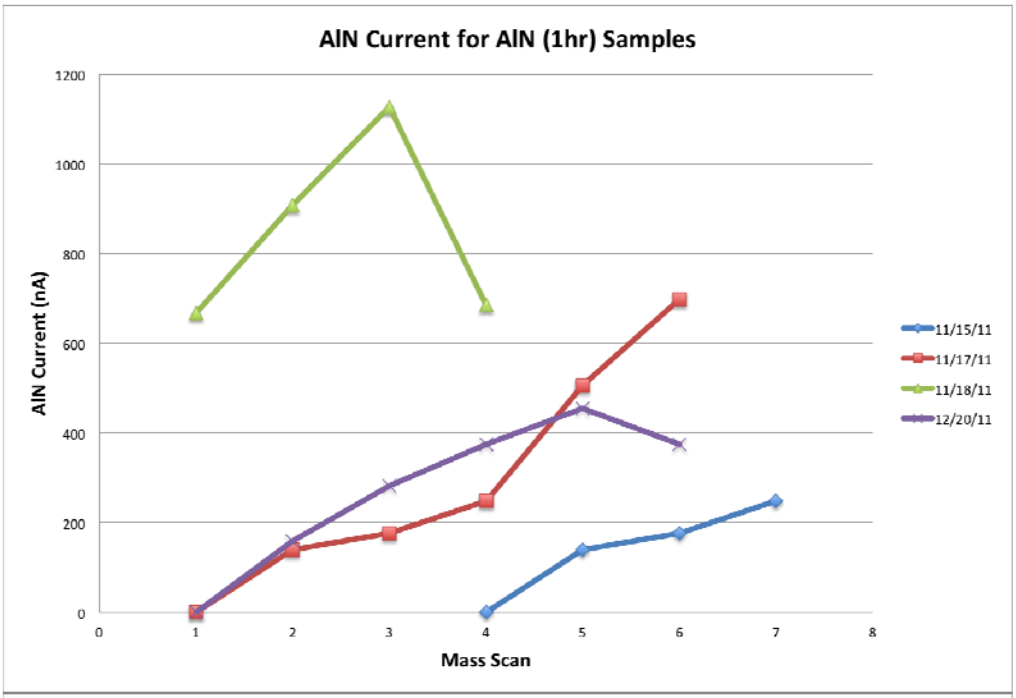
AlN Current for AlN (1hr) Samples
AlN Current (nA)
Mass Scan
11/15/11
11/17/11
11/18/11
12/20/11

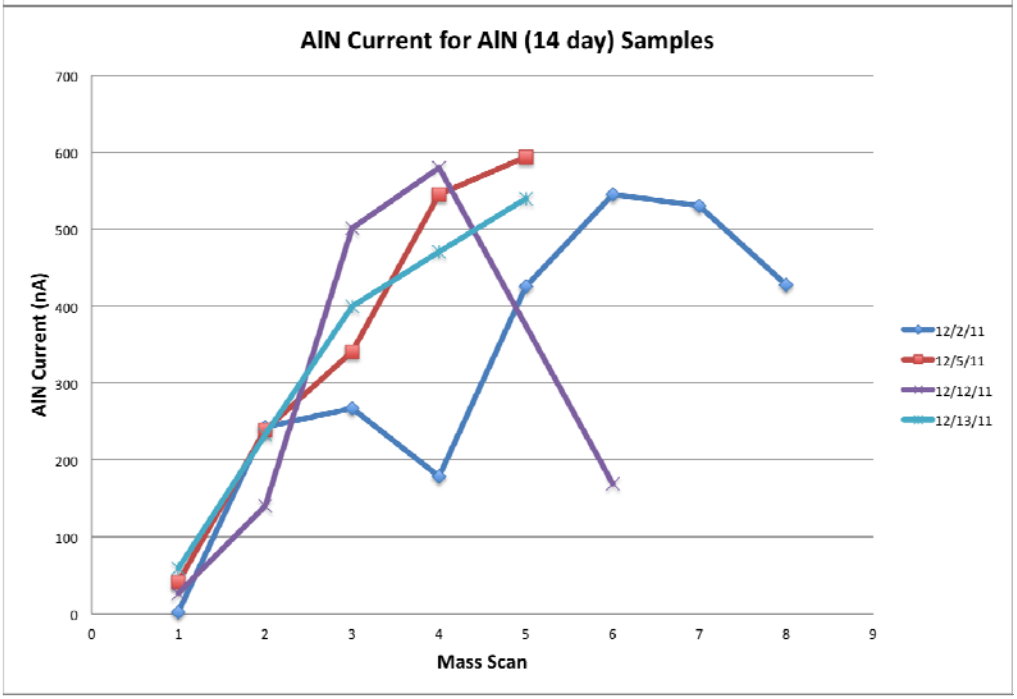
AlN Current for AlN (14 day) Samples
AlN Current (nA)
Mass Scan
12/2/11
12/5/11
12/12/11
12/13/11

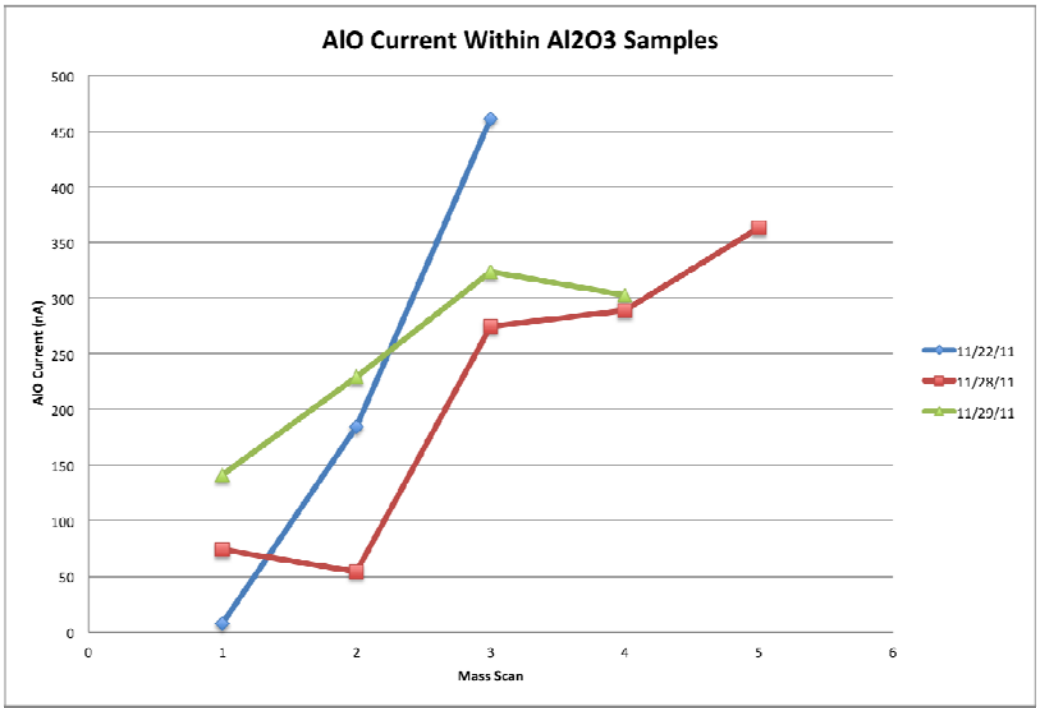
AlO Current Within Al2O3 Samples
AlO Current (nA)
500
450
400
350
300
250
200
150
100
50
0
0
1
2
3
4
5
6
Mass Scan
11/22/11
11/28/11
11/29/11

Appendix 7: AlN^-/AlO^- and Al^-/Al^- negative ion current ratios between AlN (of varying exposure times) samples and Al_2O_3 samples. The sample currents were only compared if the source conditions were the same and the samples were run within a couple weeks of each other. In addition currents recorded after 1.5 hours of running were only compared to other 1.5 hour currents as the currents increase over the course of a day (highlighted orange). The same was done for currents recorded at 6.5 hours (highlighted yellow). The averages for each of the compared runs are given in purple.

Table 8: AlN^-/AlO^- and Al^-/Al^- negative ion current ratios between AlN (of varying exposure times) samples and Al_2O_3 samples.

AlN Sample	Date of AlN Sample	Time after run began	Date of Al_2O_3 Sample	Time after run began	AlN^-/AlO^-	Al^-/Al^-
AlN (1hr)	6/4/12	1.5	5/31/12	1.5	4.112149533	14.13793103
				6.5	2.444444444	8.2
			6/14/12	1.5	4.4	10.12345679
				6.5	2.404371585	5.578231293
		6.5	5/31/12	1.5	6.635514019	17.24137931
				6.5	3.944444444	10
			6/14/12	1.5	7.1	12.34567901
				6.5	3.879781421	6.802721088
AlN (1hr)	6/5/12	1.5	5/31/12	1.5	5.981308411	15.34482759
				6.5	3.555555556	8.9
			6/14/12	1.5	6.4	10.98765432
				6.5	3.49726776	6.054421769
		6.5	5/31/12	1.5	7.102803738	17.24137931
				6.5	4.222222222	10
			6/14/12	1.5	7.6	12.34567901
				6.5	4.153005464	6.802721088
AlN (1hr)	9/17/12	1.5	9/7/12	1.5	3.832335329	15
				6.5	2.633744856	8.644067797
			9/10/12	1.5	3.585434174	7.364620939
				6.5	1.725067385	2.837273992
		3.5	9/7/12	1.5	3.832335329	12.86764706
				6.5	2.633744856	7.415254237
			9/10/12	1.5	2.147651007	6.317689531
				6.5	1.725067385	2.433936022
		6.5	9/7/12	1.5	3.74251497	12.86764706
				6.5	2.572016461	7.415254237
			9/10/12	1.5	2.097315436	6.317689531
				6.5	1.684636119	2.433936022
AlN (1hr)	9/17/12	1.5	9/7/12	1.5	6.347305389	17.42647059

Table 8: Continued

AlN Sample	Date of AlN Sample	Time after run began	Date of Al_2O_3 Sample	Time after run began	AlN^-/AlO^-	Al^-/Al^-
				6.5	4.362139918	10.04237288
			9/10/12	1.5	3.55704698	8.555956679
				6.5	2.857142857	3.296244784
		3.5	9/7/12	1.5	4.580838323	12.20588235
				6.5	3.148148148	7.033898305
			9/10/12	1.5	2.567114094	5.992779783
				6.5	2.061994609	2.30876217
		6.5	9/7/12	1.5	2.613772455	4.419117647
				6.5	1.796296296	2.546610169
			9/10/12	1.5	1.464765101	2.16967509
				6.5	1.176549865	0.835883171
AlN (1hr)	9/18/12	1.5	9/7/12	1.5	3.71257485	12.86764706
				6.5	2.551440329	7.415254237
			9/10/12	1.5	2.080536913	6.317689531
				6.5	1.67115903	2.433936022
		3.5	9/7/12	1.5	3.203592814	10.73529412
				6.5	2.201646091	6.186440678
			9/10/12	1.5	1.795302013	5.270758123
				6.5	1.442048518	2.030598053
		6.5	9/7/12	1.5	6.497005988	29.55882353
				6.5	4.465020576	17.03389831
			9/10/12	1.5	3.640939597	14.51263538
				6.5	2.924528302	5.591098748
Avg AlN (1hr)		1.5			4.400869158	11.81262545
Std dev		1.5			1.411231838	3.377143052
Avg AlN (1hr)		6.5			2.751946924	6.054438268
Std dev		6.5			1.097571266	4.112371821
AlN (2 days)	6/6/12	1.5	5/31/12	1.5	1.906542056	5.172413793
				6.5	1.133333333	3
			6/14/12	1.5	2.04	3.703703704
				6.5	1.114754098	2.040816327
		6.5	5/31/12	1.5	1.91588785	5
				6.5	1.138888889	2.9
			6/14/12	1.5	2.05	3.580246914

Table 8: Continued

AlN Sample	Date of AlN Sample	Time after run began	Date of Al_2O_3 Sample	Time after run began	AlN^-/AlO^-	Al^-/Al^-
				6.5	1.120218579	1.972789116
Avg AlN (2 days)		1.5			1.973271028	4.438058748
Avg AlN (2 days)		6.5			1.129553734	2.436394558
AlN (no exposure)	6/15/12	1.5	5/31/12	1.5	1.130841121	3.448275862
				6.5	0.672222222	2
			6/14/12	1.5	1.21	2.469135802
				6.5	0.661202186	1.360544218
		6.5	5/31/12	1.5	1.177570093	4.034482759
				6.5	0.7	2.34
			6/14/12	1.5	1.26	2.888888889
				6.5	0.68852459	1.591836735
Avg AlN (no exposure)		1.5			1.170420561	2.958705832
Avg AlN (no exposure)		6.5			0.694262295	1.965918367

Appendix 8: Tibet sample ratio for the ^{26}Al ratio calculation. The ratio calculation is done to ensure that at least 2mg of Al exists within the sample, which will produce 4mg of Al_2O_3 for an AMS target. The first two rows are the calculations for the entire quartz sample. The second two rows are the calculations for the samples once they are split in half. The number of stable atoms is calculated as the total weight of aluminum minus the number of ^{26}Al atoms. The ratio given is the ratio of $^{26}Al/^{27}Al$.

Table 9: Quartz samples TB0420 and TB0421 with their respective masses, amount of Be carrier added and the measured number of ^{10}Be atoms per gram of SiO_2.

Sample Name	Sample wt (g)	Add Be carrier (mg)	^{10}Be atoms/g SiO_2
TB0420	39.2492	0.3500	4278418
TB0421	35.9598	0.3233	4884359

Multiplier: ^{26}Al atoms = 6.7 x ^{10}Be atoms (for the Tibet region)

Table 10: Quartz samples TB0420 and TB0421 with their respective masses, calculated Al ppm, number of ^{26}Al and stable Al atoms and calculated ratio of $^{26}Al/^{27}Al$ before and after the addition of an Al carrier.

Sample Name	^{26}Al atom/g SiO_2	Mass (g)	Al Content (ppm)	Native wt (mg)	Carrier (mg)	^{26}Al atoms	Stable Atoms	$^{26}Al/^{27}Al$ ($x10^{-15}$)
TB0420	28665401	35	17	0.60	0	1003289035	1.33E+19	75538
TB0421	32725206	12	16	0.19	0	392702472	4.29E+18	91625
TB0420	28665401	18	17	0.30	1.7	501644517.5	4.46E+19	11250
TB0421	32725206	6	16	0.10	1.9	196351236	4.46E+19	4407

Appendix 9: ICP-OES results from aluminum aliquot that was removed from each quartz sample (TB0420, TB0421, TB0423 and TB0424). Sample TB0422 and TB0425 were prepared in conjunction with the quartz samples but only contain Al carrier and so there is no mass of Al from quartz in them.

Table 11: ICP-OES results from aluminum aliquot that was removed from each quartz sample (TB0420, TB0421, TB0423 and TB0424).

Sample Name	Mass of Quartz (g)	Mass of Al from Quartz (g)	Mass of ^{27}Al in Carrier (mg)	Al in Quartz (ppm)
TB0420	16.284	0.226	1.801	13.9
TB0421	5.527	0.072	1.939	13.1
TB0422	0	0.000	1.992	0.0
TB0423	20.549	0.266	1.726	12.9
TB0424	6.089	0.084	1.934	13.8
TB0425	0	0.000	2.026	0.0

Appendix 10: Table taken from F. Strelow *et al*. (1972) showing the anion exchange distribution coefficients in oxalic acid-HC1 mixtures. The oxalic acid is kept at 0.05M and the concentrations of HCl are varied. This figure is taken from Selvaduray and Sheet (1993).

	Molarity HCl							
Element	0.01*M*	0.1*M*	0.2*M*	0.5*M*	1.0*M*	2.0*M*	3.0*M*	4.0*M*
Sn(IV)	>10⁴	>10⁴	>10⁴	>10⁴	>10⁴	>10⁴	9700	3800
W(VI)	3450	>10⁴	9170	7610	6720	699	163	prec.
Pd(II)	>10⁴	>10⁴	>10⁴	>10⁴	2850	867	440	249
Mo(VI)[a]	>10⁴	>10⁴	>10⁴	>10⁴	2310	920	660	935
Bi(III)[b,c]	. . .	567	700	1330	1900	900	590	344
Pt(II)	1500	1480	1500	1470	1370	1230	837	525
Mo(VI)	>10⁴	>10⁴	>10⁴	4100	1270	487	650	930
Ta(V)[a]	378	367	364	303	201	118	17.7	10.2
Cd(II)[b]	51	48.9	269	472	171	195	289	427
In(III)	>10⁴	2900	828	173	80	44.4	28.8	24.1
Nb(V)[a]	>10⁴	7100	3410	675	78	11.5	4.7	3.7
U(VI)	>10⁴	6800	1630	250	66	24.2	38.1	71
Zn(II)[b]	28.7	3.3	2.9	5.3	30.6	35.3	61	88
Ti(IV)	>10⁴	>10⁴	>10⁴	639	26.5	0.8	<0.5	<0.5
Fe(III)[a,c]	>10⁴	2790	1580	105	14.5	6.0	9.5	39.0
Zr(IV)	>10⁴	>10⁴	4040	138	11.4	1.4	0.5	<0.5
Ta(V)	103	104	102	39.5	10.9	6.1	5.5	5.4
Hf(IV)	4030	3560	1700	85	8.1	1.7	0.9	0.5
Ga(III)	>10⁴	>10⁴	485	43.5	7.9	1.2	6.6	30.7
Ti(IV)[a]	>10⁴	1420	320	38.6	6.4	0.5	<0.5	<0.5
Pb(II)[b,c]	60	17.7	2.4	3.1	3.4	4.3	1.9	1.1
V(IV)	5180	523	152	19.1	2.7	1.5	1.1	0.9
V(V)	5370	570	160	17.1	2.3	0.6	<0.5	<0.5
Al(III)	>10⁴	1840	211	4.4	0.6	<0.5	<0.5	<0.5
Cu(II)[b]	620	39.7	8.4	1.4	0.6	0.4	1.1	2.2
Be(II)	68	8.1	1.5	<0.5	<0.5	<0.5	<0.5	<0.5
Ni(II)[b]	84	0.8	<0.5	<0.5	<0.5	<0.5	<0.5	<0.5
Co(II)[b]	9.2	<0.5	<0.5	<0.5	<0.5	<0.5	<0.5	<0.5
Mn(II), Mg, Ca, Sr, Ba, Li, Na, K, Rb, Cs		<0.5	<0.5	<0.5	<0.5	<0.5	<0.5	<0.5

[a] 1 ml of 30% H_2O_2 present.
[b] 0.05 millimole of element.
[c] 2-hour equilibration time.

Appendix 11: Results from ANOVA test run in SAS for the geological samples TB0421, TB0424 and TB0425. Because the data set is not balanced the Type III SS ANOVA table should be observed. An alpha value of 0.05 was used. These figures were taken directly from the SAS software.

Source	DF	Sum of Squares	Mean Square	F Value	Pr > F
Model	2	43373.21833	21686.60917	20.27	0.0012
Error	7	7488.06667	1069.72381		
Corrected Total	9	50861.28500			

R-Square	Coeff Var	Root MSE	current Mean
0.852775	35.88221	32.70663	91.15000

Source	DF	Type I SS	Mean Square	F Value	Pr > F
sample	2	43373.21833	21686.60917	20.27	0.0012

Source	DF	Type III SS	Mean Square	F Value	Pr > F
sample	2	43373.21833	21686.60917	20.27	0.0012

Level of sample	N	current	
		Mean	Std Dev
1	4	171.000000	49.0441978
2	3	49.933333	8.3032122
3	3	25.900000	8.1908486

Appendix 12: Results from ANOVA test run in SAS for the "one-hour" AlN using two different cathode geometries. Because the data set is balanced the Type I SS ANOVA table should be observed. An alpha value of 0.05 was used. These figures were taken directly from the SAS software.

Source	DF	Sum of Squares	Mean Square	F Value	Pr > F
Model	2	11596.86889	5798.43444	0.62	0.5671
Error	6	55712.47333	9285.41222		
Corrected Total	8	67309.34222			

R-Square	Coeff Var	Root MSE	current Mean
0.172292	49.83895	96.36084	193.3444

Source	DF	Type I SS	Mean Square	F Value	Pr > F
sample	2	11596.86889	5798.43444	0.62	0.5671

Source	DF	Type III SS	Mean Square	F Value	Pr > F
sample	2	11596.86889	5798.43444	0.62	0.5671

Level of sample	N	current	
		Mean	Std Dev
1	3	184.666667	16.743158
2	3	241.000000	140.182025
3	3	154.366667	89.021926

Appendix 13: Purdue University Sample Preparation Procedure Sheet for ^{10}Be and ^{26}Al.

^{10}Be Only ^{10}Be + ^{26}Al Procedure Sheet

Quartz Weighing & Carrier Addition

_____ Fill in the necessary information on the separate datasheet for each sample, most importantly the sample identification and the beryllium and aluminum carrier information

Sample Size	PerFluoroAlkoxy (PFA) Jar Size	For Beryllium you will need the pipettor with a 1 ml (or smaller) tip. For Aluminum you will need a 1 ml sterile graduated disposable pipette and mini glass beaker to hold the pipette. You will need the plastic weighing trays. You will need fresh deionized water for washing the weighing trays. You will need to calibrate the analytical balance (if it does not automatically auto-calibrate).
<42 grams	300 ml	
43-65 grams	500 ml	
66-140 grams	1000 ml	
141-280 grams	2000 ml	

—Label PFA jar and cap with "*sample* Be in HF/HNO3" or "*sample* Al/Be in HF/HNO3" for each sample.

Notes: Solely for beryllium-only samples: for sample sizes <10 grams, you can use the analytical balance to weigh your jar without cap (to obtain an extra significant figure).

Beryllium carrier volume should give a maximum of ~300µg Beryllium for large (and/or "old") quartz samples and a minimum of ~250µg Beryllium for small (and/or "young") quartz samples.

Aluminum carrier volume should give a maximum of ~2mg of Aluminum, including the contribution from the quartz.

—Rub all the HDPE/PP bottles holding quartz with a kimwipe to remove any grains from the outside.

Note: If you weigh the quartz out for all of your samples first, then you do not necessarily need gloves and can use the nitrile gloves for all the carrier additions. If you weigh the quartz and immediately add carrier use the low-static vinyl gloves.

_____ Run PFA jar through the anti-static device, weigh the jar (with or without cap) and record. For **^{26}Al** you MUST weigh the jar with cap!

Note: When using the 500 ml and 1 liter PFA jars, the glass top of the balance can attract the jar top through static and can result in the balance displaying a lower mass than the actual mass.

_____ Take jar out of balance, pour quartz sample into jar, run jar through the anti-static device, then reweigh the jar and record the mass

Note: The same pipette tips or pipettes can be used for all Be or all Al additions but do NOT touch or otherwise contaminate; replace tips or pipettes as needed.

—Swirl both the Beryllium carrier bottle and the Aluminum carrier bottle to mix before using.

Note: Excess Be carrier does NOT go back into the carrier jar; put excess carrier into waste Be container.

_____	Using Eppendorf pipette, transfer **Beryllium** carrier volume into tared plastic weighing pan, close the Beryllium carrier bottle while watching the mass stabilize on the balance, and record mass
_____	Pour carrier into PFA jar containing the quartz sample, wash the plastic weighing pan with about 1 ml of deionized water, pour wash into the PFA jar and then recap the jar
_____	Using sterile 1 ml transfer pipette, transfer **Aluminum** carrier volume into tared plastic weighing pan, close the Aluminum carrier bottle while watching the mass stabilize on the balance, and record mass
_____	Pour carrier into PFA jar containing the quartz sample, wash the plastic weighing pan with about 1 ml of deionized water, pour wash into the PFA jar and then recap the jar

—When finished, the pipette tip used for Be can go into the appropriate waste jar.
—The HDPE/PP bottles that held the quartz can have all HF/HNO_3 writing cleaned off with acetone/alcohol and then can be recycled.

Remember to turn off the Anti-Static unit when you are done!

Quartz Dissolution

_____ Calculate the volumes of HNO_3 (1× quartz mass) and HF (5× quartz mass) and record. Volumes for the chemistry blank are the averages of all the quartz samples.

Review the HF Binder/CHP binder for PPE and other information on working with HF/concentrated acids.
You will need a 500 ml graduated pitcher for HF and both 100 and 50 ml graduated cylinders for HF or HNO_3.
Triple-rinse all graduated cylinders/pitchers in deionized water before using. For the pitcher, the first two rinses can come from a carboy but the last rinse should be water fresh from the deionizing unit.
You will need the working bottle of concentrated HF.
You will need the working bottle of concentrated HNO_3.
Have deionized water ready in a container to fill the graduated cylinders/pitcher when you are finished before bringing cylinders out of the hood to wash.

_____ Pour the appropriate volumes of HF and HNO_3 for your sample into their respective graduated cylinders/pitcher

Note: Support graduated cylinders with both hands when you pour to keep acid from "rushing" out.

_____ Add HF to the PFA jar first and HNO_3 second, slightly tighten jar and put aside

Note: Record if you use more than ± 10 ml for HF or ± 5 ml for HNO_3 compared to the calculated values

—Do a quick inspection of your gloves between samples to make sure that no drops of acid are present. If there is acid on your gloves, wipe with kimwipe and dispose kimwipe in sodium bicarbonate container, then hold gloves under the running tap water to rinse. Gloves can be dried or replaced as needed.

—Fill (but do not overflow) your graduated cylinders with deionized water before bringing out of the hood. Triple-rinse graduated cylinders in deionized water and allow to air-dry.

Add no external heat on the samples for the first two (2) hours!

Note: Always use gloves and eye protection when handling the jars on and off the griddle.

_____ Check tightness of jar lid; lid only wants to be closed until it meets resistance

_____ Place jar on griddle set to ~150-160 ºC (Chemistry blanks do not need heat.)

Note: Samples will boil while there is still quartz to provide a nucleus for boiling. Once the quartz is dissolved the solution has too high of a density to boil at this temperature.

Note: Since jar lids are not tight, only swirl jars that have significant headspace.

Note: In lieu of swirling the jar, you can hold the top of the jar and twist the entire jar while the base is still resting on the griddle. This will drive out bubbles from the quartz and help mix the solution.

Note: If you do not see any more quartz on the bottom of the jar, you can leave the jar on the griddle for another couple of hours. This will help dry condensation in the threads from the initial stage of dissolution and keep HF/HNO_3 from dripping on your gloves when you open the dissolved sample.

_____ Sample is finished dissolving when you cannot see any remaining quartz in the bottom of the jar when the jar is held up to the light (and at arms-length from your face/body)

If you are only doing Beryllium…
Skip the Aliquot Preparation section and proceed to Sample Volume Reduction.

If you are also doing Aluminum…
Extract the ICP aliquot using the procedure on the next page before performing the Sample Volume Reduction.

Aliquot Preparation for Aluminum Determination on the ICP-OES

Review the HF Binder/CHP binder for PPE and other information on working with HF/concentrated acids.
Label both 30 ml PFA vials and lids with "*sample* Al in Acid" for each sample.
You will need a new 3 ml or 1 ml transfer pipette for each sample and a mini glass beaker to hold it.
Have a beaker of deionized water in the hood to put HF-wetted transfer pipettes in during the procedure.
You will need to calibrate the analytical balance (if it does not automatically auto-calibrate).

—Make sure that the jar is at or close to room temperature before weighing.

Note: Numbered lines correspond to lines on the datasheet where masses are recorded.

_____ Tighten the cap of the PFA jar holding the dissolved quartz sample

_____ **(1)** Run jar through the anti-static device, weigh and record the mass

Note: If the jar mass is higher than the balance limit, the top of the jar can be removed and the jar can be heated on a hotplate (temperature ~215 ºC with heatlamps and label of "NOT WEIGHED" on the jar) to evaporate some of the sample. Only evaporate enough to be able to weigh the sample.

_____ Calculate the volume of dissolved sample you want to take for your aliquot based on the equation on the datasheet. The value you calculate represents (approximately) what will be measured on the ICP-OES for one gram of solution. If less than the target value increase aliquot size.

_____ **(2)** Run the 30 ml PFA vial + lid through the anti-static device and weigh on the analytical balance and record the mass

You will need boots, chemical-resistant apron, gloves, and arm shields for opening the dissolution jars.

_____ In the hood, swirl the capped jar holding the dissolved solution to homogenize the sample

Note: If the jar lid is under suction, use the lid wrench to remove (Carefully…HF is inside!).

_____ Carefully remove top (HF is present!) of the dissolution jar and transfer with pipette your calculated value of solution to the pre-weighed 30 ml PFA vial and re-cap the vial

—Recap dissolution jar and place to the side for sulfuric acid addition.

_____ **(3)** Run the 30 ml PFA vial + lid + aliquot through the anti-static device and reweigh on the analytical balance and record the mass

—*Remember to turn off the Anti-Static unit when you are done!*

You will need the working bottles of concentrated nitric acid and concentrated hydrochloric acid.
You will need a 3 ml transfer pipette for the nitric acid and a 1 ml transfer pipette for the hydrochloric acid and mini glass beakers to hold them.

_____ Add 2 ml of concentrated HNO_3 and 1 ml concentrated HCl to the vial with aliquot

_____ With lid loosely covering the vial, turn hotplate to ~100 ºC—but not before the acid addition—and allow any reaction/gas generation to die down

—For evaporations, hotplate should be set at ~160 ºC. Only use heat lamps after the solution has dried and you want to evaporate any residual condensation at the rim of the vial.

_____ ____ Remove lid and evaporate aliquot in the PFA vial to dryness on a hotplate

—Turn down hotplate to a low setting for the addition of acid.

_____ Add 2 ml of concentrated HNO_3 and 1 ml concentrated HCl to the vial

_____ Lid can loosely cover the vial while colored gas is being evolved and can come off when the reaction dies down

_____ ____ Turn hotplate back up and evaporate the PFA vial to dryness

—Turn down hotplate to a low setting for the addition of acid.

You will only need the working bottle of concentrated nitric acid with a 3 ml transfer pipette and mini glass beaker to hold the pipette.

_____ Add 2 ml of concentrated HNO_3 to the vial

_____ ____ Turn hotplate back up and evaporate the PFA vial to dryness

—Turn off hotplate and allow vials to cool or remove vials from hotplate and allow to cool.

Label 15 ml centrifuge tubes with "*sample* Al 5% HNO3" for each sample.
You will need the bottle of 50% (1:1 V/V) nitric acid.
You will need a 1 ml transfer pipette for the nitric acid and a mini glass beaker to hold it.
You will need the working bottle of deionized water.
You will need a 3 ml transfer pipette for the deionized water and a mini glass beaker to hold it.
You will need the squeeze bottle of non-pH7 deionized water.
You will need a fresh 1 ml transfer pipette for each sample and a mini glass beaker to hold it.
You will need a centrifuge tube rack to hold the 15 ml tubes for the transfer.
You will need a 50 ml glass beaker handy to weigh the centrifuge tube on the analytical balance.
You will need to calibrate the analytical balance (if it does not automatically auto-calibrate).

_____ **(4)** Run the 15 ml centrifuge tube through the anti-static device and weigh (in the tared glass beaker) on the analytical balance and record the mass

_____ Add 1 ml of 1:1 (50%) HNO_3 solution to the dried aliquot in the cooled PFA vial

_____ Transfer the now-dissolved aliquot (with pipette) to the pre-weighed 15 ml centrifuge tube

_____ Rinse vial 3 times with ~2-2.5 ml of deionized water each time and transfer (with pipette) to the 15 ml centrifuge tube

_____ Dilute the centrifuge tube to 10 ml total solution with the squeeze bottle of non-pH7 deionized water

Note: With **10 ml** of total solution, the acid content is **5% HNO_3**, matching the ICP-OES standards.

_____ **(5)** Weigh centrifuge tube with the 10 ml of solution (in the tared glass beaker) on the analytical balance and record the mass

—*Remember to turn off the Anti-Static unit when you are done!*

_____ Shake/vortex the centrifuge tube to homogenize the sample

Sample Volume Reduction

Review the HF Binder/CHP binder for PPE and other information on working with HF/concentrated acids.
You will need the working bottle of trace-metal grade concentrated sulfuric acid.
You will need a 3 ml transfer pipette for the sulfuric acid and a mini glass beaker to hold it.

You will need boots, chemical-resistant apron, gloves, and arm shields for opening the dissolution jars.

Note: If the jar lid is under suction, use a lid wrench to remove (Carefully…HF is inside!).

_____ Remove lid from the dissolution jar and place off to the side, separated by kimwipes

Note: Each jar gets the same amount of sulfuric acid no matter how much HF/HNO_3 solution is in the jar.

_____ Add 5 ml of the trace-metal grade concentrated sulfuric acid to the sample

_____ Place jar on hotplate

—For evaporations, hotplate should be set at ~215 ºC—160 ºC if you have to leave jars unattended—and aim two heat lamps at each hotplate to aid in heating and reduce condensation at the lips of the jars.

Note: Overnight the hotplates are turned off but the heat lamps are left on.

Note: When rearranging jars or picking a jar up for inspection do not reach over other open jars. Remove jars from the side of the jar you are interested in so you can remove it from the side of the hotplate.

==>Sample is finished—and only sulfuric acid is left—when no more bubbles appear in the liquid after removing the jar from the hotplate, swirling the solution, and placing the jar back on the hotplate.

Note: The heat from the hotplate and heat lamps can superheat the sulfuric acid and send its temperature well over 100 ºC, possibly melting the jar; do not leave samples heating if only sulfuric acid is left.

_____ Remove jar, allow to cool, and cover with the correct lid.

Fuming for the Removal of HF

Review the CHP binder for PPE and other information on working with concentrated acids.
You will need the working bottle of trace-metal grade concentrated sulfuric acid.
You will need a 3 ml transfer pipette for the sulfuric acid and a mini glass beaker to hold it.
You will need the fuming crucibles and a small kimwipe for them to sit on in the hood.

—Using the green (xylene-free) marker, write the PL/Sample IDs on the outside of each crucible at least three times.

Note: You want to pour from the same spot on the dissolution jar each time.

_____ Pour sample out of the PFA dissolution jar into the crucible

_____ With a transfer pipette, add ~2 ml of the trace metal-grade H_2SO_4 to the jar, rinse across the bottom of the jar, and pour the H_2SO_4 rinse into the crucible

_____ Rinse with 2 ml of the H_2SO_4 as above two (2) more times and transfer to the crucible

_____ Transfer crucible to hotplate

Note: crucible should not be much more than half-full or spattering/creeping can occur.

Note: Aluminum sulphate decomposes at 770 ºC, beryllium sulfate decomposes at 550-600 ºC.

_____ ____ Turn up hotplate; target temperature is 400 ºC < T < 425 ºC, evaporate to complete dryness

Note: Heatlamps are not needed for this evaporation.

Note: Give each dissolution jar and cap a single rinse in deionized water in preparation for cleaning.

—Turn off hotplate and/or transfer crucibles off the hotplate.

You will need the working bottle of 6N hydrochloric acid.
You will need a small kimwipe for the crucible to sit on in the hood.
You will need a small kimwipe in the hood with a scrunched kimwipe on it to clean HCl from your gloves.

!!! If the solution in the crucible turns hot orange when HCl is inside it means that nitric acid/fumes are present…it also means that the crucible is dissolving and that you must get your sample out *Immediately*!

_____ Add at least as much 6N HCl to the crucible as there was H_2SO_4, making sure that the level of HCl is higher than any visible "bathtub ring" in the crucible

_____ Tilt (carefully!) the crucible to soak any dried material close to the rim

_____ ____ Let crucible sit for ~½ hour to soak sample material, especially $CaSO_4$

Note: Beryllium chloride boils at 480 ºC while aluminum chloride decomposes at 180 ºC—but Al is not lost from the sample above that temperature.

—Hotplate should be set at ~150 ºC; no heat lamps for this step since we want a chemical conversion.

_____ ____ Evaporate crucibles to complete dryness

—Turn off hotplate and/or transfer crucibles off the hotplate.

Label small PTFE beakers with "*sample* in HCL" for each sample.
You will need the working bottle of 6N hydrochloric acid.
You will need a 3 ml disposable transfer pipette for the HCl and a mini glass beaker to hold it.
You will need a fresh 1 ml disposable transfer pipette for each sample and a mini glass beaker to hold it.
You will need a small kimwipe for the crucible to sit on in the hood.
You will need a small kimwipe in the hood with a scrunched kimwipe on it to clean HCl from your gloves.
You will need a beaker or other container with deionized water available to add to empty crucibles.

_____ Add 2 ml of 6N HCl to the crucible, Swirl or roll (carefully!) the crucible to dissolve dried material

_____ Transfer with a 1 ml transfer pipette to the small PTFE beaker

_____ Wash crucible with 2 ml of 6N HCl three (3) times and transfer with transfer pipette to Teflon vial/beaker. Swirl/roll or wash the sides of the crucible with transfer pipette.

Note: If you are doing multiple samples you can add the 2 ml of HCl to the next crucible on the third wash.

Note: Three washes is the minimum number but you want your last wash to be "clean." If your third wash still shows color or you are still picking up solid material then add another wash (and note that).

Note: When finished with crucible, place in sink and fill with deionized water in preparation for cleaning.

—Hotplate should be set at ~150 ºC; no heat lamps for this step since we want a chemical conversion.

_____ ____ Evaporate vials/beakers to complete dryness

Label 50 ml centrifuge tubes with "*sample* in NaOH" for each sample.
Fill each centrifuge tube with 25 ml of 12.5% NaOH; any NaOH in excess of 25 ml can be transferred with a 1 ml disposable pipette to the next tube.
You will need the small bottle of 6N hydrochloric acid.
You will need a 1 ml disposable transfer pipette for the acid and a mini glass beaker to hold it.
You will need a fresh 1 ml disposable transfer pipette for each sample and a mini glass beaker to hold it.

_____ Take up the dried bead of material in the Teflon vial/beaker with 2 ml 6N HCl

Note: Only transfer dissolved material; if material is not dissolved get it in the next wash but if material has not dissolved by the third wash it will not dissolve and can be transferred.

_____ Transfer solution with 1 ml disposable pipette to the 50 ml centrifuge tube that has the 12.5% NaOH

_____ Rinse the Teflon jar/beaker with 1 ml of 6N HCl three (3) times and transfer with disposable pipette to the 50 ml centrifuge tube

Note: You only want 5 ml total of 6N HCl added to the centrifuge tube but ½ or 1 ml of extra acid is fine. If you add more than 1 ml of extra acid you should add NaOH at a quantity of 5 ml per extra ml of acid

Note: If you are doing multiple samples you can add the 2 ml 6N HCl to the next beaker on the third wash.

Note: Rinse PTFE beaker one time in deionized water in preparation for cleaning.

_____ Vortex on maximum the 50 ml "*sample* in NaOH tube (with tightened cap) for 1 minute

_____ ____ Let tubes sit for 1 hour

Fe/Ti Removal by Precipitation

_____ Centrifuge 50 ml "*sample* in NaOH" tubes for 5 minutes at >3200×*g* Relative Centrifugal Force (RCF)

Label 50 ml centrifuge tubes with "*sample* Al-Be 1" if the sample is run only for beryllium or "*sample* Al-Be 1,3" if the sample is to be run for both aluminum and beryllium.

You will need the dropper bottle of 6N HCl.

_____ Decant liquid from the "*sample* in NaOH" tube into the "*sample* Al-Be" tube

_____ In the "*sample* in NaOH" tube with the precipitate add 20 drops of 6N HCl

_____ Vortex the "*sample* in NaOH" tube on half-speed to dissolve the precipitate

Note: If you need to add more than 20 drops 6N HCl to dissolve the sample note on the datasheet.

The Eppendorf pipettor is used for this step.

The long Eppendorf pipette stem must be triple-rinsed inside and out before using or if the tip is touched to anything during the procedure.

_____ To the "*sample* in NaOH" tube with dissolved precipitate add 5 ml of 12.5% NaOH

_____ Vortex the "*sample* in NaOH" tube (with tightened cap) to mix

_____ ____ Let tube sit 1 hour

_____ Centrifuge 50 ml "*sample* in NaOH" tube for 5 minutes at >3200×*g* RCF

_____ Add supernatant from the 50 ml "*sample* in NaOH" tube to 50 ml "*sample* Al-Be" tube

—Done with "*sample* in NaOH" tube—Save.

Al/Be Hydroxide Precipitation

You will need the dropper bottle of 30% ammonium hydroxide.
You will need a 1 ml disposable transfer pipette for the hydroxide.

_____ Add 1 ml of 30% NH_4OH (with transfer pipette) to the 50 ml "*sample* Al-Be" tube

Review the CHP binder for PPE and other information on working with concentrated acids.
You will need the working bottle of concentrated hydrochloric acid and beaker with DIW for waste.
You will need a 3 ml disposable transfer pipette and a 1 ml disposable transfer pipette for the HCl and mini glass beakers to hold them.
You will need a fresh 1 ml disposable transfer pipette for each sample and a mini glass beaker to hold it.
You will need a watch glass or petri dish resting on a kimwipe and a piece of pH paper for each sample.
Always use fresh gloves when tearing the pH paper for use with samples.
You will need a small kimwipe in the hood with a scrunched kimwipe on it to clean drops and dribbles.
You will need a kimwipe to wrap around the centrifuge tube to collect dribbles during the procedure.

Note: If you were tight with your solution additions it should take 9½ to 9¾ ml of HCl to reach pH 8.

_____ Adjust solution in the "*sample* Al-Be" tube to pH 8 with concentrated HCl

Note: Use a new transfer pipette for each sample to touch a drop onto a fresh pH strip.
Note: If you reach the endpoint and still have HCl in the pipette, discard in the DIW waste beaker.
Note: If endpoint is passed, use 30% NH_4OH out of the dropper bottle to go back up to the endpoint.

_____ Let "*sample* Al-Be" tube sit ~15 minutes for hydroxides to precipitate
_____ Centrifuge 50 ml "*sample* Al-Be" tube for 5 minutes at >3200×*g* RCF

Label acid-cleaned 125 ml bottles with "*sample* SUPN" for each sample.
You will need the squeeze bottle of pH7 deionized water.

_____ Decant supernatant into the 125 ml "*sample* SUPN " bottle
_____ Rinse precipitate left in tube to the 10 ml line with pH7 deionized water and vortex to mix
_____ Centrifuge 50 ml "*sample* Al-Be" tube for 5 minutes at >3200×*g* RCF
_____ Decant supernatant into the 125 ml "*sample* SUPN " bottle
_____ Rinse precipitate left in tube to the 10 ml line with pH7 deionized water and vortex to mix
_____ Centrifuge 50 ml "*sample* Al-Be" tube for 5 minutes at >3200×*g* RCF

You will need the bottle of *clean* 0.4M oxalic acid, a 3 ml transfer pipette and mini glass beaker to hold it.

_____ Decant supernatant into the 125 ml "*sample* SUPN " bottle
_____ Using a disposable pipette, add 2 ml of *clean* 0.4M oxalic acid to the "*sample* Al-Be" tube
_____ Vortex the "*sample* Al-Be" tube at half speed to dissolve the hydroxide gel

Note: If gel does not dissolve in the initial 2 ml of oxalic acid you can:
1) add more oxalic acid but not more than 6 ml; or 2) wait overnight to allow the oxalic acid to work.

Al/Be Separation by Cation/Anion Exchange

The Eppendorf pipettor is used for all solution deliveries ≥4 ml.
The long Eppendorf pipette stem can be used for all reagents but must be triple-rinsed inside and out between solutions or if the tip is touched to anything.
You will need the column rack and the associated solutions.
Position 100 ml glass beakers below the columns to catch the conditioning solutions.
When unpacking columns, repeatedly invert the column to move beads into the reservoir and remove bubbles. Remove top first, then break bottom tab off last using a crisp front-to-back motion and place into the column rack to drain; if you twist the bottom tab the outlet will become blocked.

Note: Column volume is 2 ml.

Anion Column Conditioning (for Aluminum)

—You can fill the column reservoir with deionized water when draining to collect any dried resin.

_____ Drain the resin (AG 1-X8) bed
_____ Add 4 ml (2 column volumes) of 9N HCl and drain
_____ Add 8 ml (4 column volumes) of 0.012 N HCl and drain
_____ (If columns are not to be used immediately, cap the bottom, add DIW up to the bend in the column, and put cap back on loosely)

Cation Column Conditioning (for Beryllium)

_____ Drain the resin (AG 50W-X8) bed
_____ Add 10 ml (5 column volumes) of 6N HCl and drain
_____ Add another 10 ml (5 column volumes) of 6N HCl and drain
_____ Add 6 ml (3 column volumes) of non-pH7 deionized water and drain
_____ (If columns are not to be used immediately, cap the bottom, add DIW up to the bend in the column, and put cap back on loosely)

Load the Samples

You will need both 1 ml and 3 ml disposable transfer pipettes throughout these procedures.

_____ Using a 1 ml disposable transfer pipette, load both cation and anion columns with 1 ml of *clean* 0.4M oxalic acid and drain

—Conditioning solution goes into the non-HF waste acid container.

Label the columns with the PL/Sample ID. Label acid-washed 60 ml bottles with "*sample* OXALIC" for each sample.

_____ [If you are doing aluminum, rearrange (if need be) and stack columns, cation over anion]
_____ Rearrange columns (if need be) & place "*sample* OXALIC" bottle below the columns
_____ Using a 1 ml disposable transfer pipette, add sample solution from the "*sample* Al-Be" tube to the top of the cation column and drain. (Pipette can then be left inside the tube.)
_____ Using a 3 ml disposable transfer pipette, add 2 ml *clean* 0.4M oxalic acid to the "*sample* Al-Be" tube. (1 ml transfer pipette can be bent out of the way during addition.)
_____ Swirl the "*sample* Al-Be" tube to rinse and transfer rinsate to columns and drain

—Done with "*sample* Al-Be" tubes—triple rinse and discard.

_____ Add 10 ml *clean* 0.4M oxalic acid to the cation column and drain
_____ [If doing aluminum, pull columns and do the first two steps under **Anion Columns (Aluminum)** now]

Cation Columns (Beryllium)

_____ Place "*sample* OXALIC" bottle under column

_____ Using a 3 ml transfer pipette, add 2 ml of non-pH7 deionized water to column and drain

_____ Add 10 ml 0.5N HCl to column (to elute sodium) and drain

Label 15 ml centrifuge tubes with "*sample* Be" for each sample.

_____ Replace "*sample* OXALIC" bottle with "*sample* Be" centrifuge tube under column

_____ Add 10 ml 1.2N HCl to column (to elute beryllium) and drain

_____ Replace "*sample* Be" centrifuge tube with "*sample* OXALIC" bottle under column

—Transfer centrifuge tubes to one of the other tube racks; the acrylic rack should only be used for elution.

_____ Add 10 ml of 6N HCl to column (to elute remaining cations) and drain

_____ **If doing Aluminum**, add 10 ml of non-pH7 deionized water and drain…Otherwise:

—Push exchange beads out of column into waste bead bottle with syringe and water and discard column.

Beryllium: Precipitation, Drying, and Conversion to Oxide

Note: Do not start these steps if you do not have 1¼ to 1½ hours available to get to vial drying.

You will need the dropper bottle of 10% Na_2-EDTA.
You will need the dropper bottle of 30% ammonium hydroxide.
You will need a fresh 1 ml disposable transfer pipette for each sample and a mini glass beaker to hold it.
You will need a watch glass or petri dish resting on a kimwipe and a piece of pH paper for each sample.
Always use fresh gloves when tearing the pH paper for use with samples.

_____ To the "*sample* Be" tube add 10 drops of 10% EDTA solution, cap, and invert to mix

_____ Adjust solution in the "*sample* Be" tube to pH ~9 with 30 drops of 30% NH_4OH

_____ ____ Wait 30 minutes for beryllium hydroxide precipitate to form

—OH^- will out-compete the EDTA over time allowing unwanted species—B, Mn, Zn etc.—to precipitate as hydroxides (along with the $Be(OH)_2$) so do not leave the samples much longer than the noted time.

_____ Centrifuge 15 ml "*sample* Be" tube for 5 minutes at >3200×*g* RCF

—Inspect each tube to make sure you have the expected yield of beryllium hydroxide.

If you are doing ^{10}Be only, you can use the existing "*sample* SUPN" bottle; if you are also doing ^{26}Al, then label 30 ml acid-cleaned with "*sample* SUPN" and use them for these beryllium washes only.
You will need the squeeze bottle of pH7 deionized water.

Note: There is no need to excessively tap the centrifuge tube to try and get the supernatant water out.

_____ Decant centrifuge tube into appropriate "*sample* SUPN" bottle

_____ Add pH7 deionized water from the squeeze bottle up to the **7** ml line and vortex the tube

_____ Centrifuge 15 ml "*sample* Be" tube for 5 minutes at >3200×*g* RCF

_____ Decant centrifuge tube into appropriate "*sample* SUPN" bottle

_____ Add pH7 deionized water from the squeeze bottle up to the **6** ml line and vortex the tube

_____ Centrifuge 15 ml "*sample* Be" tube for 5 minutes at >3200×*g* RCF

_____ Make map of heating block or firebrick where each sample will be placed

—If $Be(OH)_2$ yields are not as expected, note on your datasheet so you can adjust niobium during mixing.

_____ Decant centrifuge tube into appropriate "*sample* SUPN" bottle

You will need a self-sealing bag with a Hazardous Waste sticker on it: fill in the Principle Investigator (Marc Caffee/Darryl Granger), Content line as "Beryllium Hydroxide" and Percentage as "Trace."
You will need a heating block or firebrick and kimwipe to put firebrick on.
You will need the deionized water dropper bottle with fresh non-pH7 deionized water in it.

You will need clean quartz-glass vials and tweezers; clean tweezers in acetone before using with vials.
You will need 1 ml transfer pipettes for each sample.

_____ To the 15 ml centrifuge tubes add 3 drops of non-pH7 deionized water from the dropper bottle (being careful not to touch the bottle tip to the tube)

_____ Put a 1 ml transfer pipette into each tube

Note: Only add one vial at a time; do not put vials in the block/firebrick for each sample before starting.

_____ Put a clean quartz-glass vial into block/firebrick

Note: Do not collect stray drops on centrifuge wall with pipette in this first transfer; collect drops in wash.

_____ Mix the water/gel slurry with the pipette and carefully transfer to the quartz glass vial.

NOTE 1: Do not allow slurry to move into the bulb of the transfer pipette; the beryllium hydroxide should come back out but you could lose sample.

NOTE 2: Keep the tip of the pipette inside the vial when transferring; sometimes the last drop that comes out of the pipette creates a large bubble that can leave beryllium hydroxide on the rim of the vial.

_____ Holding the top of the transfer pipette out of the way, add 3 drops of non-pH7 deionized water from the dropper bottle into the tube (being careful not to touch the bottle tip to the tube or transfer pipette)

_____ Mix the water and any remaining gel with the pipette and carefully transfer to the quartz glass vial

—Centrifuge caps are NOT beryllium waste but the centrifuge tubes, transfer pipettes, and used gloves are. These items go into the Hazardous Waste bag and the bag goes into the appropriate receptacle.

_____ ____ Dry vials under heat lamps but with no caps; this typically takes ~6-7 hours

_____ [If vials are not already on the firebrick, make a map of the firebrick and where each sample will be placed and transfer vials to the firebrick]

You will need clean quartz-glass caps and tweezers; clean tweezers in acetone before using with caps.

_____ Add caps to the vials

_____ Place the firebrick into the muffle furnace and set the temperature to 900 °C

_____ ____ Fire for <u>one hour</u> after the furnace hits 900 °C

_____ Turn furnace off/down to ~50 °C and let cool (which will take a couple of hours).

Mixing Beryllium Oxide with the Niobium Binder and Loading the Holder

Note: Inhalation of BeO can cause Berylliosis: read the posted symptom sheet in the laboratory.

You will need a self-sealing bag with a Hazardous Waste sticker on it: fill in the Principle Investigator (Marc Caffee/Darryl Granger), Content line as "Beryllium Oxide" and Percentage as "Trace."
If you have samples that need less than the full complement of Niobium, you can use a Post-It® to make a map of your samples, showing which samples need less, and stick it someplace visible.
You will need the dropper bottles of trace-metal grade acetone and (regular) methyl alcohol.
Place large kimwipe down in front of the loading area, place aluminum loading block on the kimwipe and put a small kimwipe over the block.
Cut a piece of silicon carbide sandpaper (400 grit) suitable for sanding all your tamping rods and place on the large kimwipe.
You will need the point anti-static unit on.
You will need the tweezers; clean tweezers in acetone before using.
You will need a heating block to place your vials in once they have been mixed.
You will need the trashcan placed convenient to the loading area for tamping rod-cleaning kimwipes.
You will need tight-fitting nitrile gloves, possibly a size smaller than you usually use.
Clean the curette scoop with trace-metal grade acetone and return to resting place, making sure that the clean end of the scoop does not touch any other surface. Scoop can be re-cleaned as needed.
You will need clean 1.15 mm diameter drill blanks to use as tamping rods.
You will need the Niobium powder for mixing the beryllium oxide.
When working with the beryllium oxide during mixing you will use acetone to keep any powder contained within the vial so a mask is not necessary.

_____ If you do not need the vial cap, place it with tweezers into dirty cap jar in the loading hood

_____ Hold the quartz glass vial with tweezers to the anti-static head; do not touch the head

Note: The curette we use gives ~1.2 mg of niobium per scoop.

Note: If your beryllium yields were less than expected or if you are using a very small carrier spike adjust your niobium addition amount accordingly.

_____ Using the curette, add three scoops of niobium to the vial and return curette to its place

_____ Using silicon carbide sandpaper, wet sand (in alcohol—not acetone!) approximately one half of the tamping rod shaft and also the end; dry with a kimwipe when sanded

Note: Each rod gets its own spot on the piece of sandpaper. Keep rod flat when sanding. When clean, hold the non-sanded end of the tamping rod and do not touch to any other surface.

_____ Add 2 drops of acetone to the vial

_____ Grind the sample around the bottom, across the bottom, and up & down around the lower portion of the walls of the vial

_____ When finished, the vial (with the tamping rod inside) goes into heating block to air dry

—When finished with all samples, small kimwipe goes into the Hazardous Waste bag.
—Let samples dry at least 30 minutes before beginning the loading process.

Fill in datasheets or lab book with the holder number corresponding to each sample. If you get out of that sample/holder sequence make sure that you stop and update your list before continuing to load.
If necessary, stand as many cryovials (1.2 ml volume) or shell vials as you have samples on the counter/table for easy access.
You will need the hammer.
You will need a dust mask.

_____ Place a new small kimwipe (folded to give two layers) over the aluminum loading block
_____ Extract a stainless steel holder from the holder box, double-check the holder number against your datasheet, and push holder into the hole in the aluminum plate, pushing the small kimwipe down in the process
—Holders should be packed to the top of the well with the BeO/Nb mix.
Note: For quantities of carrier near 350 μg of Be, two scoops of niobium are sufficient to get the BeO/Nb mix near to the top of the well. For quantities of carrier below 300 μg of Be, three scoops of niobium will be necessary. Adjust the quantity of make-up niobium as needed.
_____ Using the curette, add two/three scoops of niobium to the face of the holder and return curette to its place.
—Using tweezers, hold vial—including tamping rod—to the anti-static head, and place vial down, making sure that it does not fall over.
_____ Using tamping rod, push make-up Nb into the well and tamp down with the hammer
_____ Loosen BeO/Nb mix with the tamping rod (carefully), tap bottom of vial with rod to help
_____ Hold vial back up to the anti-static head to loosen powder
_____ Pour/tap powder from the vial onto the holder face
_____ Use tamping rod to move powder on the holder face down into the well
—Do not hold the tamping rod vertical while moving powder or you can flick powder off the holder.
_____ With hammer, tamp down the powder in the well using the tamping rod
—It can take multiple cycles of tapping/scraping the vial, anti-static, adding more mix to the holder, and tamping to fill the well to the top.
_____ Remove holder from the block, turn the holder upside down and rap on the kimwipe
_____ [If the sample does fall out of the well, pour off the kimwipe into the holder and re-tamp]
—The used tamping rod goes into the "not clean" beaker in the loading hood.
_____ Put holder face-down into cryo- or shell vial (so you can read the holder number) and return vial to the holder's original spot in the holder box
—Small kimwipe is folded over with used/empty vial and goes into the Hazardous Waste bag.

—When finished, mask, large kimwipe in front of the loading area, sandpaper, and gloves go into the Hazardous Waste bag and bag goes into the proper receptacle.

Remember to turn off the Anti-Static unit when you are done!

Anion Columns (Aluminum)

_____ Place "*sample* OXALIC" bottle under column
_____ Using a 3 ml transfer pipette, add 2 ml of non-pH7 deionized water to column and drain
_____ Place columns in other rack while you elute the beryllium from the cation column

Label acid-washed 60 ml bottles with "*sample* OXALIC2" for each sample.

_____ Stack columns but this time with the anion column over the cation column
_____ Place "*sample* OXALIC2" bottle below the columns
_____ Add 8 ml 0.05M oxalic acid/0.5M HCl solution to anion column and drain
_____ Add 8 ml 0.05M oxalic acid/0.5M HCl solution to anion column and drain
_____ Add 8 ml 0.05M oxalic acid/0.5M HCl solution to anion column and drain
— Place anion columns in another rack until you can elute any remaining anions
_____ Place cation columns in the main rack and place "*sample* OXALIC2" bottle underneath
_____ Add 10 ml of non-pH7 deionized water and drain
_____ Add 10 ml 1.2N HCl to column (to elute titanium) and drain

Label 15 ml centrifuge tubes with "*sample* Al" for each sample.

_____ Add 10 ml of 2.5N HCl to column (to elute aluminum) and drain
_____ Replace "*sample* Al" centrifuge tube with "*sample* OXALIC2" bottle under column
—Transfer centrifuge tubes to one of the other tube racks; the acrylic rack should only be used for elution.
_____ Add 10 ml of 6N HCl to column (to elute remaining cations) and drain
—Push exchange beads out of column into waste bead bottle with syringe and water and discard column.
_____ Place anion columns in the main rack and place "*sample* OXALIC2" bottle underneath
_____ Add 4 ml (2 column volumes) of 6N HCl to column and allow to drain
_____ Add 4 ml (2 column volumes) of 9N HCl to column and allow to drain
_____ Add 8 ml (4 column volumes) of 0.012 N HCl to column and allow to drain
—Push exchange beads out of column into waste bead bottle with syringe and water and discard column.

Aluminum: Conversion to Oxide

You will need the dropper bottle of 30% ammonium hydroxide. You will need the dropper bottle of 3N HCl.

You will need a fresh 1 ml disposable transfer pipette for each sample and a mini glass beaker to hold it.
You will need a watch glass or petri dish resting on a kimwipe and a piece of pH paper for each sample.
Always use fresh gloves when tearing the pH paper for use with samples.

_____ Adjust solution in the "*sample* Al" tube to pH ~7 with ~41 drops of 30% NH_4OH

Note: Unlike for the beryllium precipitation, there is less pH leeway for the aluminum precipitation.

Note: Use 3N HCl from the dropper bottle to adjust the pH down if it is much greater than 7.

_____ Wait 15 minutes for aluminum hydroxide precipitate to form

Note: Aluminum hydroxides compact easier than beryllium hydroxides and at higher RCF than ~3200 it takes a lot of vortex time to get the hydroxide out of the bottom of the centrifuge tube.

_____ Centrifuge 15 ml "*sample* Al" tube for 5 minutes **at** 3200×*g* RCF

—Inspect each tube to make sure you have the expected yield of aluminum hydroxide.

Note: There is no need to excessively tap the centrifuge tube to try and get the supernatant water out.

_____ Decant centrifuge tube into the 125 ml "*sample* SUPN" bottle

_____ Add pH7 deionized water from the squeeze bottle up to the **7** ml line and vortex the tube

_____ Centrifuge 15 ml "*sample* Al" tube for 5 minutes **at** 3200×*g* RCF

_____ Decant centrifuge tube into the 125 ml "*sample* SUPN" bottle

_____ Add pH7 deionized water from the squeeze bottle up to the **6** ml line and vortex the tube

_____ Centrifuge 15 ml "*sample* Al" tube for 5 minutes **at** 3200×*g* RCF

_____ Make map of heating block where each sample will be placed

—If $Al(OH)_3$ yields are not as expected, note on your datasheet so you can adjust silver during mixing.

_____ Decant centrifuge tube into the 125 ml "*sample* SUPN" bottle

You will need a heating block.
You will need the 6N HCl dropper bottle.
You will need clean quartz-glass vials and tweezers; clean tweezers in acetone before using with vials.
You will need 1 ml transfer pipettes for each sample.

_____ To the 15 ml centrifuge tubes add 4 drops of 6N HCl from the dropper bottle (being careful not to touch the bottle tip to the tube)

Note: Only add one vial at a time; do not put vials in the block/firebrick for each sample before starting.

_____ Put a clean quartz-glass vial into heating block

Note: Do not collect stray drops on centrifuge wall with pipette in this first transfer; collect drops in wash.

_____ Mix acid/gel (if need be) with fresh 1 ml transfer pipette and carefully transfer the solution to the quartz glass vial.

NOTE 1: Do not allow solution to move into the bulb of the transfer pipette.
NOTE 2: Keep the tip of the pipette inside the vial when transferring; sometimes the last drop that comes out of the pipette creates a large bubble that can leave sample on the rim of the vial.

_____ Holding the top of the transfer pipette out of the way, add 3 drops of 6N HCl from the dropper bottle into the tube (being careful not to touch the bottle tip to anything)

_____ Mix acid and any remaining gel with pipette and carefully transfer to the quartz glass vial

_____ ____ Dry vials under heat lamps but with no caps; this typically takes ~6-7 hours

You will need clean quartz-glass caps and tweezers; clean tweezers in acetone before using with caps.

_____ Add caps to the vials

_____ Place heating block on hotplate set to ~400ºC and heat for one (1) hour after the top of the heating block reaches 250ºC.

You will need a firebrick and kimwipe to put firebrick on. You will need tweezers; clean tweezers in acetone before using with vials.

_____ Make a map of the firebrick where each sample will be placed (if not the same as on the heating block)

_____ Transfer vials to firebrick

_____ Place the firebrick into the muffle furnace and set the temperature to 1100 °C

_____ ____ Fire for <u>one hour</u> after the furnace hits 1000 °C

_____ Turn furnace off/down to ~50 °C and let cool (which will take a couple of hours).

Mixing Aluminum Oxide with the Silver Binder and Loading the Holder

You will need the dropper bottles of trace-metal grade acetone and (regular) methyl alcohol.
Place large kimwipe down in front of the loading area, place aluminum loading block on the kimwipe and put a small kimwipe over the block.
Cut a piece of silicon carbide sandpaper (400 grit) suitable for sanding all your tamping rods and place on the large kimwipe.
You will need the point anti-static unit on.
You will need the tweezers; clean tweezers in acetone before using.
You will need a heating block to place your vials in once they have been mixed.
You will need the trashcan placed convenient to the loading area for tamping rod-cleaning kimwipes.
You will need tight-fitting nitrile gloves, possibly a size smaller than you usually use.
Clean the curette scoop(s) with trace-metal grade acetone and return to resting place, making sure that the clean end of the scoop does not touch any other surface. Scoop can be re-cleaned as needed.
You will need clean 1.15 mm diameter drill blanks to use as tamping rods.
You will need the Silver powder for mixing the aluminum oxide.

_____ If you do not need the vial cap, place it with tweezers into dirty cap jar in the loading hood

_____ Hold the quartz glass vial with tweezers to the anti-static head; do not touch the head

Note: The cathode holds ~15 mg of packed silver powder. For samples where you have recovered >3 mg of Al, then you can use one #3 curette scoop of silver to mix and no makeup silver. For samples where you have recovered ~2 mg of Al, then you can use one #2 and one #1 curette scoop of silver to mix and one #1 curette scoop of silver for makeup. If you have recovered <2 mg of Al, then you can use one #2 curette scoop of silver to mix and one #2 and one #1 curette scoop of silver for makeup.

_____ Using the curette(s), add the appropriate amount of scoops of silver to the vial and return curette to its place

_____ Using silicon carbide sandpaper, wet sand (in alcohol—not acetone!) approximately one half of the tamping rod shaft and also the end; dry with a kimwipe when sanded

Note: Each rod gets its own spot on the piece of sandpaper. Keep rod flat when sanding. When clean, hold the non-sanded end of the tamping rod and do not touch to any other surface.

_____ Add 2 drops of acetone to the vial

_____ Grind the sample around the bottom, across the bottom, and up & down around the lower portion of the walls of the vial

_____ When finished, the vial (with the tamping rod inside) goes into heating block to air dry

—Let samples dry at least 30 minutes before beginning the loading process.

Fill in datasheets or lab book with the holder number corresponding to each sample. If you get out of that sample/holder sequence make sure that you stop and update your list before continuing to load.

If necessary, stand as many cryovials (1.2 ml volume) or shell vials as you have samples on the counter/table for easy access.

You will need the hammer.

_____ Place a new small kimwipe (folded to give two layers) over the aluminum loading block

_____ Extract a stainless steel holder from the holder box, double-check the holder number against your datasheet, and push holder into the hole in the aluminum plate, pushing the small kimwipe down in the process

—Holders should be packed to the top of the well with the Al_2O_3/Ag mix.

—Using tweezers, hold vial—including tamping rod—to the anti-static head, run one hand under the anti-static head, transfer vial to that hand, then run the other hand under the anti-static head

_____ Loosen Al_2O_3/Ag mix with the tamping rod (carefully), tap bottom of vial with rod to help

_____ Hold vial back up to the anti-static head to loosen powder

_____ Based upon how much powder is in the vial, add enough Ag makeup to the holder well so that your Al_2O_3/Ag mix reaches the top and tamp makeup Ag down

_____ Pour/tap powder from the vial onto the holder face

_____ Use tamping rod to move powder on the holder face down into the well

—Do not hold the tamping rod vertical while moving powder or you can flick powder off the holder.

_____ With hammer, tamp down the powder in the well using the tamping rod

—It can take multiple cycles of tapping/scraping the vial, anti-static, adding more mix to the holder, and tamping to fill the well to the top.

Note: For Al you can tap excess oxide/binder mix from the holder face back into the vial for storage.

_____ Remove holder from the block, turn the holder upside down and rap on the kimwipe

—The used tamping rod goes into the "not clean" beaker in the loading hood.

_____ Put holder face-down into cryo- or shell vial (so you can read the holder number) and return vial to the holder's original spot in the holder box

—Small kimwipe is folded over and goes into the trash.

—When finished, large kimwipe in front of the loading area, sandpaper, and gloves go into the trash.

Remember to turn off the Anti-Static unit when you are done!

Appendix 14: Cathode dimensions used by the PRIME Lab at Purdue University for the ^{26}Al AMS measurements of Al_2O_3.

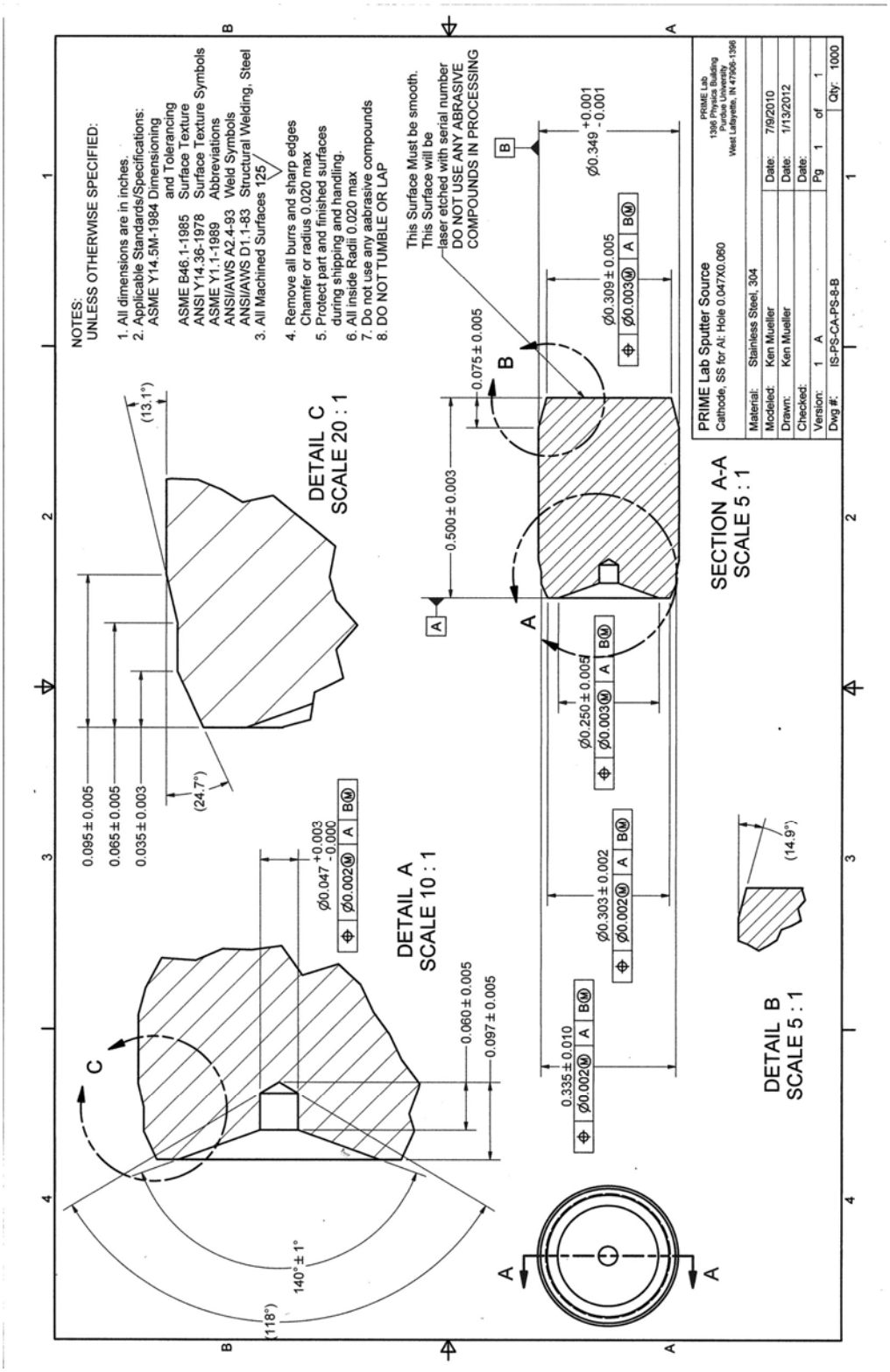

VITA

Meghan Janzen was born in Knoxville, TN, to the parents of Victor and Heather Janzen. She is the middle daughter of three children including an older brother and younger sister. A year after she was born her family returned to Canada and has lived in Deep River, Ontario ever since. Meghan attended St. Mary's Elementary school and then continued on to Mackenzie High School where an outdoor experience program sparked her interest in Earth Science. She graduated high school in 2005 and that Fall began her bachelors of science with a major in Earth and Planetary Sciences at McGill University in Montreal, Quebec. Throughout her undergraduate Meghan held student intern positions at the Deep River Science Academy, Atomic Energy of Canada Limited and Fladgate Exploration Consulting Corporation. She graduated with distinction from McGill in 2009 and shortly afterwards began working as a geologist for Atomic Energy of Canada. After working for a year she decided to return to school to get her Master of Science in Geology. She accepted a graduate research assistantship at Oak Ridge National Laboratories (ORNL) working with Dr. Alfredo Galindo-Uribarri in the nuclear physics division at the Holifield Radioactive Ion Beam Facility (HRIBF). Meghan's research at HRIBF focused on the AMS measurements of geological samples and at the same time she continued her education at the University of Tennessee, Knoxville (UTK). During her schooling at UTK Meghan accepted an internship at ExxonMobil and took a semester off to explore a career in oil and gas. Meghan then graduated with a Master of Science degree in Earth and Planetary Sciences from UTK in December 2012. She was hired on as an exploration geologist for ExxonMobil and she is now continuing her career down in Houston, Texas.